QUARTERLY PROGRESS REPORT NO. 4 ON 37-MM LIGHT ANTIAIRCRAFT WEAPON STUDY

RAD PROJECT: TR1-1051

ARMY PRIORITY PROOF PROJECT NO. EXO. 5565-1

SPERRY GYROSCOPE COMPANY
DIVISION OF THE SPERRY CORPORATION
GREAT NECK, NEW YORK

CONFIDENTIAL
SECURITY INFORMATION

QUARTERLY PROGRESS REPORT NO. 4 ON 37-MM LIGHT ANTIAIRCRAFT WEAPON STUDY

RAD PROJECT: TRI-1051
ARMY PRIORITY PROOF PROJECT NO. EXO. 5565-1

THIS REPORT COVERS THE PERIOD FROM 1 MAY 1953 TO 31 AUGUST 1953

PREPARED FOR

NEW YORK ORDNANCE DISTRICT
CONTRACT DA-30-069-ORD-607

SPERRY GYROSCOPE COMPANY
DIVISION OF THE SPERRY CORPORATION
GEAT NECK, NEW YORK

SPERRY REPORT NO. 5282-7169
SEPTEMBER 1953

COPY NO. 29
CONFIDENTIAL

CONFIDENTIAL
Security Information

CLASSIFICATION NOTICE

This document is classified as CONFIDENTIAL and contains information affecting the national defense of the United States within the meaning of the Espionage Act, 50 U.S.C., 31 and 32, as amended. Its transmission or the revelation of its contents in any manner to an unauthorized person is prohibited by law.

TABLE OF CONTENTS

TABLE OF CONTENTS (Cont.)

LIST OF ILLUSTRATIONS*

- - - - - - -

*Illustrations are presented in order by figure number at the conclusion of the text.

LIST OF ILLUSTRATIONS (Cont.)

CONFIDENTIAL
Security Information

LIST OF ILLUSTRATIONS (Cont.)

LIST OF ILLUSTRATIONS (Cont.)

CONFIDENTIAL
Security Information

LIST OF ILLUSTRATIONS (Cont.)

ABSTRACT

Results of studies conducted since 30 April 1953 are presented. Included is a description of a "fixed target rejection" system as well as a chart and over-all system schematic showing all operating modes. AA computer diagrams for use in determining overall weapon effectiveness are discussed. Sketches of single gun arrangements are included.

SECTION I

INTRODUCTION

This is the fourth in a series of quarterly progress reports being prepared for the New York Ordnance District by the Sperry Gyroscope Company on Contract DA-30-069-ORD-607. These reports describe the progress being made on the feasibility of developing an on-mount fire control system and turret design, similar to the caliber .60 weapon known as Stinger, for use with a new 37-mm gun. The program for this contract was outlined in the proposal (Neg. No. 0.16434-2) dated January 1952.

Like the Stinger, the new weapon is to be designed to engage low flying aircraft having speeds up to 800 miles per hour. The 37-mm gun provides increased range and lethality. The new weapon is to be mounted either in a self-propelled vehicle similar to Duster, in a trailer, or in a fixed installation. Its configuration and size, therefore, will have to be similar to that of the Stinger. It is required that the turret be self-contained, except for primary power and be designed to mount either two Dixon Guns T37E2 or two T172 37-mm guns with minor changes to the mount.

A major portion of the contract involves a study of the problems associated with the adoption of an improved system

to the 37-mm gun and ammunition. Although the tactical role of the new equipment is the same as for the Stinger, the ballistics will be changed considerably and the effective firing range will be increased from 2000 to 4500 yards. The ballistic changes affect only the computer, whereas the increased range will mean new requirements for both the computer and the radar. Increased range for the radar is expected through the use of improved RF components and improved receiver techniques.

Emphasis in the fire control will be placed on three major considerations: target acquisition, accuracy, and reliability. Improvement of target acquisition is essential to permit the new weapon to acquire effectively, low-flying, high-speed planes. Discussion of some methods for improving target acquisition is given in Section III B of this report. Improved accuracy is required because of the increase in firing range and higher times of flight. Reliability is influenced by many factors including simplicity, component selection, conservative design, parallel circuits, etc. All of these factors must be considered at this stage in order to avoid a change in planning in the event development is started.

While consideration will be given to the matter of minimizing redesign of some components, director accuracy will not be compromised. Many improvements to the computer are

being considered which will not involve any basic change in theory but will require a complete physical redesign. The new guns require heavier structure and larger power controls. Of the radar subassemblies it is expected that the scanner will be used as is, but all of the chassis will require complete physical and partial electrical redesign. Thus, several design studies are involved in this contract, but the number and scope will be sufficient only to determine feasibility.

SECTION II

SYSTEM CONSIDERATIONS

A. GENERAL

The proposed 37-mm fire control system is completely integrated; the radar, power controls (turret), and computer forming one closed servo loop. Within this system are several small loops. To insure overall system stability a servo analysis of the system loop has been made which takes into consideration all of the servos and other delays in the system. This analysis was presented in Progress Report No. 3 and indicated that the system will be stable throughout the required range of operation. Another important system consideration is the method of providing additional operating modes during search and aquisition. Of the three basic operations search and acquisition are the most difficult to modify when low flying high speed aircraft are considered as targets. A method of utilizing fixed target discrimination to aquire low flying targets in the presence of ground clutter is discussed in this section. A method of changing from sector search to automatic acquisition is presently being studied. All of the system modes are discussed in the following paragraphs.

B. SYSTEM OPERATING MODES

Work has been started on mode analysis and system operational procedure. A preliminary outline proposing a system embodying considerable improvements and simplifications over that of Stinger is presented here. Only one axis has been considered in detail at this time, but cognizance has been taken of the other. A complete two axis system will be presented in the final report.

Figures 2-1 and 2-2 present a general outline of the 37-mm fire control system during the several modes necessary for the successful operation of Stinger. It should be noted that, although many modes are shown, the number of switching operations required of the comprising components is held to a minimum. The gyro and the deflection servos, for example, are only required to operate in three different manners for the ten modes shown while the scanner servos operate in only two different manners. Further examples are found in the mode analysis table (fig. 2-1).

The methods of changing from both spiral and sector search to the target acquisition modes have been considerably improved and are almost identical. In both cases the gyro will be clamped (allowing no precession), and the deflection servos will be zeroed (allowing no lead angles), at the instant

the target is acquired. The scanner (and the optical sight line) will be positioned in azimuth by positioning the turret with the handle bars (scanner lead angles will be zero), and by positioning the gyro elevation servo (GYE). Wide angle displacement control will thereby be available. The method of using a follow-up synchro, located in the handle bar, to store target position, as done in the Stinger, will be retained. (A clutch is used to clamp this synchro at the proper instant.) It is expected that most of the hydraulic control features associated with the target acquisition mode of the Stinger will be used.

Sector Search

The sector search mode will be exactly the same as the acquisition mode except that the scanner will be sweeping thru a sector. When a target is seen by the radar its position will be stored. The system will then come out of sector search and seek the target position. The range gate will sweep, as described in Section III, and automatic radar lock-on will occur.

It will be noted that the sector search mode has not been included in the preliminary mode analysis. It is intended to present a proposed system, which will be integrated with the entire 37-mm mode switching system, in the final report.

It should be understood that the practicability of such a completely automatic system will be contingent upon results of breadboard tests, which is beyond the scope of this study.

Spiral Search

Automatic elevation search coverage while searching 360 degrees in azimuth defines the spiral search mode. Superimposed on the automatic elevation search signal will be the handle bar displacement signal. This will allow re-examination of a previously searched spiral sector. During this mode the guns, in elevation, and the turret, will be inoperative. (Gun elevation hydraulers are driving the scanner in 360 degree motion and the turret "B" end is being by-passed.)

Target Selector and Parallax Corrector

In the target selector mode the target selector maintains direct control over the scanner and the optical sight line by positioning the turret and the gyro elevation servos directly. The external selector mode operating from the 414C system may operate in a similar manner or may only position the system accurately enough so that the proper sector may be searched.

Gun Drive Mode

During the gun drive mode the turret will follow the motion of handle bars and the guns will follow the handle bars in elevation. The characteristics of motion will be aided tracking (rate plus displacement). The gyro elevation servo (GYE) will follow the motion of the guns in elevation. Thus, in this mode the scanner and sight line will also point along the gun line. The gun drive mode, therefore, also enables the acquisition of targets by radar using the optics or a ring sight.

In the acquisition modes mentioned above no mention was made of ranging on the target. There will be three methods of ranging, each of which is described below.

C. METHODS OF RANGING

1. Manual Lock-on

After the target appears on the PPI scope, the range gate is slewed over the target. The range gate automatically locks on the target and the system can be placed in the automatic tracking mode by throwing the "manual-automatic track" switch to "automatic". If the range gate locks on an unwanted target the operator can again press the slew button and the range gate will slew to

the next target. This method gives the operator the perogative of choosing the target he wants when there are more than one fixed or moving targets. This mode is called manual lock-on.

2. Auto Lock-on

The second method of ranging automatically causes the system to lock-on a target. The operator first slews the range gate over the target. The range gate then locks on the target which automatically places the system in automatic track. This mode is called automatic lock-on.

3. Fixed Target Rejection

The third method of ranging features fixed target rejection and an automatic range sweep. While the operator tracks a target with the target selector or ring sight, the range gate sweeps in and out, automatically stopping on the first target it comes to. It then examines said target for about 1/2 second and, if it is moving (in range), it will stay on this target and automatically switch the system to automatic track. If the target is fixed, outgoing or incoming at a rate less than about 40 yards per second, the system will reject the target and move on to the next target where the process

is repeated. Thus, the operator is able to track a target optically (or the target is tracked by the target selector) through much fixed ground clutter, and the radar will not lock on until it finds an incoming moving target.

The first ranging method described above is referred to as "AUTO TRACK" in figure 2-1 and the other two as "AUTO LOCK-ON", since in each case a switching signal is used to cause the system to switch to automatic tracking.

D. Miscellaneous Considerations

It should be noted that in all previous modes the gyro is clamped and the deflection servos are zeroed. Thus, no lead angles exist until the system is switched to a track mode.

During the track modes it is anticipated that the vertical ballistics (VB) will be added to the predicted gun position by the addition of an equivalent electrical displacement signal to the elevation power control. Lateral ballistics (LB) will be added by adding a bias rate signal, as done in Stinger.

The stabilizing cross feed signals are transmitted only during radar track since they are not needed at any other

time. A transient eliminator feature will be included to provide smooth switching from radar tracking to manual tracking. Switching from any other mode to manual tracking will also be accomplished smoothly. A fast settling circuit is included to decrease the settling time of the system. The theoretical basis for this has been shown in the previous progress report, and the practicability has been indicated in the Stinger. This is switched out at a predetermined time so as not to impair the computing procedure.

The basic mode diagram (fig 2-2) illustrates a lateral gyro system comprised of an RF servo whose output is multiplied by the lateral lead. A magnetic torquer is incorporated in order to inject the fast settling feature and to provide a creep adjustment; however it is possible that a system similar to Stinger will be used instead. This possibility is immaterial as far as the mode analysis is concerned, however, since in both cases the use of a gyro clamper is contemplated to accomplish caging because of the desirable feature obtained.

E. ORIENTATION

The 414C orientation knob is provided in order that the system may be orientated with the 414C system. The dial and slip clutch arrangement allow the dial to be adjusted to

its proper space reference. The indicator orientation knob allows the operator to orientate the indicator with respect to the direction of the sweep. Orientation of the target selector is accomplished by positioning its case.

F. CENTERING FOR POWER CONTROLS

The centering mode is initiated by releasing the safety switches of the handle bar. The azimuth and gun elevation "B" ends are then blocked which insures no motion of the guns*. The yokes are centered (preventing a gun transient motion when they are turned on), the gyro is clamped, and the deflection servos are zeroed.

---

*The gun elevation "B" end may be blocked in such a manner that the oil is trapped in the "B" end, thus preventing rapid falling until the equilibrator spring balances the downward gravity torque.

SECTION III

RADAR

A. TRANSMITTER-RECEIVER

Space studies of the transmitter-receiver unit have been completed during the past quarter. Since the heavier guns of the 37-mm system require a longer elevation power control motor this component occupies more space. This requires that the transmitter-receiver unit be deeper than the existing caliber .60 unit. The synchronizer or scanner servo chassis, therefore, must be broken up into several small functional sub-chassis which will be distributed on either side of the pedestal or relocated below decks. The transmitter-receiver unit layout (fig. 3-1) was drawn using a magic tee mixer and conventional TR-ATR duplexer. This mixer-duplexer will probably not be the final type used (Stinger Quarterly Progress Report No. 3), but it was shown because it represents the largest configuration considered.

B. SYNCHRONIZER (FIXED TARGET REJECTION CIRCUITS)

During the past quarter most emphasis was placed on the development of the final circuitry for the range gate automatic sweep and lock-on and for the fixed target rejection circuits. A complete breadboard of the synchronizer and fixed target rejector was built and checked out satisfactorily.

The operation of this circuit is described in the following paragraph.

When the system is switched to the target selector or optical acquisition mode, the range gate will automatically sweep over preset limits (nominally 1000 to 10,000 yards). The scanner will be positioned to track the target by means of either the handlebars or target selector. When a target appears in the radar beam the range gate will lock on this target and sample its range rate for 0.5 seconds. If the range rate is less than 40 yards per second the range gate will reject the target and continue sweeping until it locks on the next target in the beam. If the target range rate is greater than 40 yards per second, and, if the movement of the target is towards Stinger, the range gate will stay locked oh. After the 0.5 second sampling time the entire system will switch to automatic track. After approximately 0.5 second of tracking the reject circuits will automatically be de-energized to enable tracking through crossover at which time the range rates become zero. Additional circuits have been added to prevent the range gate from sweeping if the target is lost momentarily due to fading. If this occurs Stinger will continue to track, in both range and position, the last known motion of the target. The block diagram of the range sweep

and reject system is shown in figure 3-2 and circuit operation is described in the following paragraph.

Initial conditions for the various relays are: S_1 closed, S_2 open, and S_3 closed. When the range gate locks on a target a signal will appear at point "A". This will cause the range strobe to be turned off and will energize the 0.5 second and 1 second time delay circuits. The voltage input to the differentiating circuits is proportional to range, which means that the output voltage of the differentiator will be a voltage proportional to range rate. If the target is a fixed target its range rate will be zero and relay S_1 will remain closed. After 0.5 seconds relay S_2 will close which allows the reject voltage to be supplied to the synchronizer range tracking loop thereby causing the range gate to be driven off the target. When this happens the signal at point A will disappear and the range strobe circuits will cause the range gate to continue to sweep. If the target is a moving target a voltage will appear at the output of the differentiator causing relay S_1 to open. Therefore, when S_2 closes (after 0.5 seconds) there is no -300 volts available as a reject voltage. The closing of S_2 will also fire the automatic track relays, switching Stinger to the automatic track mode. After 0.5 seconds of tracking S_3 will open. This means that even if the signal fades, causing no signal to appear at point A, the reject voltage and range strobe voltage will not

be supplied to the ranging circuits. However, if no signal appears at point A for approximately three consecutive seconds, S_3 will reclose allowing the range strobe action to take place. The ability to discriminate against incoming and outgoing targets originates in the differentiator which supplies an output of different polarity for incoming and outgoing rates. The relay control circuit will only respond to a polarity resulting from an incoming rate.

C. EXPERIMENTAL CHASSIS

A complete synchronizer chassis (fig. 3-3) is being built incorporating the new features discussed in the synchronizer section. This chassis can be tried in the caliber .60 Stinger with a minimum of changes to the existing wiring in the Stinger.

D. INDICATORS

Development of the indicator circuitry has been started during the past quarter. Progress on design of the circuits for the development of the PPI sweeps has been temporarily halted pending delivery of a cathode ray tube from DuMont and deflection coils from Syntronic Instruments, Inc. A breadboard of the new intensifier circuit (Quarterly Progress Report No. 3) has been built and is currently undergoing testing.

SECTION IV

COMPUTER

A. GENERAL

The studies on the computer have been concerned with effectiveness and accuracy, sensitivity computation, fast settling, mechanical design of the main computer section (known as the tracking section), development of a mechanical caging mechanism, and potenticmeter tests. The status of the computer at this time can be summarized as follows:

1. Main computer section redesigned and materially simplified without sacrificing accuracy.

2. Sensitivity computer (TM computer) designed, breadboarded, and tested; and its feasibility established.

3. New gyro gimbal system designed which is more compact, rugged, and accurate.

4. Effectiveness studies are nearing completion and important accuracy factors have been evaluated.

5. Preliminary optical design is nearing completion.

6. Fast settling parameters have been chosen.

7. Wooden mockup of computer is nearing completion.

The following paragraphs contain discussions of the various studies which have been completed or are in advanced stages.

B. EFFECTIVENESS AND ACCURACY STUDIES

Because of the original nature of these studies, it has been necessary to consider several different analytical techniques in an attempt to arrive at the most satisfactory solution to the problem. This has caused changes to be made in the original study program. Now, however, as the result of concentrated study and analysis, a firm study plan has evolved, the outline of which is herewith presented:

1. The determination of kill probability

2. Target Course Data

3. System Limitations

4. AA Computer Diagrams

5. Practical Usage and Limitations

6. Optimum Firing Parameters

7. Accuracy Requirements

1. The Determination of Kill Probability

As shown in Progress Report No. 3, the single shot kill probability Pss is given by the following expression:

$$P_{ss} = \frac{1}{1 + \frac{2r_s^2}{a^2}} \, e^{\left[\frac{-\left(\frac{h}{a}\right)^2}{1 + \frac{2r_s^2}{a^2}} \right]} \qquad (4\text{-}1)$$

where

a = radius of a vulnerable circular target area A_v

r_s = random circular probable error or scatter

h = bias or systematic error

Acceptable values must now be assigned to a, r_s and h.

The target vulnerable area A_v is the product of the apparent area Ap of the aircraft at any instant of time, and the vulnerability coefficient av of the shell at that time. The apparent area of the aircraft is the area presented by the aircraft to the gun at any instant of time and, obviously, is directly dependent upon the type of aircraft engaged, the range at which it is engaged, and the course which it is flying.

It is to be expected that the type of aircraft which the Stinger will engage most frequently will be single engine

fighters especially suited for ground interdiction. In the propeller driven class an example of this type of plane would be the F-47; in the jet class the F-84F.

To calculate the apparent area presented to the gun by this class of aircraft for all attitudes on all target courses would be a staggering task. Thus, it was decided that the simple geometric mean of the areas presented by the aircraft from below, from in front, and from a side of the aircraft would be computed and the result would be assumed equal to the average apparent area of the target for all attitudes and for all target courses. For the class of aircraft described above a value between 10 and 20 square yards was computed.

The vulnerability coefficient (av) is a function of the total energy of the projectile at impact. According to an empirical equation developed by the Sperry Sysnet Group to match data supplied by the Ballistic Research Laboratories

$$av = 1 - .3^{E_t}.$$

In this equation E_t is equal to the sum of the kinetic and chemical energies of the projectile at the time of collision with the target.

Because of the high explosive content of the 37-mm H.E. Shell T81, the vulnerability coefficient (av) is relatively

independent of the kinetic energy of the projectile at impact. The maximum and minimum values of av were calculated to be .60 and .36. Since we are not, for all practical purposes, concerned with these extreme cases, the variation in av is expected to be slight over the courses to be considered, and little error should be introduced by assuming av to be a constant.

From the data derived above, the average vulnerable Av is expected to be between 3.6 and 12 square yards. A of five (5) square yards was selected as the average vulnerable area (Av) of the target under analysis in order to present a conservative picture of Stinger effectiveness.

Therefore: $\overline{Av} = 5 \text{ Yds}^2$.

The total random circular probable error, or scatter, is the sum of the random error in aim, or wander, and the random error of the gun, or dispersion. The standard deviation of wander is equal to the tracking error multiplied by the system amplification factor. From tracking data acquired to date during the Stinger caliber .60 test program, a standard deviation value of 2 mils of tracking error appears reasonable. This is an average value for both radar and manual tracking, over all target courses and at all ranges. The system amplification factor, unchanged in the 37-mm Stinger, is 3.5. Thus,

the standard deviation of wander is equal to 2 x 3.5 = 7.0 mils.

As yet no data is available on the firing dispersion of the 37-mm guns currently under development. If, however, 96% of the projectiles are assumed to fall within a circle 24 mils in diameter 50% of the projectiles will fall within a circle 8 mils in diameter and the circular probable error will be equal to 4 mils.

The scatter r_s is equal to the square root of the sum of the square of the wander and the dispersion.

$$\overline{r_s} = \sqrt{(7)^2 \pm (4)^2} \simeq 8 \text{ mils.}$$

A value for $\overline{r_s}$ of 8 mils may appear somewhat large. It does, however, represent a conservative estimate for the determination of engagement kill probability, and furthermore it is in reasonable agreement with the av standard deviation of random error in feet ($\overline{s}$) derived from the equation below. (This equation was provided by the Ballistic Research Laboratories at Aberdeen, Maryland.)

$$s^2 = (.05TV)^2 \pm \left\{2 \pm \frac{TV}{1000}\right\}^2 \left\{\frac{DP}{1000}\right\}^2 \pm (10TF)^2$$

where

s = Standard deviation of random error in ft

TV - Target velocity in ft/sec

DP = Future range in ft

TF = Time of flight in sec

For a random circular probable error r_s of 8 mils and a vulnerable circular target area of 5 square yards, it can be shown that the target area is generally small compared to the area covered by scatter under these conditions. $2rs^2 >> a^2$ and equation 4-1 can be written as follows:

$$Pss = \frac{a^2}{2r_s^2} \exp^{-\frac{h^2}{2r_s^2}} \quad (4\text{-}1a)$$

or, since a = radius of a vulnerable circular target area

$$Pss = \frac{A_v}{2\pi r_s^2} \epsilon^{-\frac{h^2}{2r_s^2}} \quad (4\text{-}1b)$$

Systematic error (h) can only be evaluated in terms of the effect it has on kill probability. However, because of the broad nature of this study, it has been found advisable to make this investigation during the conclding portion of the program. At that time quantitative evaluation of the effects of systematic error on kill probability will be considered. Until then systematic error will be assumed equal to zero.

Thus:

$$P_{ss} = \frac{A_v}{2\pi r_s^2} \qquad (4\text{-}1c)$$

where Av = an area of 5 square yds expressed in mils

and r_s = 8 mils total scatter.

It was shown in Progress Report No. 3 that the probable accumulated lethal hits N can be expressed as follows:

$$N = FR \sum_{PCTof}^{PCTcf} PCTi\,(Pss)\,i \qquad (4\text{-}2)$$

Substituting equation (4-1c) for Pss into equation (4-2) and factoring

$$N = \frac{FR}{400} \sum_{PCTof}^{PCTcf} PCTi\,((Av)\,i \qquad (4\text{-}2A)$$

where FR = Rate of fire in rounds/second

PCT_i = Present course time at $instant_i$

$(Av)_i$ = Target vulnerable area in mils at PCT_i

Equation (4-2A) forms the basis for construction of the AA Computer Diagrams.

2. Target Course Data

Kill probability, as discussed in Quarterly Progress Report No. 3, has been selected as the yardstick with which to

measure the effectiveness of the 37-mm Stinger System. The target course calculation present data on twenty-five representative target courses for which it is desired to measure system effectiveness. The results of the analysis of the target course data in terms of expected kill probabilities are shown on the computer AA diagrams (figs. 4-1, 4-2, 4-3 and 4-4).

3. System Limitations

The expected effective range of the 37-mm gun is 4500 yards. However, certain system limitations occur which may restrict and/or negate the effectiveness of the 37-mm Stinger on certain courses. These system limitations are shown on the Computer AA Diagrams.

The major system limitations are those which delay opening fire until after the aircraft has passed within the maximum effective range of the weapon and those that precipitate cease fire before the target has passed outside the effective range of the weapon. Included in the first category are the limitations arising from maximum radar detection range and time lost during acquisition and settling. Included in the latter category are limitations imposed by maximum turret rates and accelerations, maximum values of lead angle, maximum values of scanner elevation, and excessive radar beam shadowing.

The time before present position cross-over, when the prediction problem is solved and effective anti-aircraft fire can begin, is the time when the target was initially detected minus the total lost time k, or

$$PCTpps = PCTrd - k \tag{4-3}$$

where

PCTpps = Present Course Time when prediction problem is solved.

PCTrd = Present Course Time when radar detects aircraft.

k = Time lost in acquisition and settling.

From geometry

$$(TV \cdot PCTrd)^2 = R^2d - Rc^2 \tag{4-4}$$

where

TV = Target Velocity

Rd = Radar detection range

Rc = Slant range at cross-over

or

$$PCTrd = \frac{\sqrt{Rd^2 - Rc^2}}{TV}. \tag{4-4a}$$

Substituting equation (4A) into equation (3) gives

$$PCTpps = \frac{\sqrt{Rd^2 - Rc^2}}{TV} - k \quad (4\text{-}3a)$$

The time interval between the initial detection of a target and opening fire is defined as the time lost (k) and consists of the time spent in target acquisition and computer settling time. From experience and considered study it has been estimated that

Acquisition Time	=	10 seconds
Computer Settling Time	=	2 seconds
Total time lost k	=	12 seconds

Maximum radar detection range is a direct function of the size and shape of the reflecting surface. Then for different types of aircraft different maximum radar detection ranges are to be expected; the larger and less streamlined the aircraft. the longer the detection range. But the larger and less streamlined the aircraft, the lower the median speed that can be associated with the aircraft. Thus, it does not seem inconsistent to propose that maximum radar detection range can be correlated with median aircraft speed. Based on this assumption a table (table 4-1) was constructed relating maximum radar detection range and average target velocity. Data for this table was culled from the "Final Report on Study of Short

Range Anti-Aircraft Fire Control Systems" by Aircraft Armaments, Ind., and was based on experience gained on the caliber .60 Stinger.

TABLE 4-1

MAXIMUM RADAR DETECTION RANGE VS AVERAGE TARGET VELOCITY

Average Target Velocity	Maximum Radar Detection Range
100 yds/sec	16,000 yds
200 yds/sec	12,000 yds
300 yds/sec	9000 yds
400 yds/sec	7200 yds

A graphical solution of equation (4-3A) can be readily obtained since, on a graph with present course time PCT as the abscissa and Rc/TV as the ordinate, equation (4-3A) is a semi-circle of radius Rd/TV whose center is located where PCT = k and Rc/TV = 0. A typical plot, assuming a target velocity of 400 yards/second, is presented in figure 4-5. Superimposed on this graph is a semi-circle showing the total firing time available. This plot is based on a maximum effective range of 4500 yds with targets of 400 yds/sec velocity and with slant ranges at cross-over between 0 and 4500 yds.

This plot reveals that using a maximum radar detection range of 7200 yds and a total lost time (k) of 12 seconds eliminates 70% of the firing time available to the 37-mm weapon for targets of 400 yds/sec velocity. The computer AA diagram shows that for a similar speed target the loss in effectiveness is only 20%. This indicates that firing time is no criterion on which to base the measure of system effectiveness.

It appears safe to assume that if the required rate and/or acceleration of the turret exceeds the maximum rate and/or acceleration of the azimuth power control, the system will lose track of the target. It likewise appears safe to assume that if the tracking is interrupted because of excessive azimuth rate and/or acceleration, the engagement, for all practical purposes, will have terminated.

Because of the mechanization of the system, required rates and/or accelerations of the guns in elevation, in excess of the maximum rate and/or acceleration of the elevation power control, will result in errors in the pointing of the guns. However, this will not produce an interruption in the tracking of the target. The effect on system performance of excessive rates and/or accelerations in elevation is therefore felt to be of only minor importance, especially in view of the large rates and accelerations available in the elevation power control.

From geometry it can be shown that firing azimuth rate (FAR) is expressed as

$$FAR = \frac{TV \sqrt{Rc^2 - Y^2}\,(1 + TFR)}{(DP^2 - Y^2)} \qquad (4\text{-}5)$$

where TV = Target velocity

Rc = Slant range at cross-over

Y = Constant target altitude

TFR = Time rate of change of time of flight

DP = Future slant range.

Firing azimuth acceleration (FAA) is equal to the time rate of change of FAR. Performing the required differentiation of equation (4-5), and making use of the equation for the analytical trajectory of the 37-mm HE Shell T81 given in Appendix A, of Quarterly Progress Report No. 3, the firing azimuth acceleration is expressed as follows:

$$FAA = \frac{TV \sqrt{RC^2 - Y^2}}{(DP^2 - Y^2)} \left[\dot{TFR} - \frac{DP\,(1 + TFR)\; APV^2 \cdot TFR}{500\,(DP^2 - Y^2)} \right] \qquad (4\text{-}6)$$

where APV = average projectile velocity

and TFR = time rate of change of TFR

Because of the obvious complexity of determining FAA for various instances, on different target courses, it was found that equation (4-6) could be closely approximated by

$$FAA \simeq FAA' = \frac{-\,TV \sqrt{R_c^{\,2} - Y^2}}{500} \; \frac{APV^3 \cdot TFR \cdot TF}{(DP^2 - Y^2)^2} \qquad (4\text{-}7)$$

The extent of the agreement between equations (4-6) and (4-7) is shown on the graph (Course No. 4, fig. 4-6).

In order to limit the scope of this portion of the study it has been found desirable to reduce all problems to the slant plane. Obviously turret azimuth rate and accelerations are not only functions of TV and Rc but of target altitude Y as well. Thus, it now becomes necessary to select, as judiciously as possible, the median value of the slant plane inclination to the azimuth plane. Based upon a random target distribution in space, this inclination corresponds to an angle of thirty degrees.

On the basis of a slant plane inclination of thirty degrees, a maximum turret azimuth rate of 90 degrees per second, and a maximum turret azimuth acceleration of approximately 120 degrees per second per second, it is possible to determine the limitations arising from maximum turret azimuth rates and acceleration by using equations 4-5 and 4-7. This has been done and these limitations have been entered on the computer AA diagrams.

In the caliber .60 Stinger it was found advisable to limit the lead angle in the slant plane to a value of 30°. This was done by limiting the lateral and vertical components

of the lead angle to thirty degrees individually, and by rounding off cam data wherever the total lead angle function L exceeded thirty degrees. If the required value of lead angle L exceeds thirty degrees for any period of time tracking will be interrupted when

$\int_0^t (PR_{REQUIRED} - PR_{ACTUAL})\, dt$ exceeds the maximum radar signal.

Once tracking is interrupted it appears reasonable to assume that the engagement, for all practical purposes, will have terminated. Thus, it behooves us to investigate the limitations on Stinger effectiveness due to the requirement that lead angles exceed 30°.

From the course data it is possible to determine for each target course the present position, if any, at which the required lead angle exceeds thirty degrees. Such information is presented in table 4-2.

TABLE 4-2

PRESENT TARGET POSITIONS WITH
LEAD ANGLE EXCEEDING 30 DEGREES

Course No.	TV	Rc	PCT
24	300	4000	-2.400
13	400	1500	+2.800
15	400	2000	- .675
19	400	2500	-2.300
21	400	3000	-3.875
25	400	4000	-8.600

Table 4-3 lists for each target course the present position, if any, at which the required lead angle exceeds thirty-five degrees. This gives an indication of the increase in system effectiveness resulting from increasing the lead angle limit from 30 to 35 degrees.

TABLE 4-3

PRESENT TARGET POSITIONS FOR LEAD ANGLES EXCEEDING 35 DEGREES

Course No.	TV	Rc	PCT
15	400	2000	+2.050
19	400	2500	+0.250
21	400	3000	-1.475
25	400	4000	-5.450

The data furnished in tables 4-2 and 4-3 is graphically presented on the computer AA diagrams for purposes of analysis.

A minimum TM value of 0.25 seconds will place a limitation on the extent of the target courses to be considered. Unlike the limitations arising from maximum azimuth rates and accelerations, and a maximum lead angle value of 30 degrees; however, a limitation arising from a minimum value of TM will not manifest itself in the form of a tracking interruption. It will cause a systematic error in the lead input value required to achieve the desired tracking rate. This is shown as follows:

Given

$$TM\ min = 0.25 \text{ seconds}$$

$$RF\ max = 4 \text{ seconds}^{-1}$$

$$L\ max = 30°$$

$$\sin\ L\ max = 0.500$$

and since PR max = sin L max RF max (4-8)

We may substitute the above values for sin L max and RF max into equation (4-8) giving:

$$PR\ max = 2\ radians/sec.$$

Since the value of PRmax is in excess of the maximum turret rate and maximum gyro precession rate, it is obvious that forcible interruption in tracking will result from the limitation imposed by the maximum turret azimuth rate of 90 degrees per second, and not from the inability to introduce lead in excess of 30° for a minimum TM of 0.25 seconds. Thus, a minimum value of TM of 0.25 seconds does not constitute a system limitation, in that it does not delay opening fire until after the aircraft has passed within the maximum effective range of the weapon, nor precipitate cease fire before the target has passed outside the effective range of the gun.

It has been realized that, as in the case of the caliber .60 Stinger, certain target courses would require an elevation greater than 1600 mils to permit continuous tracking of the target shortly after it proceeds past cross-over. The obvious example is that of a target directly overhead. This limitation, which results from a maximum value of

SE of 1600 mils, will not apply to any target course whose slant plane has an inclination of thirty degrees or less. For that reason no SE limitation is shown on the computer AA diagrams. Further, it will be recalled that for the caliber .60 Stinger, this limitation first occurred at a future azimuth which was approximately 900 mils beyond cross-over. Stinger is not very effective in that region as can be seen from the computer AA diagrams.

Radar shadowing by the Armour gun is expected to be substantial for certain regions on various target courses. The effects of shadowing on system performance have not been quantitatively evaluated to date; thus it is not yet possible to determine the effect on system effectiveness of radar shadowing by the Armour gun. It is not believed that radar shadowing by the Dixon Gun will be significant.

4. Computer AA Diagrams

The Computer AA Diagram (figs. 4-1, 4-2, 4-3 and 4-4) is a plan view presentation of probable accumulated lethal hits (N) in future position space. This type of presentation was originally devised by the Research and Analysis Department of the Antiaircraft and Guided Missiles Branch of the Artillery School, Fort Bliss, Texas, to permit selection of optimum gun

positions which would maximize anti-aircraft defense. We shall use the Computer AA Diagram to present system effectiveness in terms of probable accumulated lethal hits, to evaluate the system limitations previously discussed, and to indicate cumulative ammunition consumption.

Future position space forms the basis of the Computer AA Diagram. Thus, the initial step in the construction of such a diagram is to draw a circle whose radius equals the maximum effective range of the 37-mm weapon which is considered to be located at the center. If all target courses are drawn parallel to the abscissa the ordinate is graduated in values of slant range at cross-over, from 0 to 4500 yds. The distance along the abscissa, then, is equal to X, the product of future course time and target velocity. Four Computer AA Diagrams have been prepared for targets with 5 square yds of vulnerable area and velocities of 100, 200, 300 and 400 yds/sec.

In Quarterly Progress Report No. 3 it was concluded that engagement kill probability is the only realistic measure of the effectiveness of the 37-mm Stinger System. Engagement kill probability, however, is not cumulative, in that the engagement kill probability on one segment of a target course added to the engagement kill probability on other segments of the target course does not equal the engagement kill probability

over the entire course. For this reason it was decided to use the probable accumulated lethal hits (equation 4-2A) on the Computer AA Diagram since these are cumulative.

The curves of probable accumulated lethal hits are calculated assuming firing is begun at the maximum effective range of the weapon. However, because of the cumulative nature of the probable accumulated lethal hits N, this does not restrict consideration to situations where firing is begun at 4500 yards. To measure system effectiveness over any segment of any target course it is only necessary to determine N_1 at open fire and N_2 at cease fire. N_2-N_1 is then the probable accumulated lethal hits and $1-\epsilon^{-(N_2-N_1)}$ is the engagement kill probability for that segment of that particular course. To eliminate the necessity of calculating the engagement kill probability a graph has been provided on each Computer AA Diagram giving the survival probability as a function of probable accumulated lethal hits N. Since, by definition, one minus the engagement survival probability is equal to the engagement kill probability the engagement kill probability can easily be determined.

Inspection of the Computer AA Diagram reveals that only at target velocities of 400 yds/sec do maximum radar detection range, and time lost during acquisition and settling,

appreciably limit system effectiveness. As previously shown, a maximum radar detection range of 7200 yards and a total lost time k of 12 seconds eliminates 70 percent of the firing time available to the 37-mm Stinger for targets of 400 yds/sec velocity. Figure 4-2 shows that a 7200 yd maximum radar detection range and a total lost time k of 12 seconds causes 45 percent of future position space to be unavailable for gun firing purposes. In terms of probable accumulated lethal hits, however, and hence in terms of system effectiveness, the limitation is slight. It is only at longer values of cross-over range, where the system effectiveness rapidly attenuates, that this limitation become very appreciable.

A greater maximum radar detection range might be desirable for high speed targets. More desirable, however, would be a decrease in the time lost in acquisition and settling. It is certainly conceivable that an enemy aircraft could, due to topographical or other obstacles, come within maximum radar range before detection. Under those conditions a decrease in lost time k is to be desired while an increase in radar range would be of no avail.

As previously discussed settling time was estimated to be two seconds and acquisition time at ten seconds. While the former probably could not be much improved, three features

proposed for the 37-mm Stinger are expected to reduce, perhaps by as much as half, the 10 second acquisition time. These are:

1. Use of a 5-inch radar scope.
2. The addition of elevation synchro control.
3. The use of a new range gate sweep with automatic lock-on and reject features.

The four Computer AA Diagrams indicate that a maximum lead angle of 30° imposes no limitation on any targets except those whose speed is in excess of 300 yds/sec. It can be seen from the diagram that for a target flying at a speed of 400 yds/sec, no limitation exists within a slant range at cross-over of 1500 yds. For comparative purposes, the limitation which would arise from a maximum lead angle value of 35° has been added to the Computer AA Diagram. Careful analysis of this data reveals the gain in system effectiveness caused by increasing the maximum lead angle value from 30 to 35° to be slight.

Figure 4-2 indicates that the limitation imposed by a maximum lead angle value of 30° combines with the limitations arising from a maximum radar detection range of 7200 yds and a total lost time, k, of 12 seconds, to prohibit fire on any

target flying with a velocity of 400 yds/sec on a course which exhibits a slant range at cross-over in excess of 3000 yds. However, the proposed reduction in acquisition time would extend this cross-over range to beyond 3500 yds. In this region the engagement kill probability is less than 0.2.

The limitations resulting from maximum turret rates and accelerations, shown on the Computer AA Diagrams for a slant plane inclination of 30°, merit little discussion since the reduction of overall system effectiveness resulting from these limitations is negligible. However, it is expected that at higher slant plane elevations these limitations will become appreciable, but only on the receding leg of the future position target. Similarly, at higher elevation a scanner elevation limitation of 1600 mils, and the expected radar shadowing by the Armour gun, may combine to make firing on the receding leg of the target course almost impossible against high velocity aircraft.

Different firing rates have been allocated for the four different target speeds shown on the Computer AA Diagrams. This, however, should not be construed as a recommendation that firing rate should be linked to target speed. This is only an attempt to distribute the consumption of available ammunition throughout the target courses. Further, it does

not place any restriction on interpretation of the Computer AA Diagram. Ammunition consumption, like probable accumulated lethal hits, is cumulative. Doubling the firing rate doubles ammunition consumption and doubles the number of probable accumulated lethal hits. The Computer AA Diagrams clearly illustrate the ammunition shortage and the need for a very thorough study of the tactical requirements of the 37-mm weapon. Such a study is now in progress as a part of the program entitled "Tactical Limitations", and there is every reason to believe that satisfactory results will be obtained. On the basis of these results, optimum firing parameters will be determined which will husband the available ammunition. A more intelligent decision can then be reached concerning the accuracy requirements of the system. This information will be presented in the final report of the 37-mm Stinger study project.

C. SENSITIVITY COMPUTER

1. General Status

The laboratory breadboard of the model A sensitivity computer was completed two months ago and is now undergoing system accuracy tests and component studies. Only one major change has been made to the solution schematic as a result of the component study on the TF tachometer and its driving

isolation amplifier. This change provides VCRF in the RF equation

$$RF = SRF + RCRF - VCRF$$

through mechanization.

This equation may be approximated by the expression

$$VCRF = APV.\ TFR.\ (KVC.AK)\ .\ RD.$$

The previous laboratory mechanization method, which was also used with the caliber .60 Stinger, required that the TFR isolation amplifier be driven by the high sensitivity APV signal and that the KVC, AK, and RD attenuation follow the TF tachometer differentiations. Thus, the TFR booster amplifier was forced to deliver excessive power to the low impedance tachometer with the resulting signal being attenuated by about 75 percent. This arrangement was found to put a strain on the isolation amplifier and drove it into minor oscillation. This oscillatory effect was then transferred to the other isolation amplifiers in the system (as electrical pickup through their common power supplies) and forced the entire computer into constant jitter.

This problem was solved by relocating the attenuator at the input to the TFR booster amplifier rather than at the tachometer output, effectively reducing the power required from the amplifier by a factor of 16.

Thus the VCRF term, as provided in the laboratory mockup through mechanization can be written as

VCRF = APV. (KVC.AK).RD.TFR.

This change immediately stopped the jitter in the laboratory mockup, removing a serious obstacle to further testing of the computer system.

2. Static Tests

Tests have been run on the laboratory mockup for static points on general flight courses. These static tests presumed zero values for both DOR and TFR, and solved for TF and RF as the inputs DO and cos L were varied statically.

These tests were limited in their mechanized range because, for higher values of DO (above approximately 4500 yards) the TF servo drove into its upper limit (TF max = 10 secs) which yielded an increased error in RF. For very low values of DO (below approximately 1000 yards), errors appeared in both TF and RF due to the linearity and resolution of the Do potentiometers, which supply data to both these servos. However, throughout the intermediate range of DO, computer accuracies were good. TF was accurate to 0.01 secs and RF to 0.002 sec^{-1}, maximum errors being considered. This represents an accuracy (with respect to the true solution) greater than 0.3 percent in TF and 0.5 percent in RF.

For the values of Do which drove TF into its limit stop, extreme accuracy in determining RF is not required because gun firing range is limited (at a DP of 4500 yards) below the TF value of 10 seconds. Laboratory tests indicate that for values of DO up to 7500 yards (with the TF servo in its limit) RF accuracy increases to approximately five percent as DO increases.

At the other extreme, as DO decreases below 1000 yards, RF is increasing rapidly due to the DO reciprocation required by the mathematics, and the linearity resolution effects of the DO potentiometers are magnified in the RF servo. In this region the RF accuracy increases to approximately 1.5 percent with the potentiometers now used. Specially constructed Helipots with extremely high linearity and resolution at the low end have been purchased to increase accuracy for higher RF values.

These static tests are not indicative of typical flight courses as computed in the effectiveness and flight studies, but serve only to indicate the accuracy that might be expected for dynamic problems. Dynamic tests on the sensitivity computer have been begun and will be discussed in the next progress report.

3. Tachometer Studies

A component study was made on the Kearfott Mark I, Mod I a-c tachometer which is used in the sensitivity computer to measure the DOR and TFR quantities. These studies were undertaken so that simple networks could be devised to correct for the zero-speed null and phase shift error of the tachometers, and to investigate the linearity and interchangeability of these units. A simple voltage divider correcting circuit was devised which succeeded in reducing the zero-speed null to about one yd/sec. and it was found that adding an RC filter at the tachometer compensated for the inherent six degree phase shift. The later modification was adopted directly from the T26 computer while the former is a change towards increased rate accuracies in the TM solution.

Linearity and replaceability tests were run employing these dual tachometer corrections. Four tachometers were tested and indicated an individual linearity of 0.5 percent, which corresponds to an error in the DOR quantity of one yard/sec. The transfer functions of the four units were found to differ by a maximum of one percent.

This tachometer study indicates that if each tachometer were packaged with its zero-speed null network and its phase

shift circuit, the entire tachometer package would be interchangeable and would function within allowable tolerances.

4. Power Drain

The d-c power required to operate the laboratory mockup of the sensitivity computer was measured and servo interaction due to common power sources was analyzed. The electronic components of the sensitivity computer comprise three sets of servo amplifiers, each set containing both a preamplifier and a power amplifier, and seven [illegible] isolation amplifiers. All higher voltage d-c power in the mockup is obtained from electronically regulated power supplies. The computer, however, must be capable of operation with the [illegible] current +250 volt source taken directly from a dynam[illegible]. The currents required by the computer employing the re[illegible] power supplies for all voltages other than the +27 vo[illegible] ment supply, are listed in table 4-4.

TABLE 4-4

COMPUTER CURRENT REQUIREMENT

VOLTAGE	CURRENT
+27 volts	[illegible]
-300 volts	[illegible]
+150 volts	[illegible]
+300 volts	[illegible]
+250 volts	[illegible]
Isolation [illegible]	[illegible]
DC and IF servos	[illegible]
RF servos	[illegible]

No interaction between servos was noticed while using the regulated power supplies as a voltage source due to the low output impedance of these components. With the +250 volt loads tied to a common dynamotor no change in computer operation occurred. It can be concluded, therefore, that interaction between the isolation amplifiers and the computing servos, due to an unregulated common +250 volt supply, will not effect system operation.

5. Future Studies

The operation of the DO servo following a constant-speed dynamic course as a preliminary to its operation from synchronizer data must be analyzed to complete the study program. This will involve a change in the servo preamplifier since the radar range data is a d-c error voltage while during previous tests the DO servo has been operated from a-c signals.

A second test will be run eliminating the tachometer unit test fixture and supplying the DOR and TFR signals from the DO and TF servos respectively, rather than from the auxiliary mockup. Stability difficulties, in the form of servo jitter, is anticipated in this closed loop test of the sensitivity computer. The minor vibrations of the servo motors, which has been hardly noticeable in our previous tests, will

now appear at the tachometers as primary data and may cause significant oscillation in both the TF and RF servos.

D. FAST SETTLING FOR USE WITH THE PRECESSION TORQUE MULTIPLIER

Stinger Quarterly Progress Report No. 3 (Section IV, F), which covered the fast settling problem, discussed two methods of introducing fast settling and developed an equation, equation 4-9, expressing lead angle as a function of elapsed time after lock-on. In developing this equation it was assumed that the aided laying constant, AK, was replaced by the fast settling constant, AKFS (=AK-KFS), under all conditions, as it is when the Stinger type precession mechanism is used. If the precession torque multiplier is used this assumption cannot be true for the reasons given in Stinger Quarterly Progress Report No. 3, namely:

1. The RF servo cannot produce the negative signals required under certain fast settling conditions.
2. The amount of lead angle rate (KFSI) the magnetic torquer can introduce is limited by size and inertia considerations.

During this quarter, both methods of introducing fast settling, as limited by practical considerations, were analyzed. The following symbols are used in this discussion.

OE - Stinger Sight Line Elevation

L - Lead angle between Stinger gunline and Stinger sight-line

RF - 1/TM, or the response factor from the TM computer

SRF - Constant value of RF, analogous to a circular target course condition where range and range rate are zero

RFFS - Fast settling correction to RFOR, in the following analysis, to SRF.

EO - Elevation of the line from Stinger to the target

E_1 - Error between EO and OE at the time of lock-on

E_e - Error between EO and OE at any time

AK - Aided laying constant

AKFS - Aided laying constant during fast settling

KFS - Fast settling constant (AKFS=AK-KFS)

KRL - Rate lag constant of the system

t - Elapsed time from lock-on

NOTE: Dotted quantities are time derivatives.

1. Fast settling introduction through the RF servo.

Referring to Stinger Quarterly Progress Report No. 3:

$$\dot{OE} = L \cdot SRF + AK \cdot \dot{L} - KFS \cdot \dot{L} = L \cdot SRF + AKFS \cdot \dot{L}$$

and $RF_N = RF - RFFS = RF - KFS \cdot \dot{L}/L$.

Therefore:

$$\dot{O}E/L = SRF + AK\frac{\mathring{L}}{L} - KFS\frac{\mathring{L}}{L} = SRF + AK\cdot\frac{\dot{L}}{L} - RFFS$$

OR

$$OE = L(SRF-RFFS) + AK\cdot\mathring{L}$$

If SRF-RFFS is within the limits of the RF servo the following equation, developed in Progress Report No. 3, holds:

$$L = C_1\epsilon^{\left(-\frac{AKFS}{2KRL} + \sqrt{\frac{AKFS^2}{4KRL^2} - \frac{SRF}{KRL}}\right)t} + C_2\epsilon^{\left(-\frac{AKFS}{2KRL} - \sqrt{\frac{AKFS^2}{4KRL^2} - \frac{SRF}{KRL}}\right)t} + L_c \qquad (4\text{-}9)$$

Where RFFS $\geqq$ SRF, SRF-RFFS becomes zero and the new equation results:

$$\dot{O}E = AK\cdot\mathring{L}$$

This equation when integrated becomes

$$L = C_1 + C_2\epsilon^{-\frac{AK}{KRL}t} + \frac{L_c SRF\ t}{KRL} \qquad (4\text{-}10)$$

Where SRF-RFFS exceeds the upper limit of the RF servo a third equation results:

$$p\ (OE) = L\cdot SRF\ max + AK\cdot\dot{L}$$

This equation when integrated becomes:

$$L = C_1 \epsilon^{\left[-\frac{AK}{KRL} + \sqrt{\frac{AK^2}{4KRL^2} - \frac{SRFmax}{KRL}}\right] t} + C_2 \epsilon^{\left[-\frac{AK}{2KRL} - \sqrt{\frac{AK^2}{4KRL^2} - \frac{SRFmax}{KRL}}\right] t} + L_c \qquad (4\text{-}10a)$$

The initial conditions at lock-on are:

$t = 0$ where t = time
$L = 0$ L = lead angle
$\dot{L} = E_1/KRL$

Under these conditions RF_N is usually less than zero and equation 4-10 must be used until RF_N comes within the range of the RF servo. At that time equation 4-9 is used, with integration constants determined by the lead and lead rate at the particular time in question. Where the upper limit of the RF servo is exceeded equation 4-10A is used. The curve must be plotted step by step, transferring to the applicable equation whenever the RF servo limits are passed in either direction, until settling is complete.

Fast settling introduction through the RF servo has been discarded as a practical solution, primarily because the nature of the fast settling signal ($-KFS \cdot \mathring{L}/L$) requires a complex electronic reciprocator. Further, it can be seen from figure 4-7, with reference to figures 4-8 and 4-9, that the $-KFS \cdot \mathring{L}/L$ correction circuit will go from plus to minus infinity (or vice-versa) where L goes through zero, causing the RF servo

to run immediately from one limit to the other. Figure 4-10 represents settling to a fixed target where $\dot{L}/L \rightarrow 0/0$ and becomes indeterminate. In practice additional circuitry would be required to ground the fast settling signal when L is in the ±5 mil range. In short, this solution requires excessive electronics and the settling curves are not smooth continuous functions of time.

2. Introduction through Magnetic Torquer:

In Stinger Quarterly Progress Report No. 3, the equation for fast settling,

$$\dot{OE} = L \cdot SRF + AK \cdot \dot{L} - KFS \cdot \dot{L} = L \cdot SRF + AKFS \cdot \dot{L},$$

was shown to be composed of the normal Stinger equation

$$\dot{OE} = L \cdot SRF + AK \cdot \dot{L}$$

and the fast settling component, $-KFS \cdot \dot{L}$, which must be superimposed on the sight line rate. It is sufficient that a magnetic torquer cause the gyro to precess this additional amount, since the sight line is mechanically connected to the gyro line.

The gyro torque equation is

$$T = AM \cdot PR$$

where

$$AM = 32 \text{ in. oz sec} \left[1 \frac{\text{mil}}{\text{sec}}\right] \left[\frac{2\pi \text{ rad}}{6400 \text{ mil}}\right] \cong .03 \text{ in. oz.}$$

Consider a torquer or microsyn, acceptable as to size and inertia, with a maximum output of 1.5 in.oz. The maximum gyro rate produced by this torquer would be

$$\frac{1.5 \text{ in.oz.}}{.03 \text{ in.oz.}/\frac{\text{mil}}{\text{sec}}} \cong 50 \text{ mils/sec}$$

This value would then be equivalent to a maximum lead angle rate of

$$\mathring{L} = -\frac{DPR}{KFS} = \frac{-50}{.27} = 180 \text{ mils/sec}$$

Therefore, the normal fast settling equation would apply only where $-180 < \dot{L} < +180$

The normal fast settling equation, as developed in Stinger Quarterly Progress Report No. 3, is equation 4-9. The normal Stinger equation without fast settling is

$$L = C_1 \epsilon^{\left[-\frac{AK}{2KRL} + \sqrt{\frac{AK^2}{4KRL^2} - \frac{SRF}{KRL}}\right] t} + C_2 \epsilon^{\left[-\frac{AK}{2KRL} - \sqrt{\frac{AK^2}{4KRL^2} - \frac{SRF}{KRL}}\right]} + L_c \qquad (4\text{-}11)$$

In the case where $\mathring{L}$ exceeds the torquer limits, the original conditions must be changed, since the torquer now puts in a constant, $-KFS \cdot \mathring{L}$ max, instead of the variable $- KFS \cdot \dot{L}$, as shown below. Normally

$$\mathring{OE} = L \cdot SRF + AK \cdot \mathring{L} - KFS \cdot \mathring{L} = L \cdot SRF + AKFS \cdot \mathring{L}$$

but, where the torquer limit is exceeded

$$\dot{OE} = L \cdot SRF + AK \cdot \dot{L} - KFS \cdot \dot{L}\ max$$

This equation when integrated becomes

$$L = C_1 \epsilon^{\left[-\frac{AK}{2KRL} + \sqrt{\frac{AK^2}{4KRL^2} - \frac{SRF}{KRL}}\right] t} + C_2 \epsilon^{\left[-\frac{AK}{2KRL} - \sqrt{\frac{AK^2}{4KRL^2} - \frac{SRF}{KRL}}\right] t} + L_c + \frac{KFS}{SRF} \dot{L}\ max \tag{4-12}$$

which is the same as the normal Stinger tracking equation, except for the KFS/SRF$\cdot\dot{L}$ max factor, which changes the lead angle to which the system tends to settle. Therefore, it is seen that no fast settling takes place during the time when $\dot{L}$ exceeds the torquer limits.

To discover how settling times are affected by a limitation in $\dot{L}$ max, it is necessary to use equations 4-9 and 4-12 in the same way equations 4-9 and 4-10 were used, in conjunction with the RF servo. Where $\dot{L}$ exceeds $\dot{L}$ max, equation 4-12 must be used, the curve being transferred to equation 1 when $\dot{L}$ max > $\dot{L}$ > - $\dot{L}$ max.

Figures 4-11 through 4-22 show settling curves for several critical combinations of lead angle and STM. All of these settling curves are smooth and continuous. In figures 4-11 and 4-12 the lead angle curve representing a torquer limited to an $\dot{L}$ max of ± 250 mils/sec settles faster than the curve of the unlimited torquer since the unlimited torquer

curve, while its settling slope is steeper, initially rises to 200 mils and must settle from that point. Figure 4-12 graphically emphasizes the fact that the derivatives of equations 4-12 and 4-13 are equal. In figures 4-13 and 4-14 the data is the same as in figures 4-11 and 4-12, except for the sign of L_c. In the case where E_1 and L_c are of the same sign, the overshoot condition aids the unlimited torquer curve and it settles first.

Figures 4-15, 4-16, 4-17 and 4-18 show curves for $L_c = \pm 451$ mils. Here the same conclusions may be drawn as were for figures 4-11 through 4-14 except that, in figures 4-17 and 4-18, the slope of the unlimited torquer curve is steep enough to allow it to settle before the ± 200 mil/sec curve, in spite of the initial overshoot. Figures 4-19 and 4-20 represent a less critical case in which the curve representing a torquer limited to ± 100 mils/sec settles faster than the unlimited curves. Figures 4-21 and 4-22 is a less critical case, similar to figures 4-13 and 4-14, in that the curve limited to ± 100 mils/sec settles faster than the unlimited curve. It can be seen that in most normally encountered courses the overshoot inherent in the unlimited equation actually causes the settling times to be somewhat longer than those of the limited curves, in spite of the rapid exponential decay which is constantly present. Only under the severest

conditions (high speed and short crossover range) does the unlimited curve settle first. The gain in settling time, however, is significant for the limited curves shown. Study of these and other curves not included in this report establishes the optimum value for $\dot{L}$ max to be 200-250 mils/sec. This value requires a torquer whose output is approximately 2 in.oz.

A microsyn torquer developed by M.I.T. has been obtained and tested satisfactorily up to an output of 4 in.oz. (Microsyn Torque Generator Assy, SPG 683422, with 500 turn coils replacing those designated). This torquer operates on an amplified ac signal from the appropriate LG tachometer and will require a power amplifier equivalent to that used with a Kearfott motor. Design studies, now complete, have successfully located these microsyns in the rotating element.

E. COMPUTER TRACKING SECTION

The hand control assembly has been modified to enable the azimuth gearing to be absorbed into the main body of the tracking section (fig. 4-23). This change was made to provide easier access into the cockpit from the tank under the computer. The manual range wheels will be replaced by a knob on the hand control assembly. The range wheels were used on the T26 computer in conjunction with stadiametric ranging which will not be used in the 37-mm computer. The range knob on the T37

computer will be used to track manually in range through clutter while in auto-track.

Electrical connection to the computer from the turret will be by two cables and plug boxes under the tracking section which provides protection from impacts and the weather. The problem of tight water seals to the computer and turret is thereby eliminated.

Redesign of the shock mounts has resulted in a simpler, more rugged unit. The tracking section of computer T26 must be tilted on the shock mounts to enable the installation and removal of the radar indicator chassis. Such an arrangement is not needed for the 37-mm tracking section since the single indicator can easily be installed and removed. (fig 4-24)

Changes in the periscope and radar optics are being studied by Kollsman Instrument Corporation. The new periscope design will reduce astigmatism, thereby facilitating optical acquisition of distant targets. There will be two eyepieces, one for the periscope optics and one for the single 5-inch radar indicator tube. An improved eyeshield design and increased eye relief will give an improved view and lessen operator fatigue.

F. MECHANICAL CAGE

A device to mechanically cage the gyro during acquisition, gun drive, target selector, etc, has been developed and designed as a part of the rotating element. The device consists of a solenoid-actuated pin with a tapered end, and a socket unit consisting of three miniature ball bearings mounted 120° apart with rims toward the center. The taper is designed to cover the pickoff motion of the gyro in any direction (± six degrees). The solenoid and pin are located on the outer gimbal, which rotates in LLG and the ball bearing socket is located on the gyro housing. Actuating the solenoid drives the pin into the socket, thereby centering the gyro in elevation and azimuth. The solenoid is located on the outer gimbal so that the centering may take place before the lead angle motors have driven to zero.

Locating the solenoid on the rotating element frame would require that LLG be driven to zero before centering could take place. Not only would such an arrangement require more time for the caging operation, but serious damage to the gimballing could result should LLG, for some abnormal reason, start driving before the pin had been removed from the socket. With the present arrangement, it is estimated that the time required for the centering operation only will be approximately

one-half second. The lead angle servos will require approximately 3/4 seconds to center from either extreme. It may be assumed that since the solenoid must operate against additional torques while the LLG servo is running to zero, some of the centering operation will remain after the lead angles are zero. Therefore, the caging time will vary from slightly more than zero to a maximum of 1 to 1-1/8 secs under the worst conditions of full pickoff error displacement and maximum lead angle.

G. POTENTIOMETER STUDIES

A life test on ten turn potentiometers was mentioned in Stinger Quarterly Progress Report No. 2. This test was performed primarily to compare the durability of the Giannini slide-wire potentiometer with conventional finite resolution units. The slide-wire potentiometer would probably be a valuable improvement to the precession servo and RF servo if satisfactory life characteristics are exhibited. This life test has now been completed and the results are being evaluated.

It is too early to report many conclusions regarding the test results, except that the slide-wire potentiometers have remained operative after undergoing 345,600 cycles of oscillation. This probably means that the tests will be carried further with an increased number of samples. Although final linearity and backlash measurements are still in progress no

marked defects are expected to develop due to wear, except in the case of the SAN33B roller wiper helipot. This component has exhibited noise and backlash, caused no doubt by wear of the roller contact. One sample of the two slide wire potentiometers has developed a noisy spot which is not expected to be characteristic of the Giannini design. There is also some doubt as to whether it existed before the resistor was subjected to wear. Although it is too early to be sure, there is some evidence that the Electromath design needs improvement to avoid binding. This judgement is based only on the results of one sample.

The method used to conduct this life test was unique as far as can be determined (fig. 4-25). Instead of revolving the potentiometers at constant speed throughout their ten turns of travel, they were oscillated sinusoidally through a double amplitude of only 1/8 of one turn, or 45 degrees. This is considered to be much more typical of servo applications. Two frequencies of oscillation were provided, 48 cpm and 240 cpm, each for 40 hours. These frequencies produced speeds of 20 and 100 rpm respectively, at the center of each cycle. A rest period of five minutes out of every ten minutes of testing was provided. The test included linearity measurements of 0.01%, running noise tests, and backlash measurements to 0.01%. (Figure 4-25) shows the dial arrangement that was used to assure mechanical reliability of the linearity observations.

SECTION V

SERVOS

A. GENERAL

During the past quarter work was nearly completed on the azimuth power control electronic and hydraulic breadboards. Test data was taken using a completely electronic breadboard, to show the feasibility of the complete servo system and to verify certain assumptions made in the theoretical design. The azimuth power control breadboard was operated with a magnetic d-c amplifier. The test data taken, although not conclusive, indicates that the use of the magnetic amplifier is feasible.

Some investigation has been made, into the use of transistors and subminiature tubes in the azimuth turret servo and in the small deflection servos in an effort to miniaturize and improve reliability.

The status of the servo studies to date can be summarized as follows:

1. System Loop Analysis - The stability study on the complete system loop has been completed and has established the feasibility of the system.

2. Deflection Servos - Breadboard tests are complete and feasibility has been established. (See Quarterly Progress Report No. 3.)

3. Scanner Servos - No breadboards are required. Feasibility has been established on the basis of Stinger operation.

4. Small Computer Servos - No breadboards are required. Feasibility has been established on the basis of Stinger operation.

5. Azimuth Power Control - Breadboard is complete and has been tested. Feasibility has been established using electronic and magnetic amplifiers. (See paragraph D below.)

6. Elevation Power Control - No breadboard is required. Theoretical study is not complete but feasibility appears assured. Complete discussion will be presented in final report.

B. ELECTRONIC CONTROL CIRCUITS

In the theoretical design of the turret servo the electronic system was separated into three components. These components were: the error channel, the feedback channel, and the d-c amplifier. The requirements of these components were

indicated in Quarterly Progress Report No. 3 (Sect. V, Par. C 2f) and are repeated below.

1. Error channel KeGe (+) = $\frac{300\ (1 + jw/1.5)}{1 + jw/.15}$

2. Voltage gain = 10 from output of the "E" pickoff circuit

3. Feedback channel K_hH (+) = $\frac{6.5\ jw}{1 + jw/15}$

4. Voltage gain = 0.111 from output of yoke position synchro

5. D-C Amplifier KaGa (+) = 0.143 amp/volt

The d-c amplifier KaGa value is frequency insensitive.

The electronic system built for breadboard tests is shown in figure 5-1. This figure indicates the number of vacuum tubes that would be required. The servo system was tested using these electronic components. The lag network in the error channel and the lead network in the feedback channel were adjusted to give the best compromise between synchronization time and acceleration errors. The acceleration error obtained experimentally after transient had settled (figs. 5-2a, 5-2b and 5-2c) was 12 mils per 100°/sec. The error predicted in the theoretical design was 10 mils per 100°/sec. As a

further test of servo design the system was set up to follow the firing azimuth cam on the Stinger dynamic tester. This cam represents the future position of a target flying at a velocity of 400 yds/sec with a slant range of 670 yds and a horizontal range of 300 yds. The maximum error recorded was 11.5 mils (fig. 5-5). With the "E" pickoff slug displaced 100 mils the servo synchronized within 1.88 sec. (fig. 5-6). It should be realized that these data were taken under ideal laboratory conditions and results may be somewhat less favorable in practice.

The tests conducted above were performed both with an electronic demodulator and a transistor demodulator in the feedback circuit. The schematic of the transistor demodulator is shown in figure 5-7. Some consideration has been given to the packaging of this demodulator in a plug-in chassis (fig. 5-8).

After completing the test during which electronic components were used in the servo system, the system was altered to accomodate the magnetic d-c amplifier (fig. 5-9). Of special interest is the elimination of the demodulator output filters. Since these filters are no longer required for the magnetic amplifier the isolation cathode follower between the filter and the lag or lead network is no longer required.

This system was tested for an acceleration of $110°/sec^2$ and the error recorded was 12 mils (fig. 5-10). This compares favorably with the error obtained with the fully electronic system. Work will continue on the magnetic amplifier system during the next quarter.

In comparing the electronic and magnetic amplifier systems, servo performance being equal, consideration should be given to size, number of tubes, power requirements, heat generated, and reliability. The magnetic amplifier system uses eight tubes as compared with 11 for the all electronic system.* The expected improvement in reliability is based on the difference in the number of vacuum tubes and associated components, wires, and connections. Overall system requirements may change the tube compliment slightly.

C. MINIATURIZATION

An important consideration in Stinger was the packaging problem. With this in mind some thought has been given to the use of sub-miniature tubes and to the packaging problem associated with them. A d-c power amplifier for the azimuth turret servo has been built (fig. 5-11). In addition two other sub-miniature tube chassis have been built for the

- - - - - - -

*If transistor demodulators were used the number of tubes used with the all electronic system would be reduced to four.

deflection servos. One contains a single d-c power amplifier (fig. 5-13). The use of sub-miniature tubes would greatly reduce the size of the electronic components and thus reduce the packaging problem for the 37-mm Stinger. Some additional work will be done along these lines during the next quarter.

D. AZIMUTH POWER CONTROL SOLENOID

The solenoid consists of a spring loaded armature (fig. 5-14) mounted in a magnetic field. The mmf is supplied by current which is proportional to the error signal. A quiescent current also flows through the coils. The force exerted on the solenoid armature is given by the expression:

$$f = K \; \Delta I \; I_q \; N^2$$

where f = force

K = constant of proportionality

ΔI = differential current

I_q = quiescent current

N = number of turns in one coil

The solenoid armature on which the force acts is centered by a torsion spring with a constant of 150 pounds per inch.

The pilot valve was designed to yield a volumetric rate of flow of 1.15 gallons per minute per .0075 inches displacement. This yields an acceleration of 400°/sec^2 when the

pilot valve strokes the power piston which has an area of 2 square inches a stroke of 2 inches. The diameter of the pilot valve is 5/16 inch.

It is desired that 20 ma differential current in coils of 10,000 turns (for the electronic d-c amplifier) produce a turret acceleration of $400°/sec^2$. A proper quiescent current must be found, using equation 5-1, to give this result. Further, due to Bernoulli effects, this stroke rate (which determines the turret acceleration) must be measured and not inferred from flow rate and displacement data at the pilot valve. The additional required quiescent flux was obtained by raising the quiescent current in the dither coils so as not to disturb the control coil operating point and the associated amplifiers.

When the magnetic amplifier is used 4500 turns are used in the solenoid coils. This necessitates a corresponding change in the required differential ampere turns, and the associated quiescent current.

E. ASYNCHRONOUS GUN FIRING

In Quarterly Progress Report No. 3 it was pointed out that when both 37-mm guns are firing in synchronism there is no net torque transmitted to the azimuth power controls. However, when the guns are firing 180 degrees out of phase, the torques

due to the first harmonics will double and the average torque will cancel. This situation causes a total peak torque of 1530 in. lb and a total peak pressure of 6260 psi to be produced. (Model 915 Vickers aircraft-type hydraulic pump and motor is rated at 1088 in. lb at 4500 psi.) It is obvious, therefore, that there is some maximum angle at which the guns may fire out of phase and still not exceed the peak rating of the power controls. The first assumes the turret stationary and the other assumes that the turret will be moving at a maximum acceleration of 120°/sec^2. (These represent the two extreme conditions.)

The maximum angle assuming the turret fixed was found to be 85° 16' (25 milliseconds on the time scale). With the turret moving at 120°/sec^2 the angle is reduced to 68.6° or 19 milliseconds. These figures are derived explicitly in the following paragraph for the 37-mm Armour guns. This analysis is based on the revised recoil force vs time diagram furnished by the Armour Foundation in January, 1953.

The azimuth hydraulics, which absorb the gun reaction forces, are a Model 3915 Vickers aircraft-type hydraulic pump and motor. These units operate at a maximum pressure of 4500 psi. Only the fundamental frequency (computed by a Fourier Analysis of the force time curve) was used in calculating to

torque and transfer functions since all the other harmonics were attenuated to such a degree as to be negligible.

Let us first consider the equation

$$G_2'' = \frac{\theta_o(t)}{T_L} \qquad y(t) = 0^* \qquad (5\text{-}2)$$

which is the transfer function of transmission used for pressure studies. In this expression y(t), the yoke position, is zero

$\theta_o(t)$ = Turret servo output times 232 and

$T_L(t)$ = Gun reaction torque.

From equation 5-1 we may write

$$\theta_o(t) = G_2'' \; T_L(t).$$

Now consider the guns firing out of synchronism by an angle ψ. Then

the torque due to No. 1 gun = T cos wt and

the torque due to No. 2 gun = T cos (wt - ψ)

where T is the input load torque due to the fundamental frequency (fig. 5-1).

- - - - - - -

*Developed in Section V C, Quarterly Progress Report No. 3.

Total Torque = $T \cos wt - T \cos (wt - \psi)$

$$T_T = T [\cos wt - \cos (wt - \psi)]$$

$$T_T = T [\cos \alpha - \cos B] \tag{5-3}$$

$$T_T = T [-2 \sin 1/2 (\alpha + B) \sin 1/2 (\alpha - B)]$$

$$T_T = T [-2 \sin 1/2 (wt + wt - \psi) \sin 1/2 (wt - wt + \psi)]$$

$$T_T = T [-2 \sin (wt - \frac{\psi}{2}) \sin \frac{\psi}{2}]$$

where $-2 T \sin \frac{\psi}{2}$ = amplitude and

$\sin (wt - \frac{\psi}{2})$ = frequency term. (5-4)*

Then:

$$\Theta_o(t) = -2 T \sin \frac{\psi}{2} G_2''$$

and

$$psi = K \Theta_o(t) = K(-2 T \sin \frac{\psi}{2} G_2'')$$

where $K = \dfrac{1.519 \ (in^3/rev) \ 238{,}000 \ (lbs/in^2)}{2\pi \ (\frac{rad}{rev}) \ 11 \ in^3}$

- - - - - - -

*Refer to figure 10 FOR GRAPHICAL PLOT OF EQUATIONS 5-2 and 5-3 AFTER CONVERSION TO PSL BASES.

$K = 5230$ lbs/in^2/rad.

$T = 34$ ft lbs for fundamental frequency

$G_2'' = .0187$ (rad/ft lb) for fundamental frequency (from pressure studies on Vickers aircraft-type hydraulic pump and motor Model 915.)

Therefore:

$$4500 = 5230 \left[-2 (34) \sin \frac{\psi}{2}\right] .0187.$$

Solving for $\sin \frac{\psi}{2}$:

$$\sin \frac{\psi}{2} = - \frac{4500}{5230 \left[68(.0187)\right]}$$

$$= -.677$$

$$\frac{\psi}{2} = -42°38'$$

$$\psi = -85°16'.$$

This then is the maximum angle that the two guns may be out of synchronism, using a type 3915 hydraulic system operating at 4500 psi.

This angle is related to the time scale as follows: $\frac{85}{360} \times .1$ sec (one cycle) = .025 sec or 25 milliseconds (for rate of fire of 10 rounds per second)

For a plot of gun reaction force versus time with the guns firing under the above conditions see figures 5-15 and 5-16.

The 4500 psi value used in the above calculations assumes that the entireload on the hydraulics is due to the gun reaction forces. However, when it becomes necessary to track and fire at the same time, as will be the case during system operation, this figure will be reduced as shown below.

The maximum tracking acceleration will be 120°/sec^2 (2.09 rad/sec^2).

Then:

$$T = J\alpha = 1750\,(2.09)\,(12) = 44{,}000 \text{ in.lb}$$

$$T = \frac{44{,}000}{232} = 190 \text{ lb in. at shaft of hydraulic motor.}$$

The pressure at 120°/sec.^{2} acceleration is then

$$\frac{1088\#\text{in.}}{4500 \text{ P.S.I.}} = \frac{190}{X}$$

$$X = 785 \text{ psi}$$

This figure when subtracted from 4500 psi leaves a remainder of 3715 psi.

Then:

$$\sin\frac{\psi}{2} = \frac{3715}{5230\,(68\,[.0187\,]\,)}$$

$$\sin\frac{\psi}{2} = .562$$

$$\frac{\psi}{2} = 34.3$$

$$\psi = 68.6°.$$

This would be the maximum angle that the guns could be out of synchronism if the turret is tracking at an acceleration of 120°/sec^2 while the guns are firing. 68.6° of the gun cycle corresponds to .019 sec on the time scale.

SECTION VI

TURRET

A. INTRODUCTION

During the past quarter engineering and design work on the turret was concerned with: the development of a method for providing gun elevation data inside the torque tube, determination of the effective rigidity of the gun mount using the Dixon Gun T37E2, the computation of the moment of inertia for this same gun, the development of a gun elevation gear box equipped with spur gears, the turret azimuth drive mechanisms, the feasibility of a ball type torque limiting clutch for the azimuth hand crank drive, study of an hydraulic ammunition booster, and the shadowing of the radar beam by the Armour gun.

B. FE POSITION MECHANISM

Conversations with gun engineers at Armour Research Foundation concerning a gun arrangement which would be suitable for use with Stinger, led to the suggestion that some of the gun components might be mounted inside the Stinger torque tube, which space would otherwise be unused. Such an arrangement would provide the reduced recoil force associated with the soft mounted gun and would also permit the two guns to be synchronized to a degree necessary for good turret azimuth power control

performance. Soft mounted guns can not ordinarily be synchronized. The arrangement proposed provides the additional advantage of reducing the moment of inertia of the gun and the shadowing of the radar beam. Gun engineers of the Armour Foundation stated that such gun component relocation might be feasible if some means of indicating FE were available inside the turret torque tube. A layout has been prepared (fig. 6-1) showing one means of providing this indication.

C. MOUNTING OF DIXON GUN

An aluminum quarter scale model of the cast steel cradle proposed for mounting the Dixon gun was made (fig. 6-2) and tested under static loads which simulated direct recoil loads as well as transverse loads. The object of this program was to determine the effective rigidity of the mounting. By combining the expected rigidity of the cradle (as determined from the model tests) with the computed rigidities of the torque tube and the gun (T37E2), an estimate of the lowest natural frequency of the mount could be made. These frequencies are listed in table 6-1. Since conversations with representatives of the Dixon Company and the Armour Foundation had indicated there was some interest in the use of a muzzle brake, additional computations were made showing the effect of a 10-pound muzzle brake on the natural frequency of the mounting. The static deflection curves used for this analysis are shown in figure 6-3.

TABLE 6-1

ESTIMATE OF LOWEST NATURAL
FREQUENCY OF DIXON GUN MOUNTING

CONDITION	LOWEST NATURAL FREQUENCY
*Gun Only	23.4
*Gun with Muzzle Brake	19.2
Gun and Cradle - Elevation Sense	21.3
Gun, Cradle, and Torque Tube - Elevation Sense	19.1
Gun, Cradle, and Torque Tube - Azimuth Sense	19.8
Gun, Cradle, Torque Tube, and Muzzle Brake - Elevation Sense	15.6

D. DIXON GUN INERTIA STUDY

The weight, cg, and moment of inertia of the Dixon Gun T37E2 (17 in. round) was estimated. The weight of one gun and the cast steel cradle required to mount it was estimated to be 895 pounds. The cg was estimated to be 21.4 inches forward of the FE axis and the moment of inertia to be 248 slug feet^2. These estimates were used in the natural frequency computations described above.

- - - - - - -

*Receiver assumed fixed to rigid base.

E. GUN ELEVATION DRIVE

Further consideration of the gun elevation drive has indicated that the worm type drive previously considered would probably not be feasible due to the fact that decelerating loads reflected to the power controls would be appreciably different from accelerating loads due to the locking characteristics of the worm. A spur type drive was laid out, therefore, and is shown in figure 6-4. Figure 6-5 shows the upper structure arrangement which includes this gear box.

F. TURRET AZIMUTH DRIVE

In the lower structure of the turret were arranged the gear box, electric motor, hydraulic motor, and pump necessary for control of the turret (figs. 6-6 and 6-7). These units are larger than the units previously proposed. They will provide the required turret azimuth accelerations if the guns are synchronized within a reasonable degree. If only one gun fires, or if the guns fail to synchronize, the pressure in the hydraulic lines will cause the relief valves to blow. During hand crank operation, however, no such safety feature is available. To avoid excessive gear loads under these conditions a torque limiting clutch has been proposed. Figure 6-8 shows the location of the clutch in the gear train.

A ball type clutch was considered the most dependable type for use as a torque limiting device since its torque would be relatively unaffected by the extremes of temperature and humidity expected or by the presence of lubricating oil (fig. 6-9). The value of torque which actuates the clutch is such that a load of 3000 pounds must be shared among the clutch balls. With this type of clutch, in an application where little backlash can be tolerated, the edges of the clutch seats would be made sharp and the balls would seat themselves at the first few applications of break-away torque. Subsequent applications of torque would not increase the degree of seating. A mockup of the clutch face, incorporating a single ball, was made to determine permissible ball loads and the probable degree of load sharing among the balls. A cross section of the mockup is shown in figure 6-10.

Tests were made using ball bearing grade chrome steel balls against clutch faces of various materials and the results are summarized in table 6-2. It should be noted that the peak ball forces given are based on a pitch error between adjacent balls of .001 inch. The chamfer dimension listed is the maximum width of the chamfer produced on the originally sharp edged ball seat by a ball load of 3000 pounds. The tests indicate that a ball clutch with suitable hardened seats would be feasible.

TABLE 6-2

RESULTS OF BALL SEAT TESTS

Ball Seat Material	Max Expected Ball Load-lbs	Chamfer for 3000 lb Ball Load-In.
Cold Drawn Steel (SAE 1020)	620	.062
Stainless Steel (AISI 416)	585	.055
Chrome Moly Steel (SAE 4140)	650	.045
*Hardened Tool Steel	800	.010

- - - - - - -

*0.65 - 0.8% C, 0.25 - 0.45% mn, 0.90 - 1.15% cr, 1.6 - 1.8% Ni, hardened to R_c 58 - 62

G. AMMUNITION BOOSTER

The ammunition boosters previously studied were:

1. Direct d-c motor drive.
2. Direct a-c motor drive.
3. Motor driven flywheel coupled to sprocket by hydraulic pump motor combination (constant volume system).

During the past quarter a booster was studied which was similar in arrangement to 3 above except that it has what is basically a constant pressure hydraulic system. In this system an electric motor drives a flywheel which is coupled to an hydraulic pump. A combination three-way control and relief valve is

interposed between the hydraulic pump and a hydraulic motor providing control of booster operation. The hydraulic motor is geared to the booster sprocket (fig. 6-11). Such a booster, equipped with a 3/4 horsepower 10,000 rpm electric motor and with its relief valve set at 1100 psi, could accelerate the ammunition belt to 916 rounds per minute within 0.15 seconds. The same booster equipped with a 7200 rpm, 1/2 horsepower motor and with its relief valve set at 850 psi, could accelerate the belt to 452 rounds per minute in 0.2 seconds. The time required to accelerate the flywheel to operating speed would be about 12 seconds in the first case and 8 seconds in the second.

H. SHADOWING OF RADAR BEAM BY ARMOUR GUN

Quarterly Progress Report No. 3 indicated the extent of the radar beam shadowing problem. During this quarter further analysis has been made using values of FE, SE, and LL computer for six typical target courses. The extent of beam shadowing by the Armour Gun as a function of course time for the courses studies is shown in figure 6-12.

MODE ANALYSIS FOR T-37

	SPIRAL SEARCH SP		SPIRAL ACQ. SPA		SECTOR SEARCH SS		SECTOR ACQ. SA		TARGET SEL. TS		GUN DRIVE GD		AUTO TRACK AT		MANUAL TRACK (RADAR RANGING) MT				PAR. COR. 414C PC	
	VERT.	LAT.	VERT.	LAT.	VERT.	LAT.	VERT.	LAT.	VERT.	LAT.	VERT.	LAT.	VERT.	LAT.	VERT	LAT.			VERT.	LAT.
GYRO	CLAMPED	CLAMPED	CLAMPED	CLAMPED	CLAMPED	CLAMPED	CLAMPED	CLAMPED	CLAMPED	CLAMPED	CLAMPED	CLAMPED	PREC.	PREC.	PREC.	PREC.			CLAMPED	CLAMPED
DEFLECTION SERVO	ZEROED	ZEROED	ZEROED	ZEROED	ZEROED	ZEROED	ZEROED	ZEROED	ZEROED	ZEROED	ZEROED	ZEROED	FOL. RAD.	FOL. RAD.	FOL. HB	FOL. HB			ZEROED	ZEROED
SCANNER SERVO	FOL. SE SYNCHROS	FOL. LL SYNCHROS	FOL. SE SYNCHROS	FOL. LL SYNCHROS	FOL. SE SYNCHROS AND AUTO-SEARCH SIG.	FOL. SWEEP SIG.	FOL. SE SYNCHROS	FOL. LL SYNCHROS	FOL. SE SYNCHROS	FOL. LL SYNCHROS	FOL. SE SYNCHROS	FOL. LL SYNCHROS	FOL. SE SYNCHROS	FOL. LL SYNCHROS	FOL. SE SYNCHROS	FOL. LL SYNCHROS			FOL. SE SYNCHROS AND AUTO-SEARCH SIG.	FOL. SWEEP SIG.
CROSSFEEDS	OUT	OUT	OUT	OUT	OUT	OUT	OUT	OUT	OUT	OUT	OUT	OUT	IN	IN	OUT	OUT			OUT	OUT
FAST SETTLING	OUT	OUT	OUT	OUT	OUT	OUT	OUT	OUT	OUT	OUT	OUT	OUT	IN	IN	IN	IN			OUT	OUT
GYE SERVO	FOL. AUTOMATIC ELEVATION SEARCH SIGNAL, H.B., AND TILT CORRECTION		FOL. H.B.		FOL. H.B.		FOL. H.B.		FOL. T.S. SYNCHRO		FOL. GUN ELEV.		FOL. "E" PICKOFF		FOL. "E" PICKOFF				FOL. 414C SYNCHRO	
TURRET	"B" END BY-PASSED AND YOKE CENTERED		FOL. H.B.		FOL. H.B.		FOL. H.B.		FOL. T.S. SYNCHRO		FOL. H.B.		FOL. "E" PICKOFF		FOL. "E" PICKOFF				FOL. 414C SYNCHRO	
GUNS (ELEVATION)	BLOCKED		BLOCKED		FOL. GYE		FOL. GYE		FOL. GYE		FOL. H.B.		FOL. PE AND VB SIG.		FOL. PE AND VB SIG.				FOL. GYE	

CENTERING: WHEN HANDLE BAR SAFETY SWITCHES ARE NOT DEPRESSED THE POWER CONTROL YOKE CENTERS AND THE "B" END IS BYPASSED, THE GYRO IS CLAMPED AND THE DEFLECTION SERVO IS ZEROED.

FIGURE 2-1
MODE ANALYSIS FOR 37-MM FIRE CONTROL SYSTEM

CONFIDENTIAL
SECURITY INFORMATION

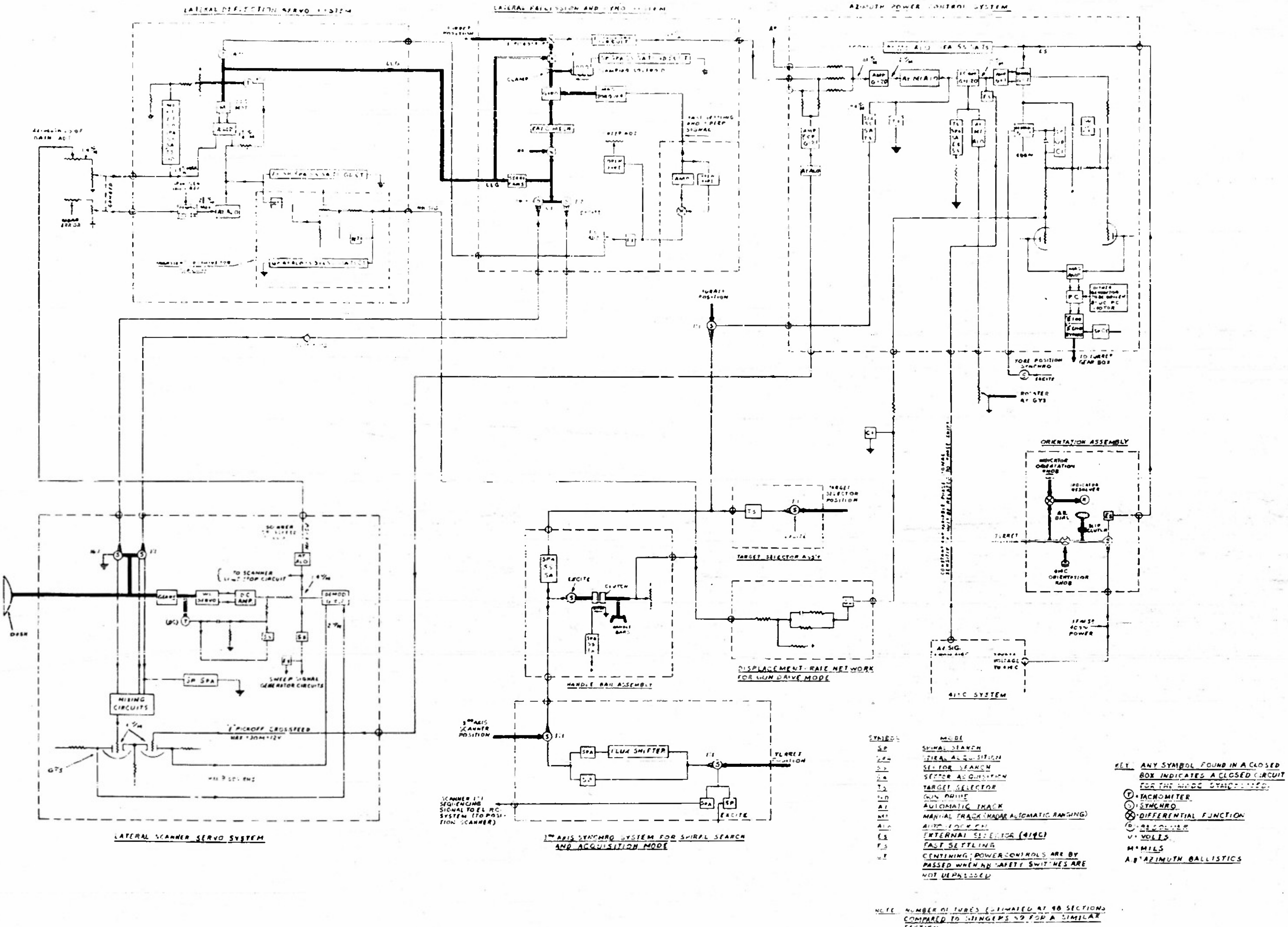

FIGURE 2-2

MODE DIAGRAM FOR AZIMUTH AXIS OF 37-MM FIRE CONTROL SYSTEM

CONFIDENTIAL

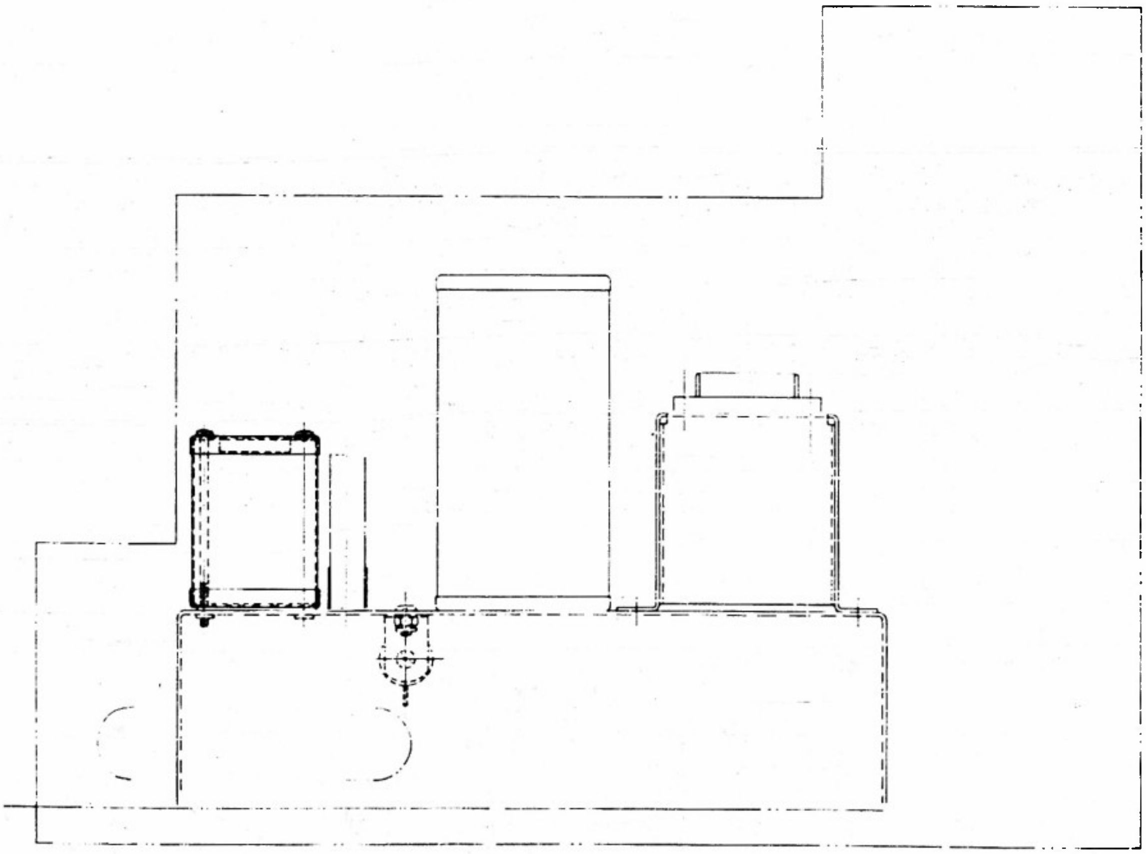

1

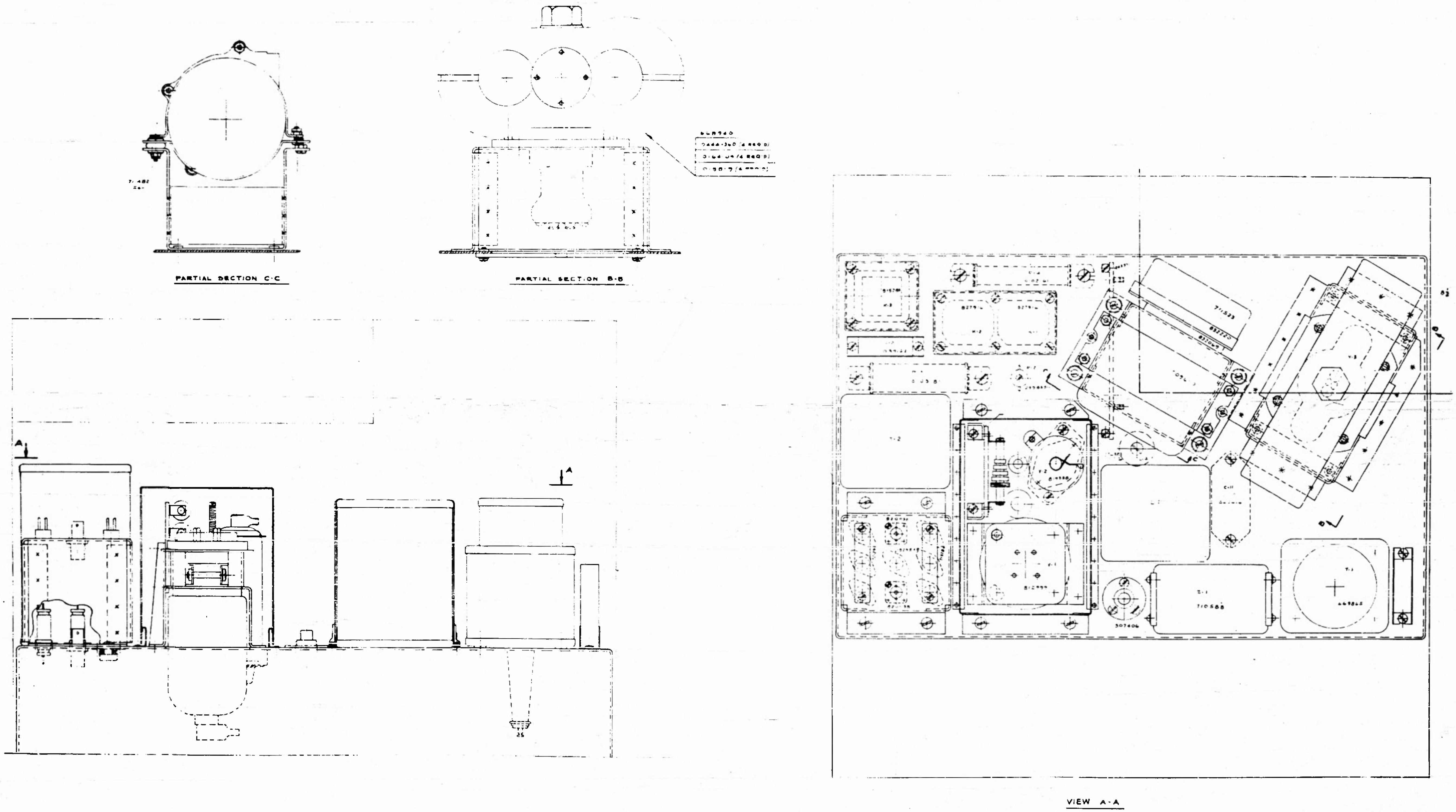

FIGURE 3-1
TRANSMITTER-RECEIVER ASSEMBLY DRAWING

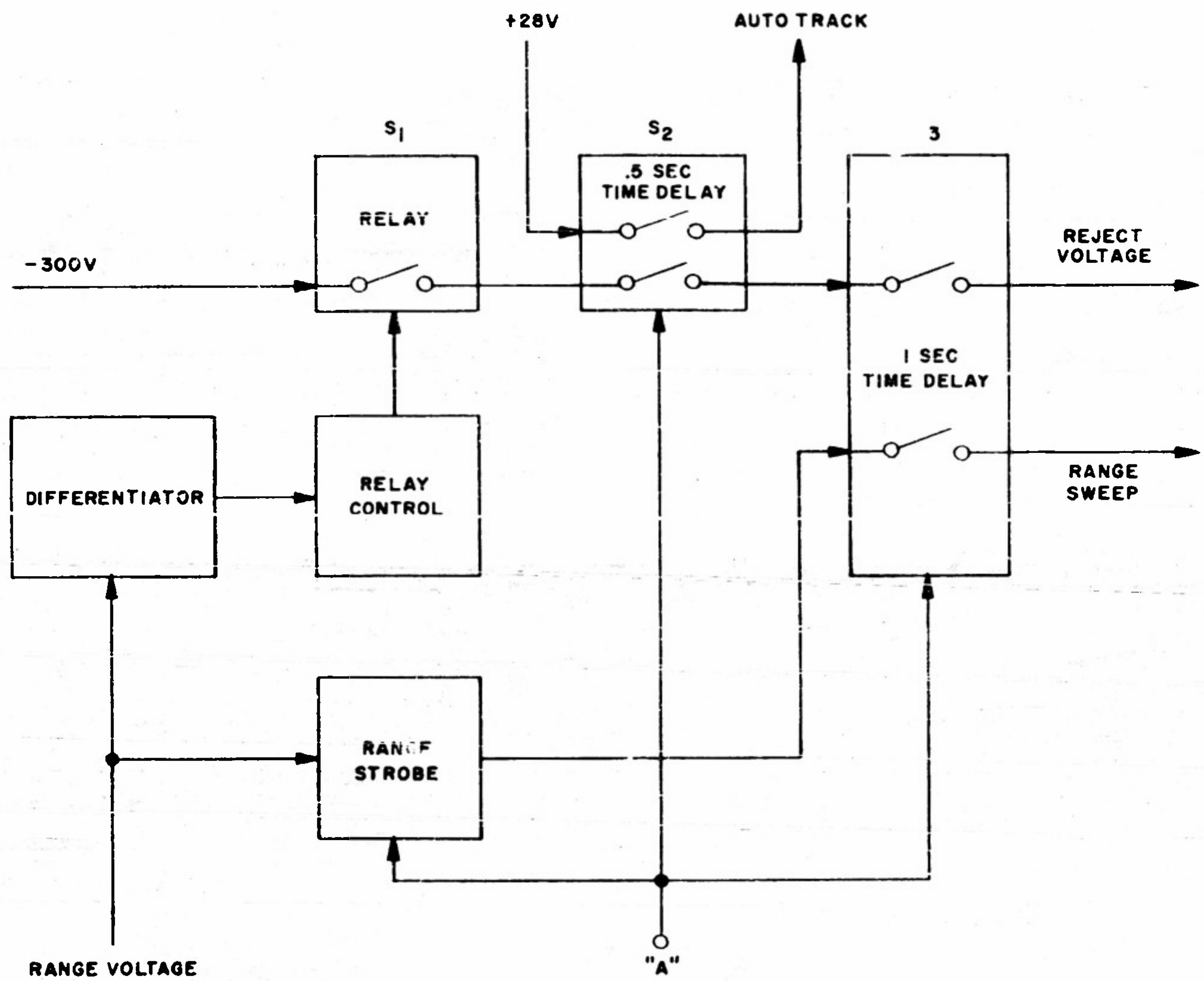

FIGURE 3-2
FIXED TARGET
REJECTION SYSTEM
BLOCK DIAGRAM

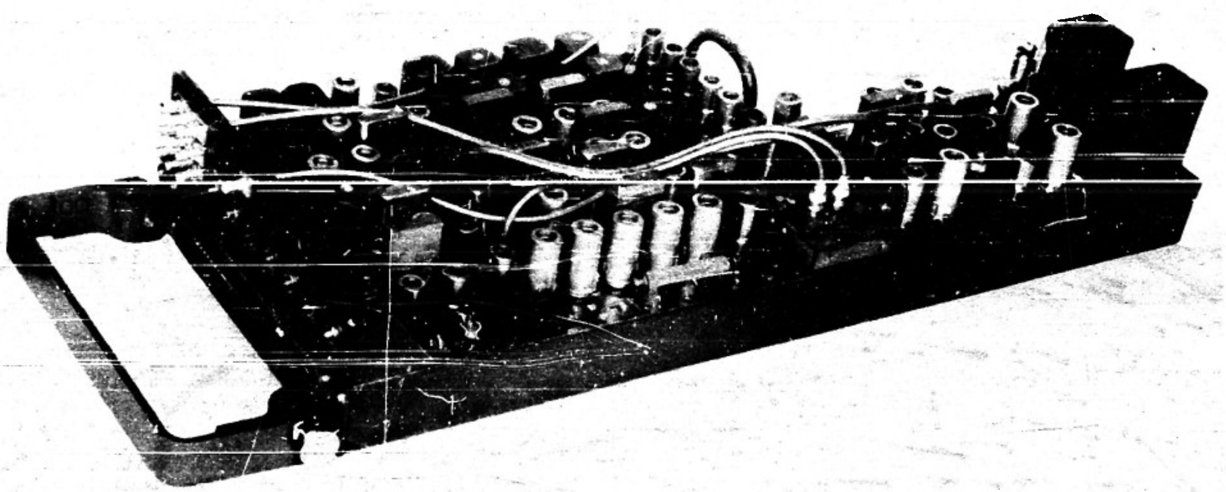

FIGURE 3-3
EXPERIMENTAL SYNCHRONIZER

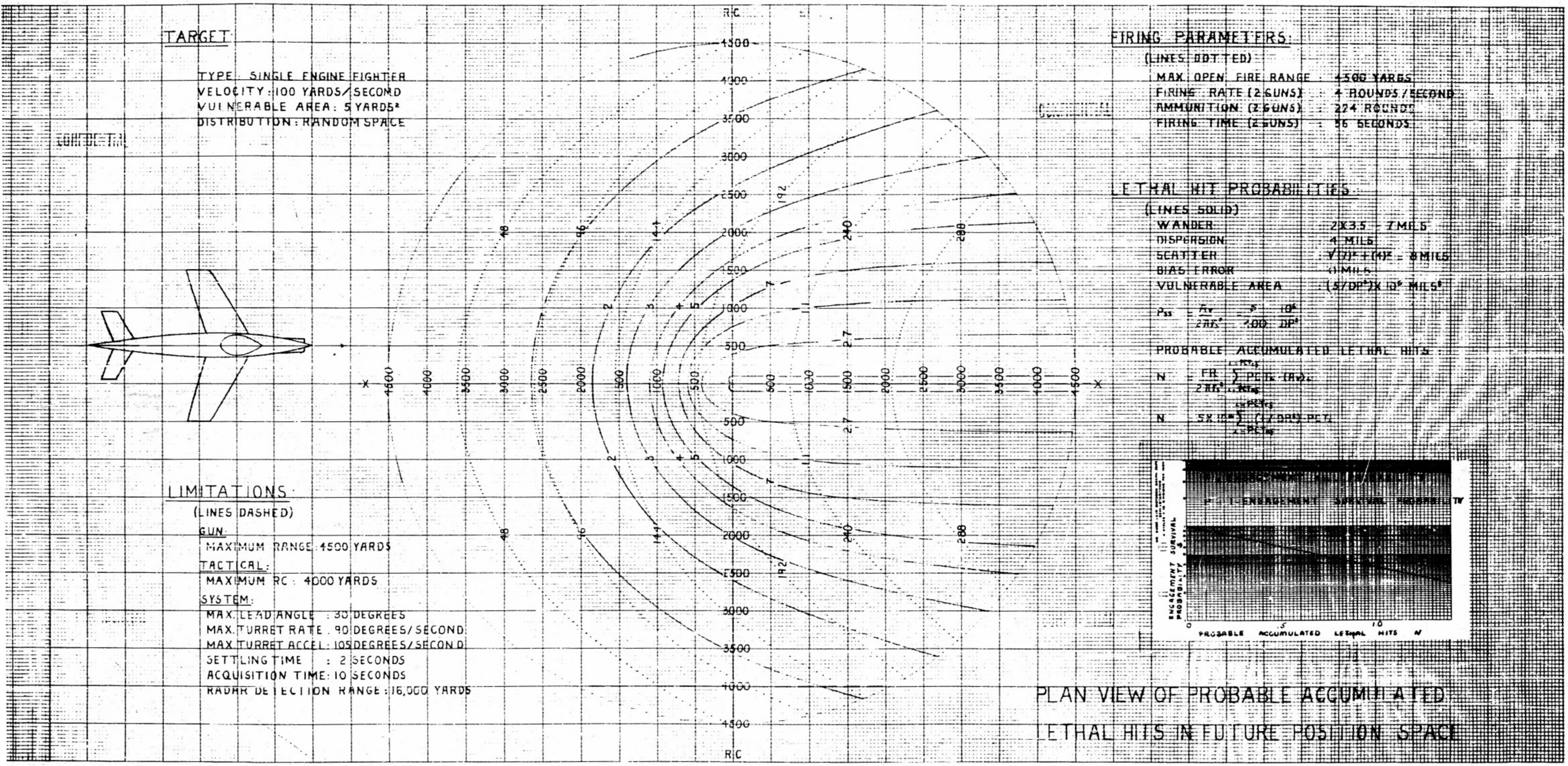

FIGURE 4—1
COMPUTER AA DIAGRAM—
TARGET VELOCITY 100 YDS/SEC

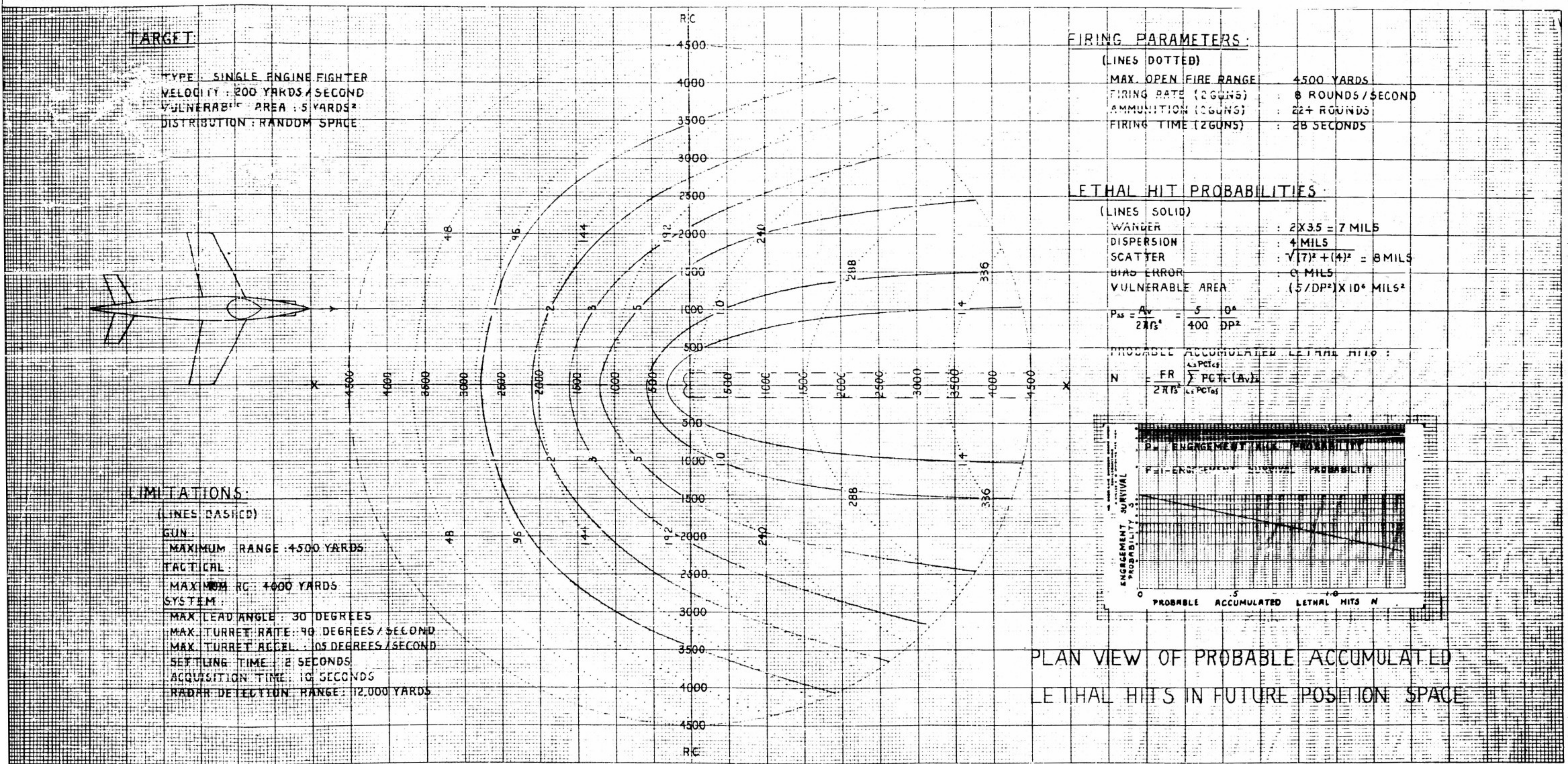

FIGURE 4-2
COMPUTER AA DIAGRAM-
TARGET VELOCITY 200YDS/SEC

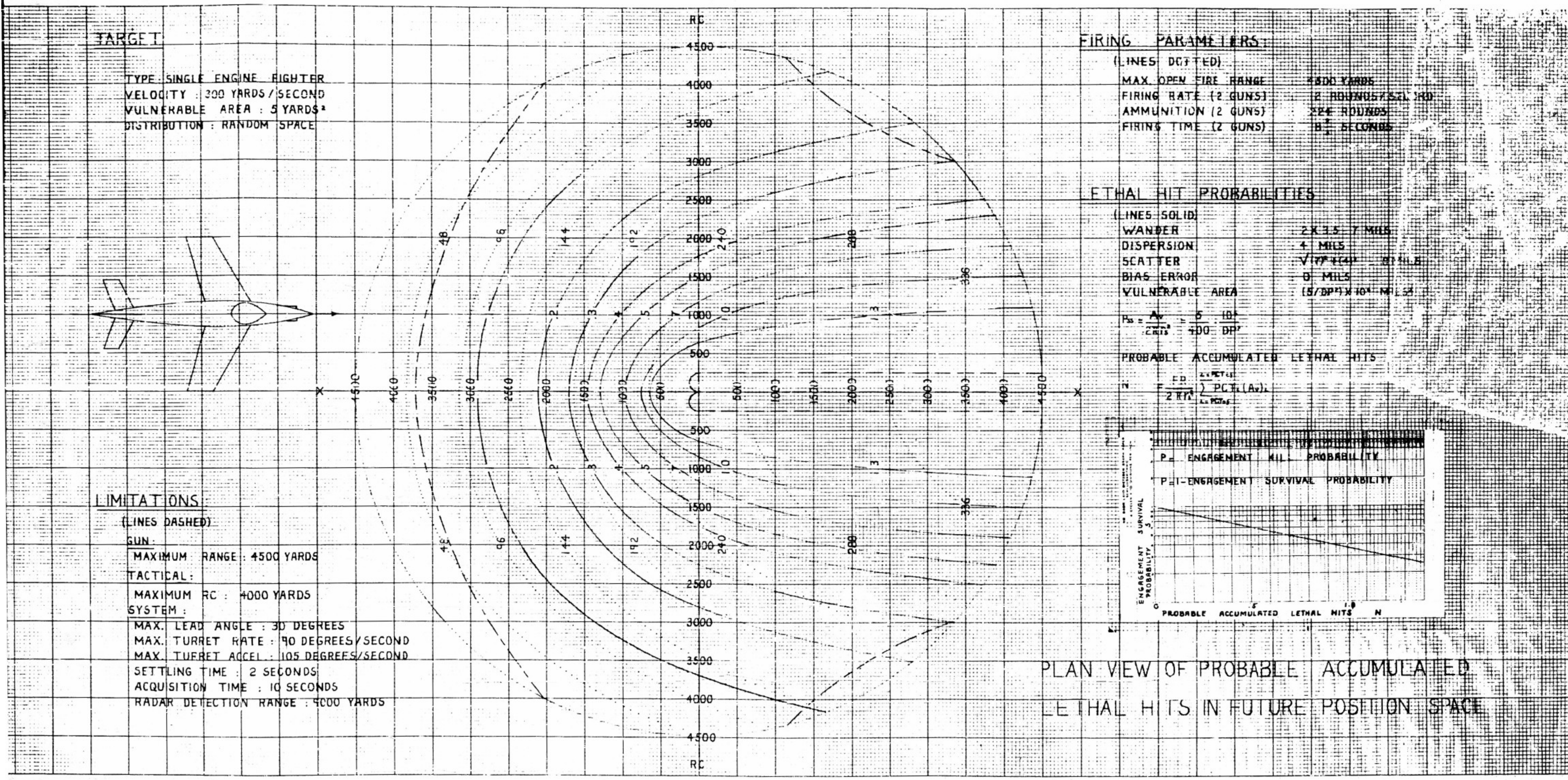

FIGURE 4-3

COMPUTER AA DIAGRAM–TARGET VELOCITY 300 YDS/SEC

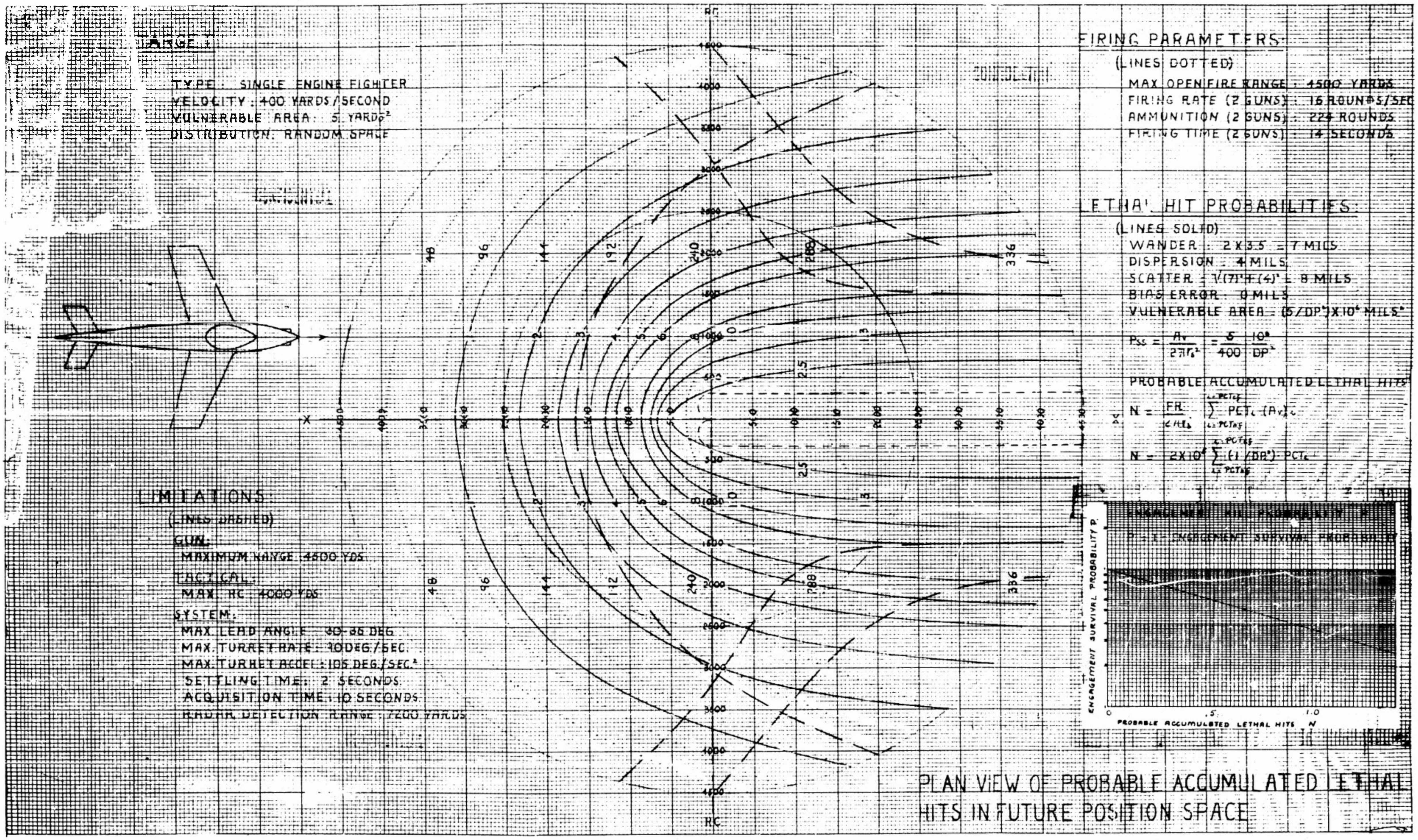

PLAN VIEW OF PROBABLE ACCUMULATED LETHAL HITS IN FUTURE POSITION SPACE

FIGURE 4-4

COMPUTER AA DIAGRAM—TARGET VELOCITY 400 YDS/SEC

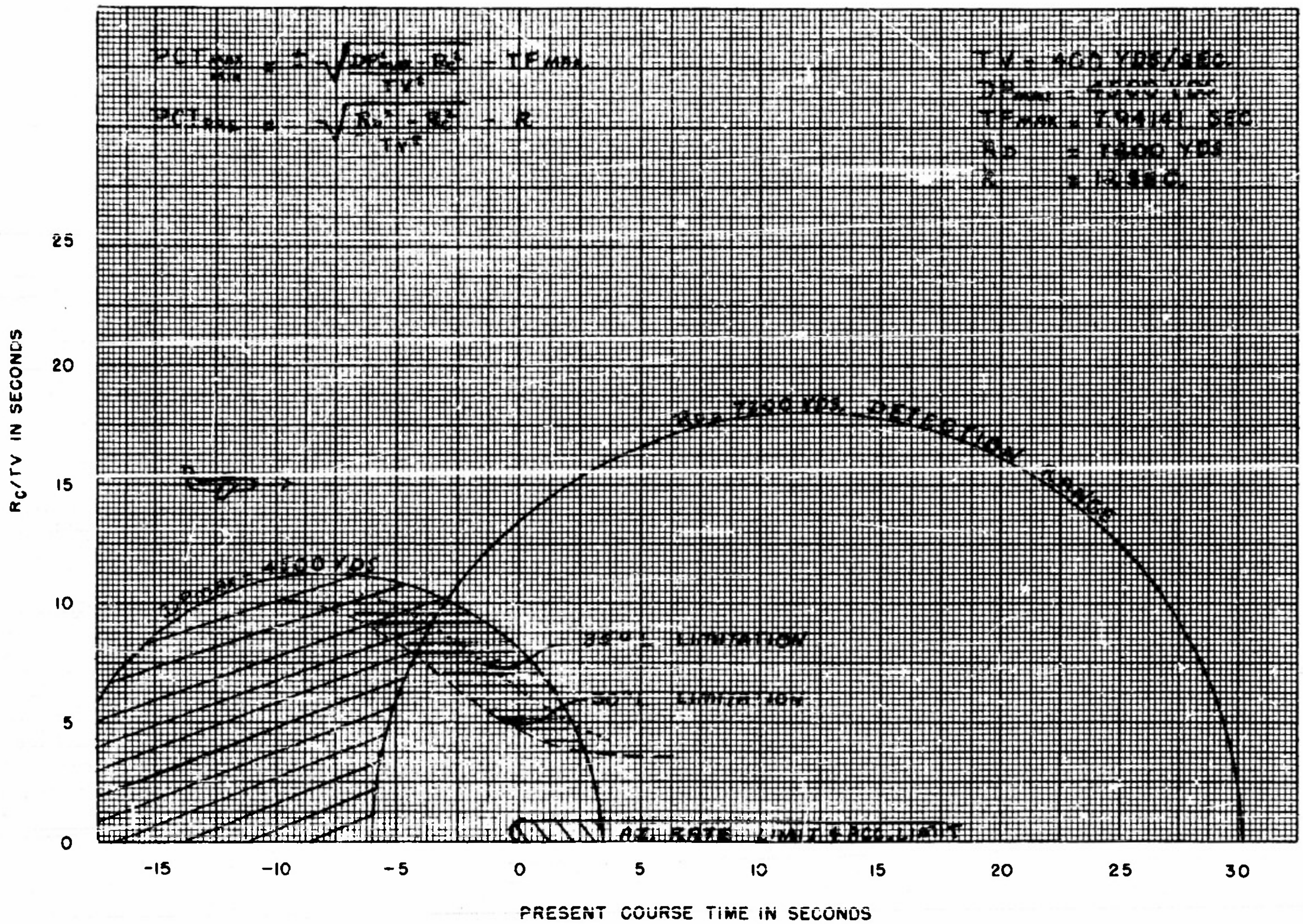

FIGURE 4-5
FIRING TIME
GRAPHICAL PRESENTATION

CONFIDENTIAL
SECURITY INFORMATION

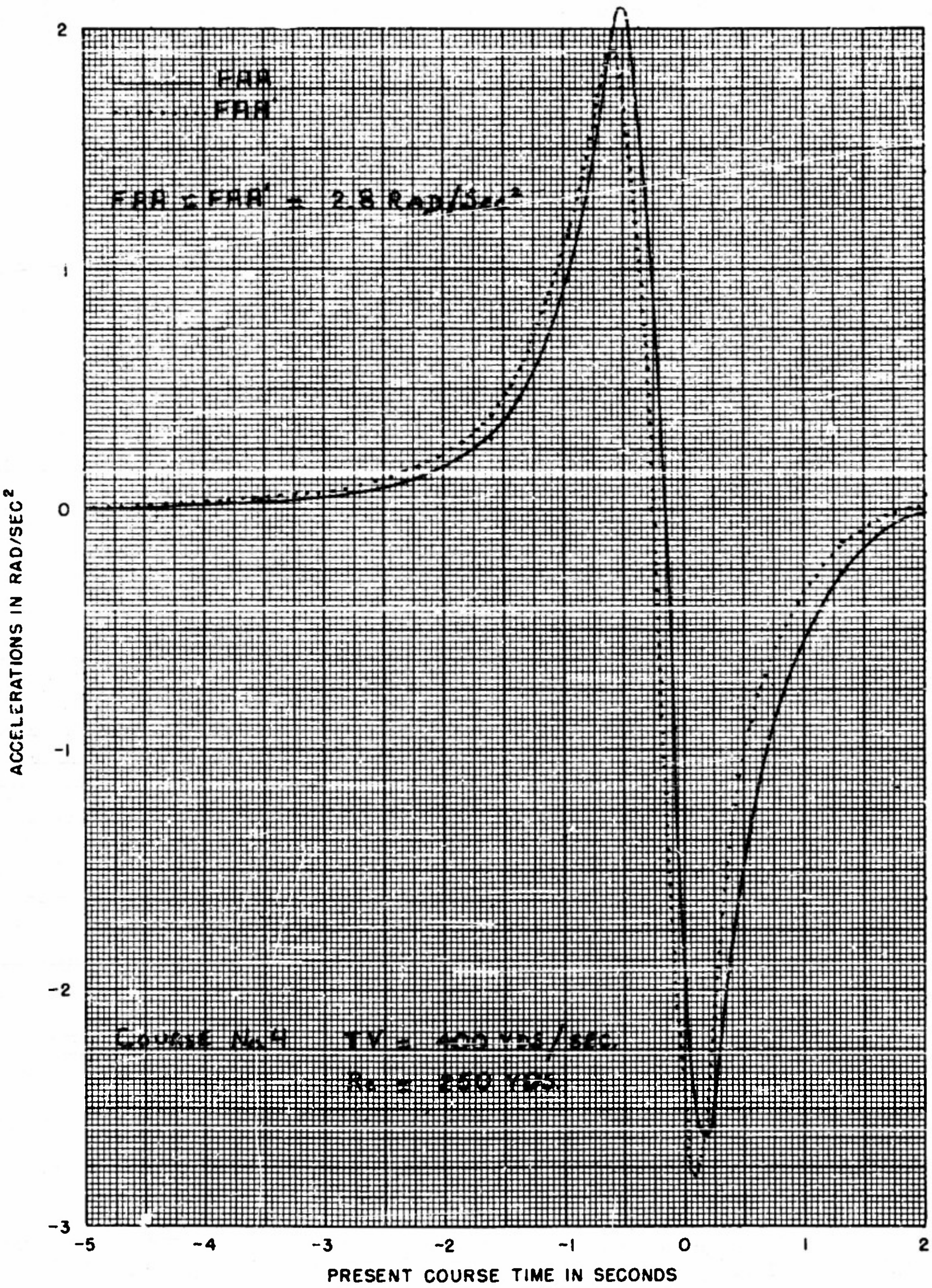

FIGURE 4-6
FIRING AZIMUTH ACCELERATIONS

CONFIDENTIAL

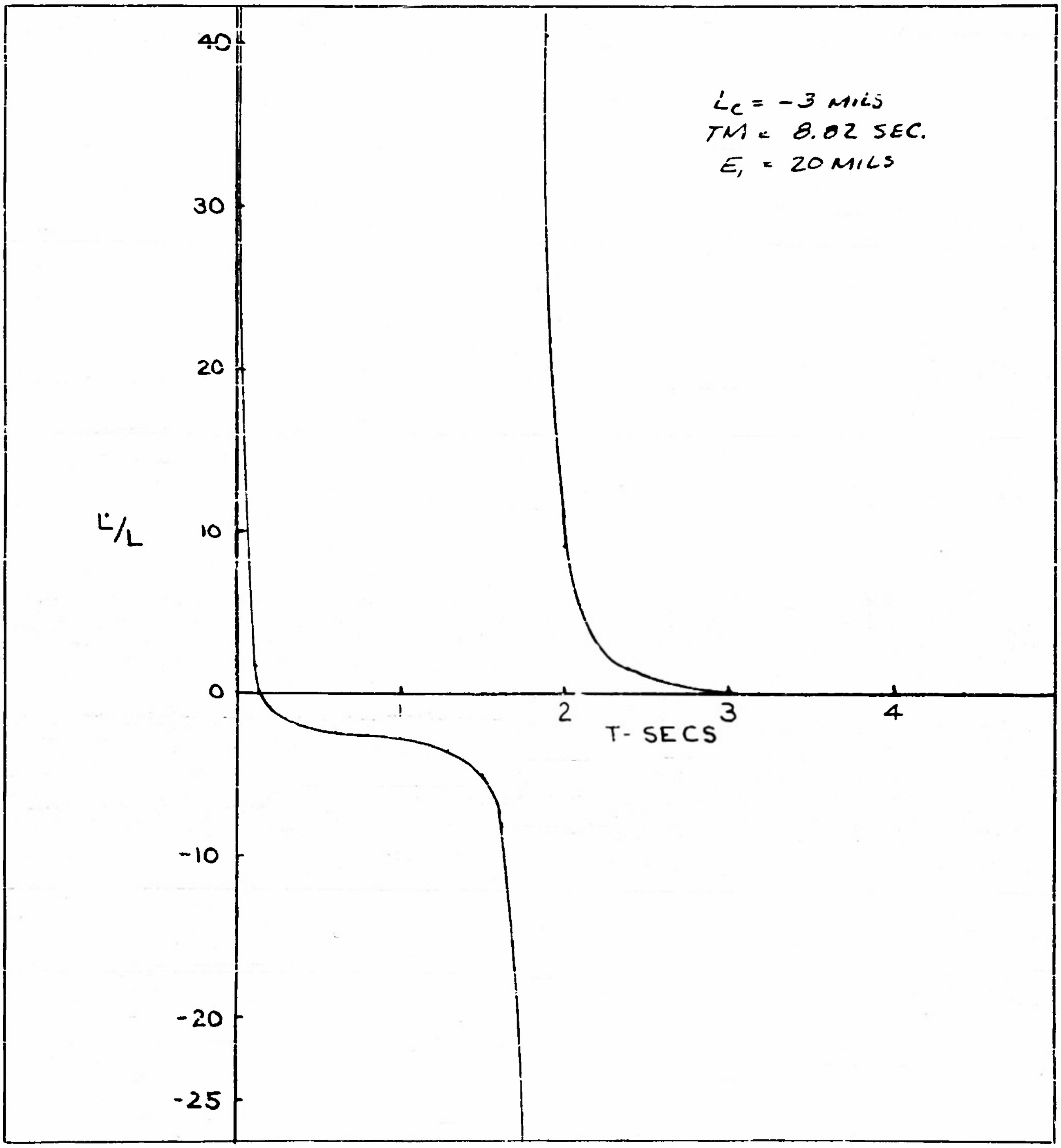

FIGURE 4-7

FAST SETTLING CURVE - L'/L vs SETTLING TIME (L_c=-3 MILS)

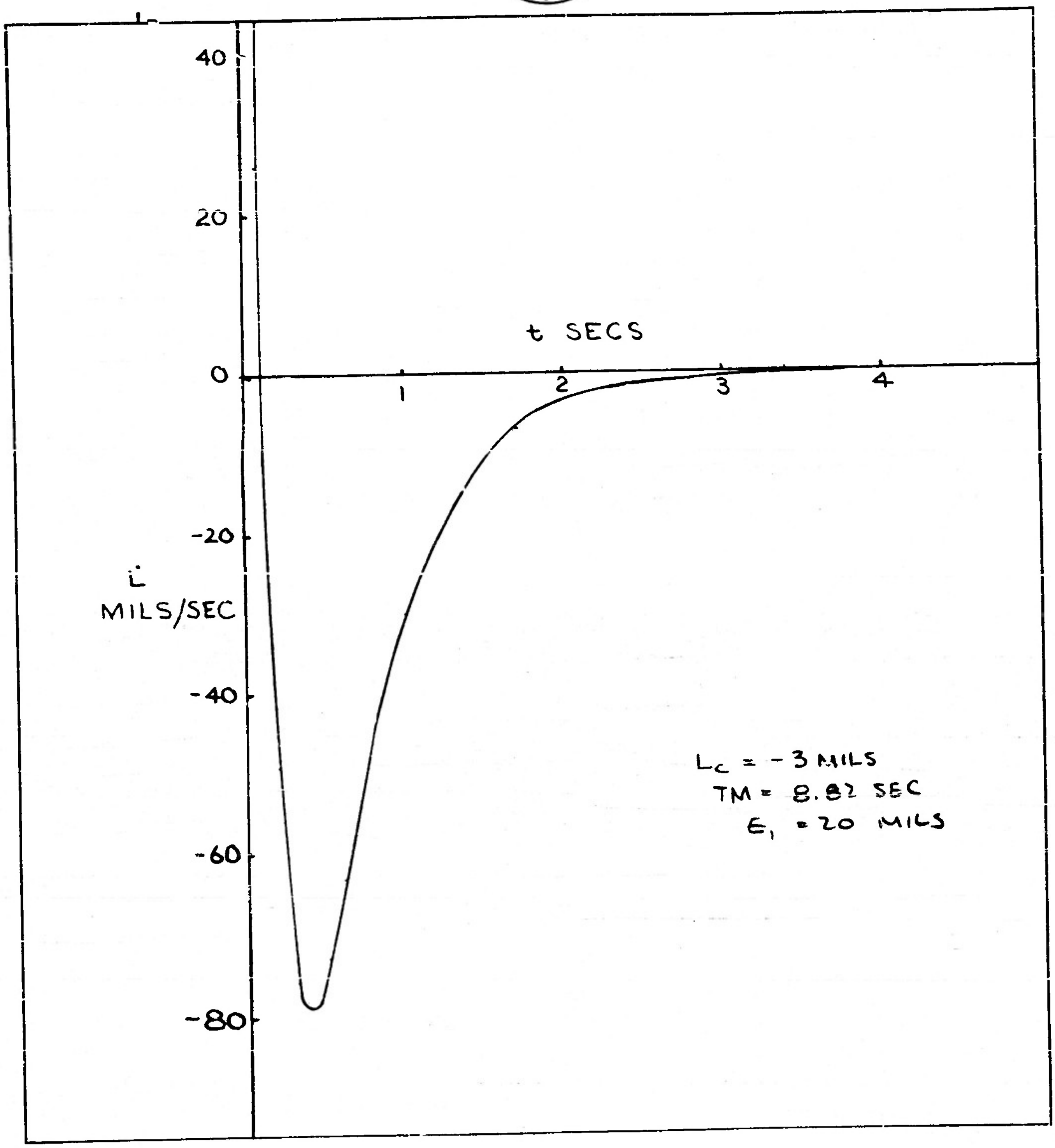

FIGURE 4-8
FAST SETTLING CURVE - L̇ vs SETTLING TIME

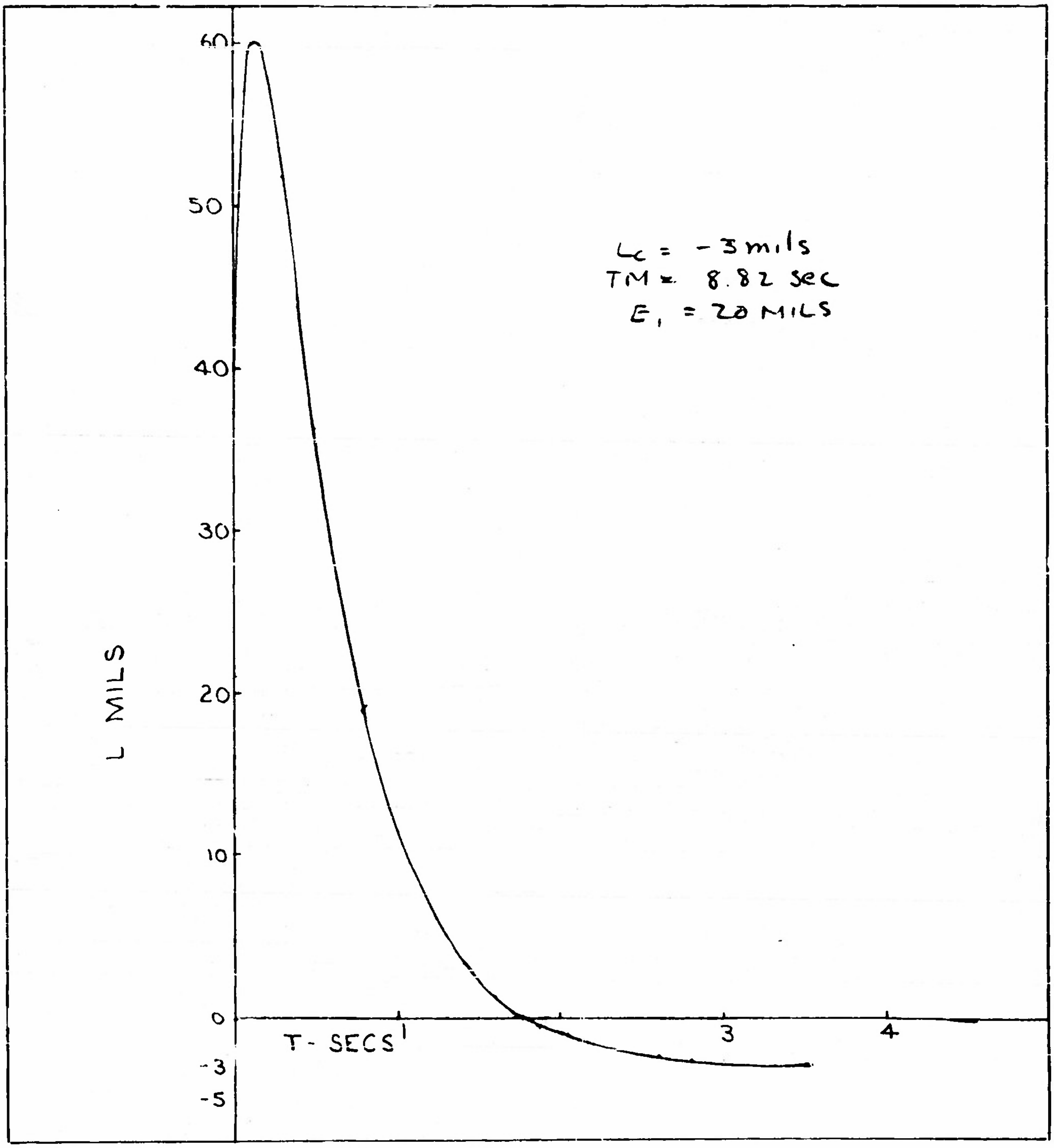

FIGURE 4-9
FAST SETTLING CURVE-L vs SETTLING TIME

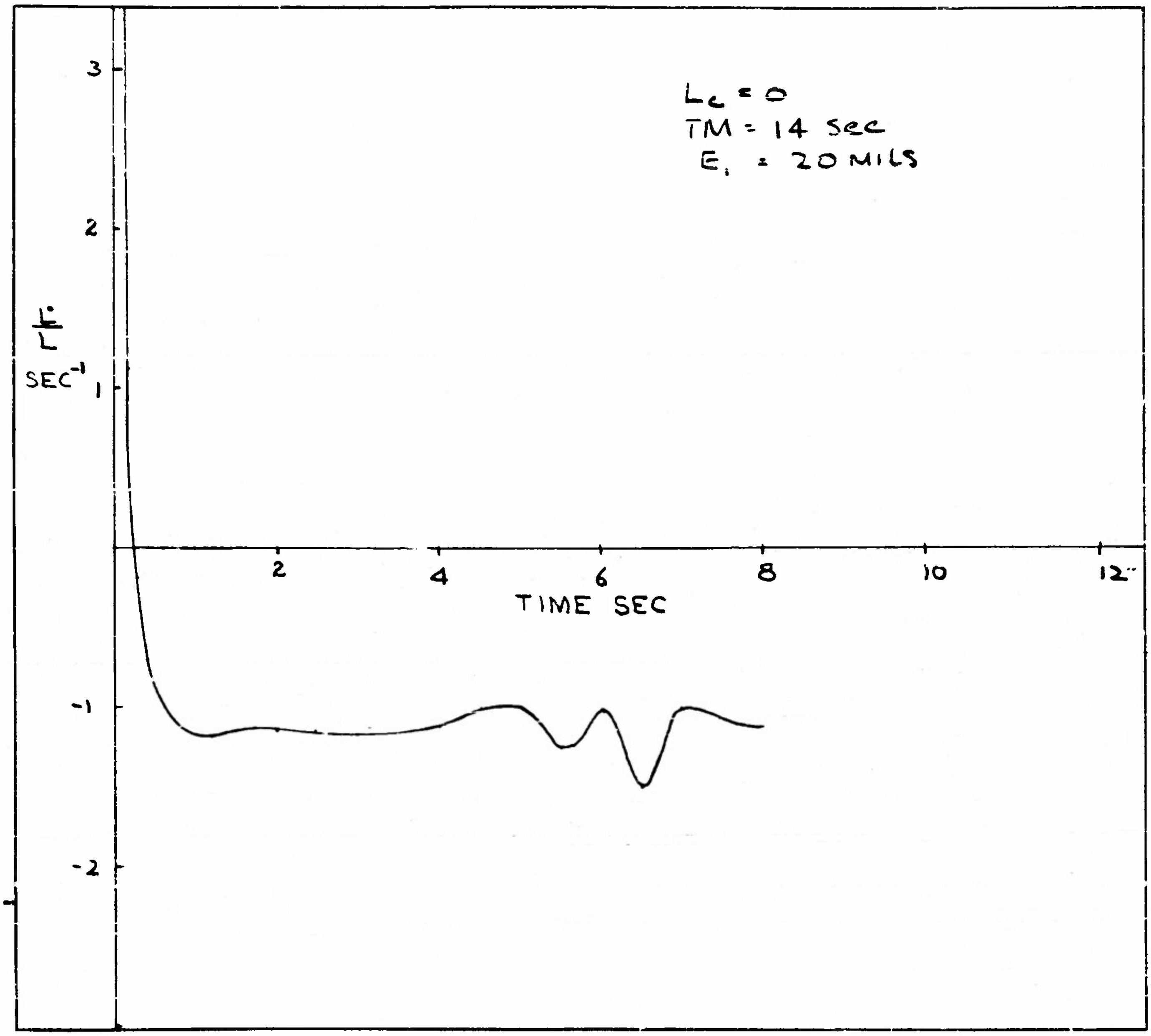

FIGURE 4—10
FAST SETTLING CURVE $-\dot{L}/L$ vs SETTLING TIME

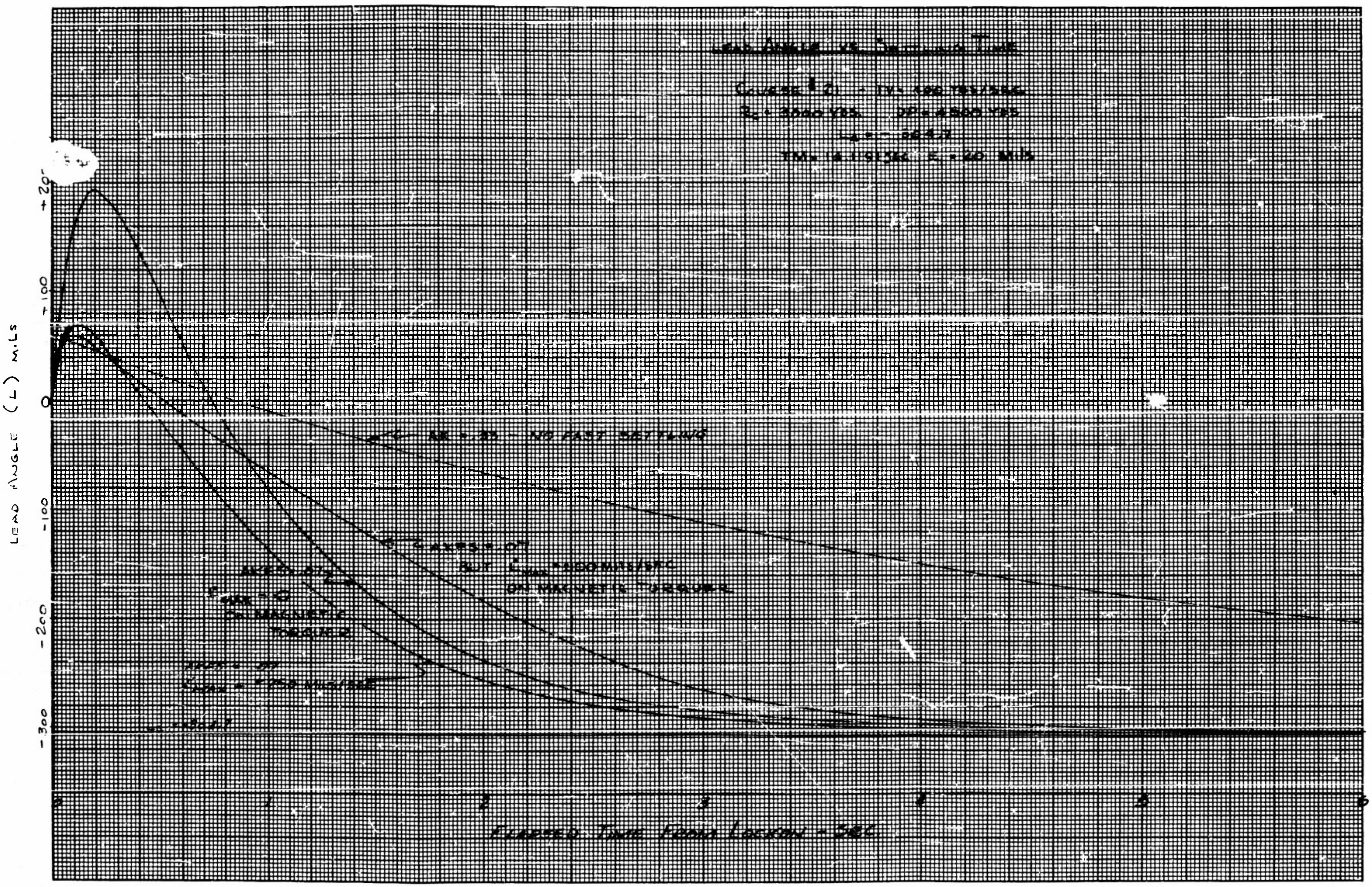

FIGURE 4—11
FAST SETTLING CURVE - LEAD ANGLE vs SETTLING TIME (L_c=-304.7 MILS)

CONFIDENTIAL
SECURITY INFORMATION

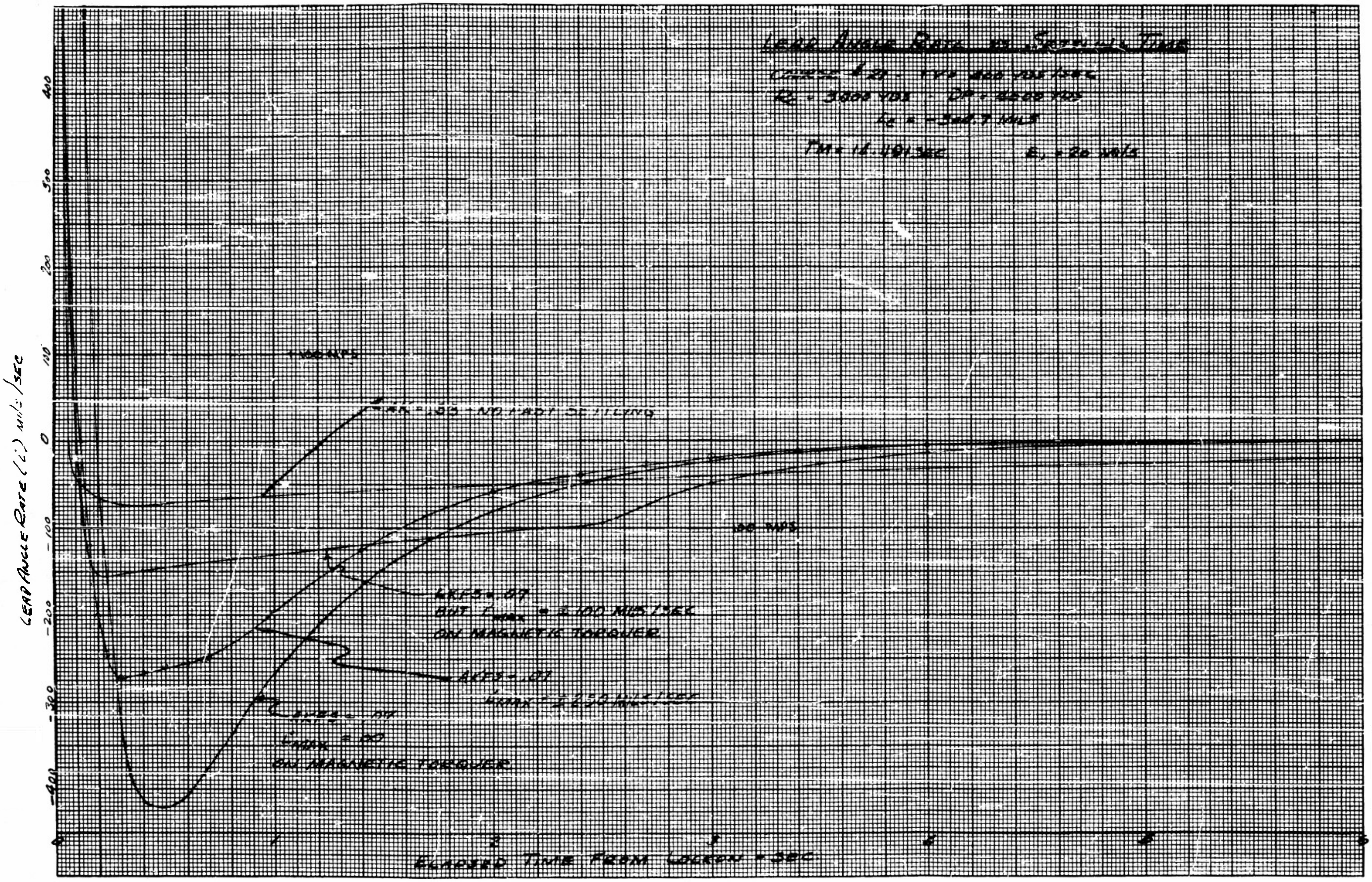

FIGURE 4-12

FAST SETTLING CURVE-LEAD ANGLE RATE vs SETTLING TIME (L_C=-304.7 MILS)

CONFIDENTIAL

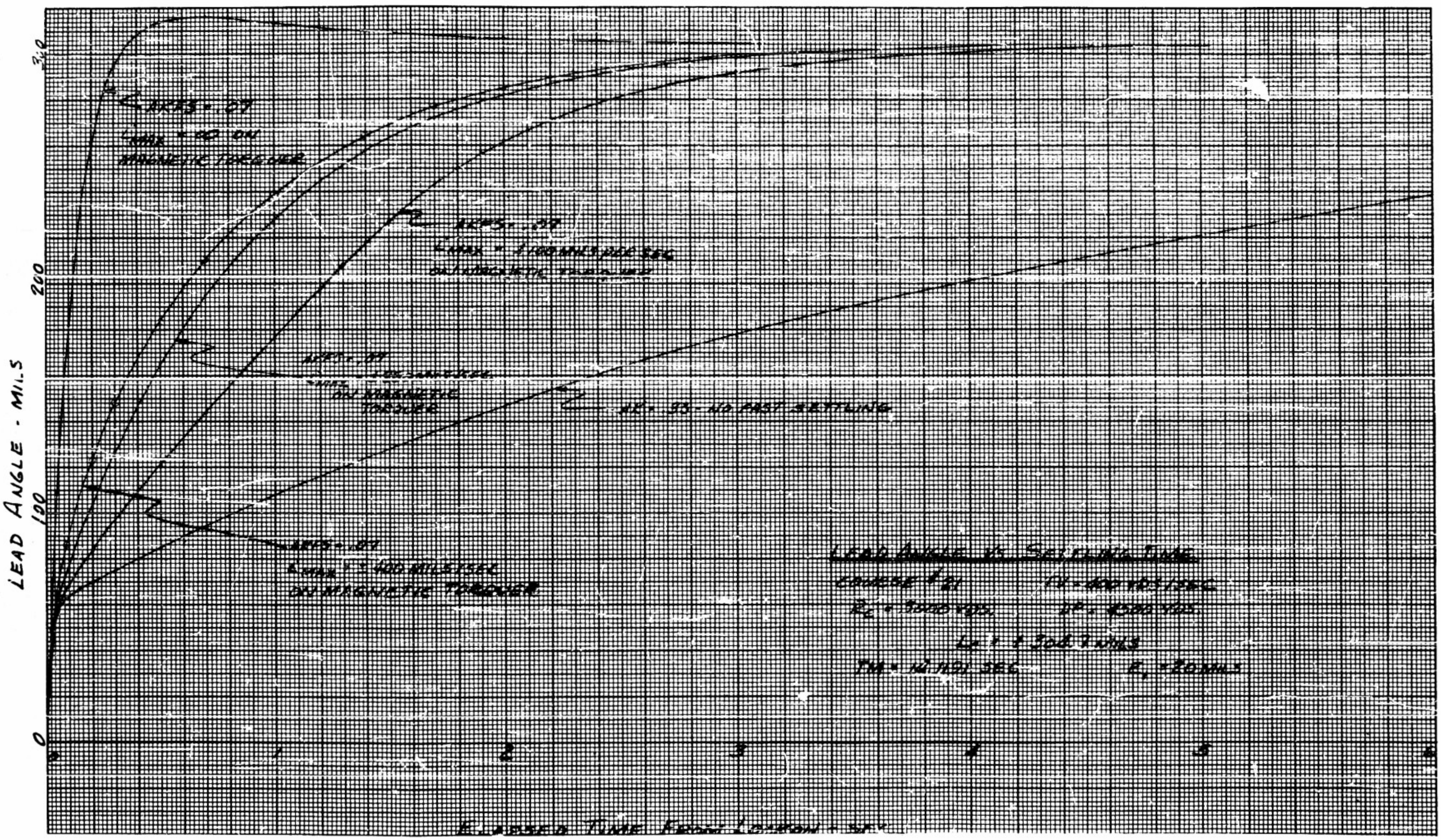

FIGURE 4-13

FAST SETTLING CURVE-LEAD ANGLE vs SETTLING TIME (L_c - 304.7 MILS)

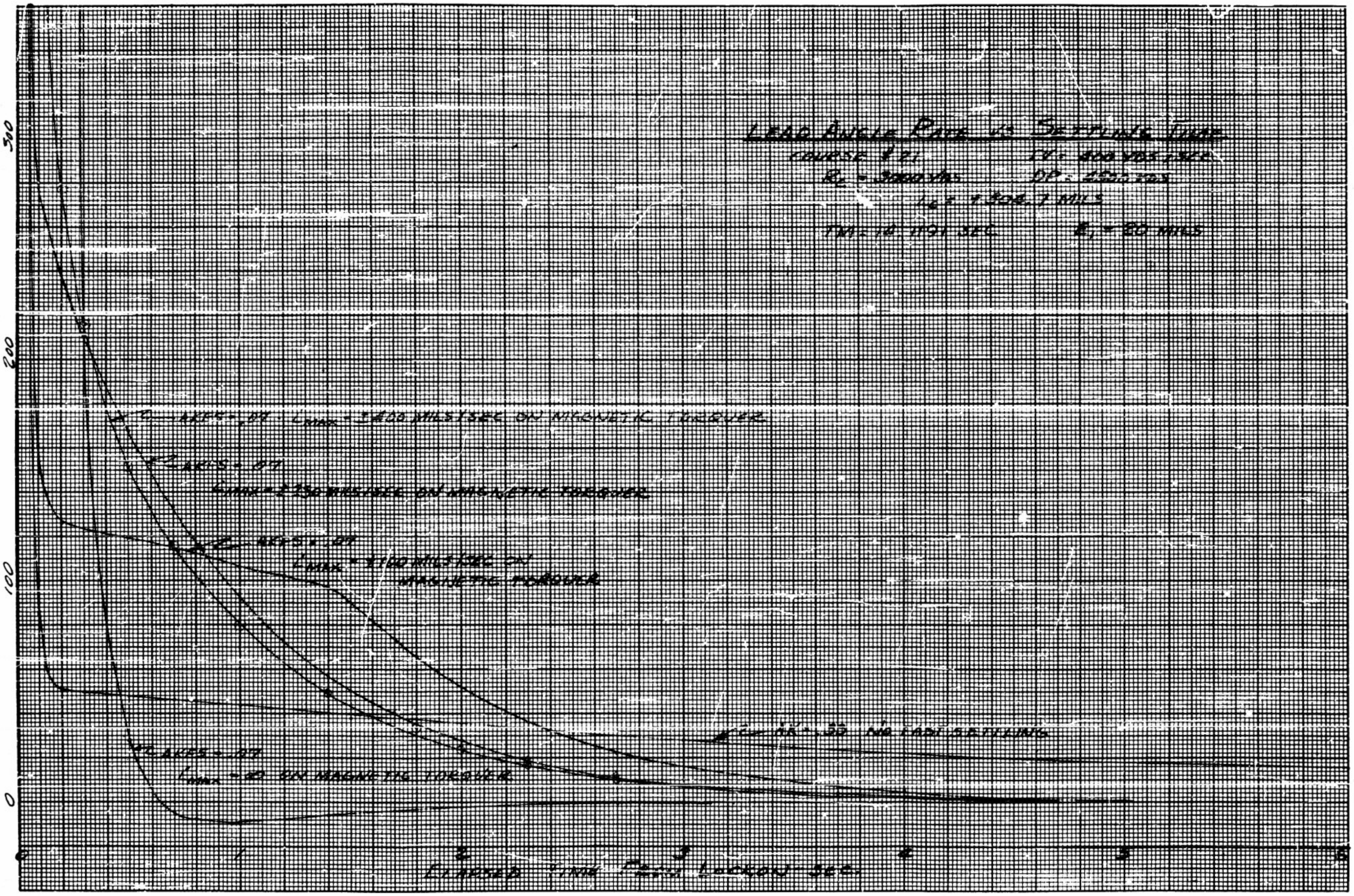

FIGURE 4-14

FAST SETTLING CURVE-LEAD ANGLE RATE vs SETTLING TIME (L_C= 304.7 MILS)

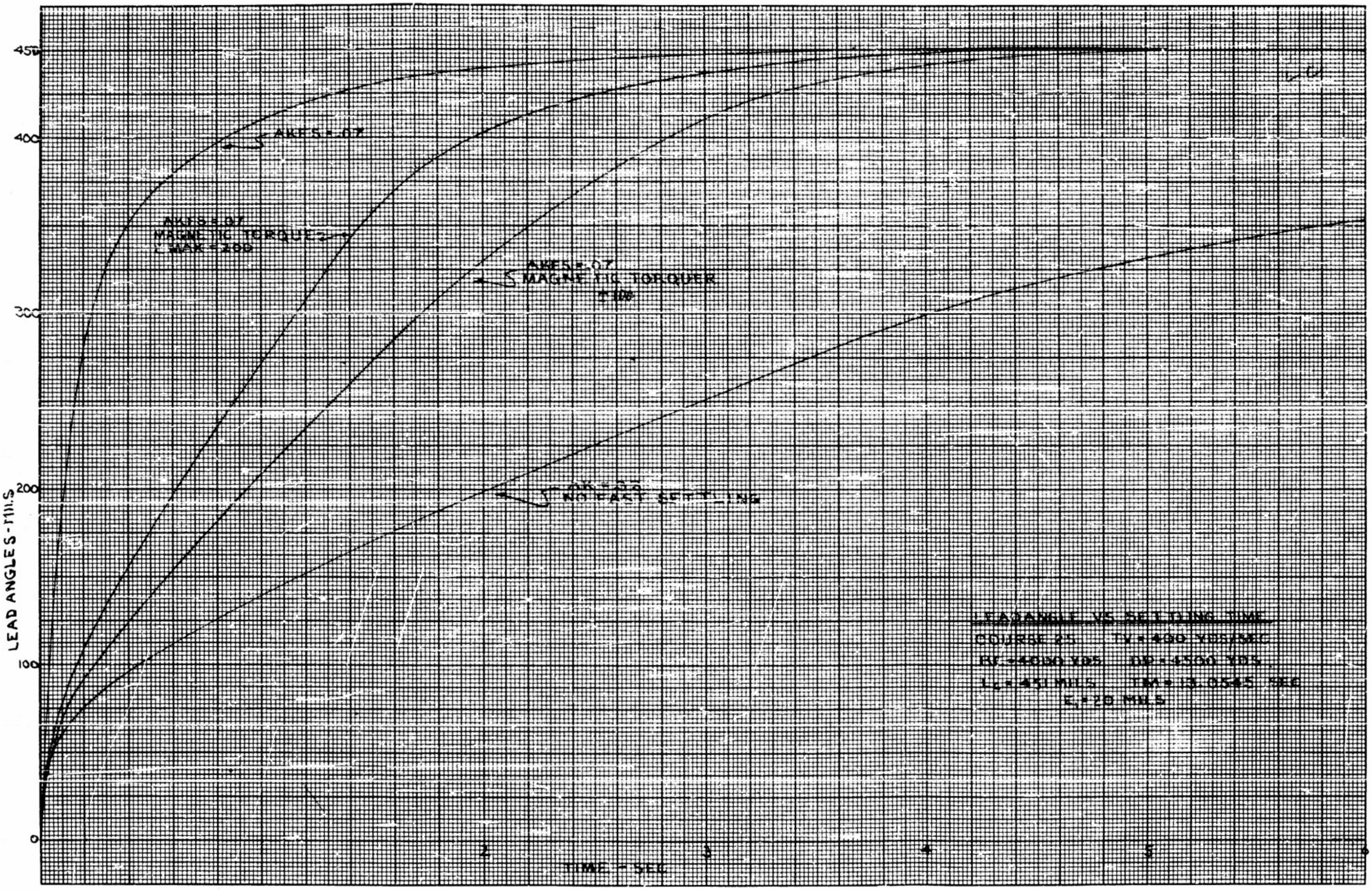

FIGURE 4-15

FAST SETTLING CURVE–LEAD ANGLE vs SETTLING TIME (L_c= 451 MILS)

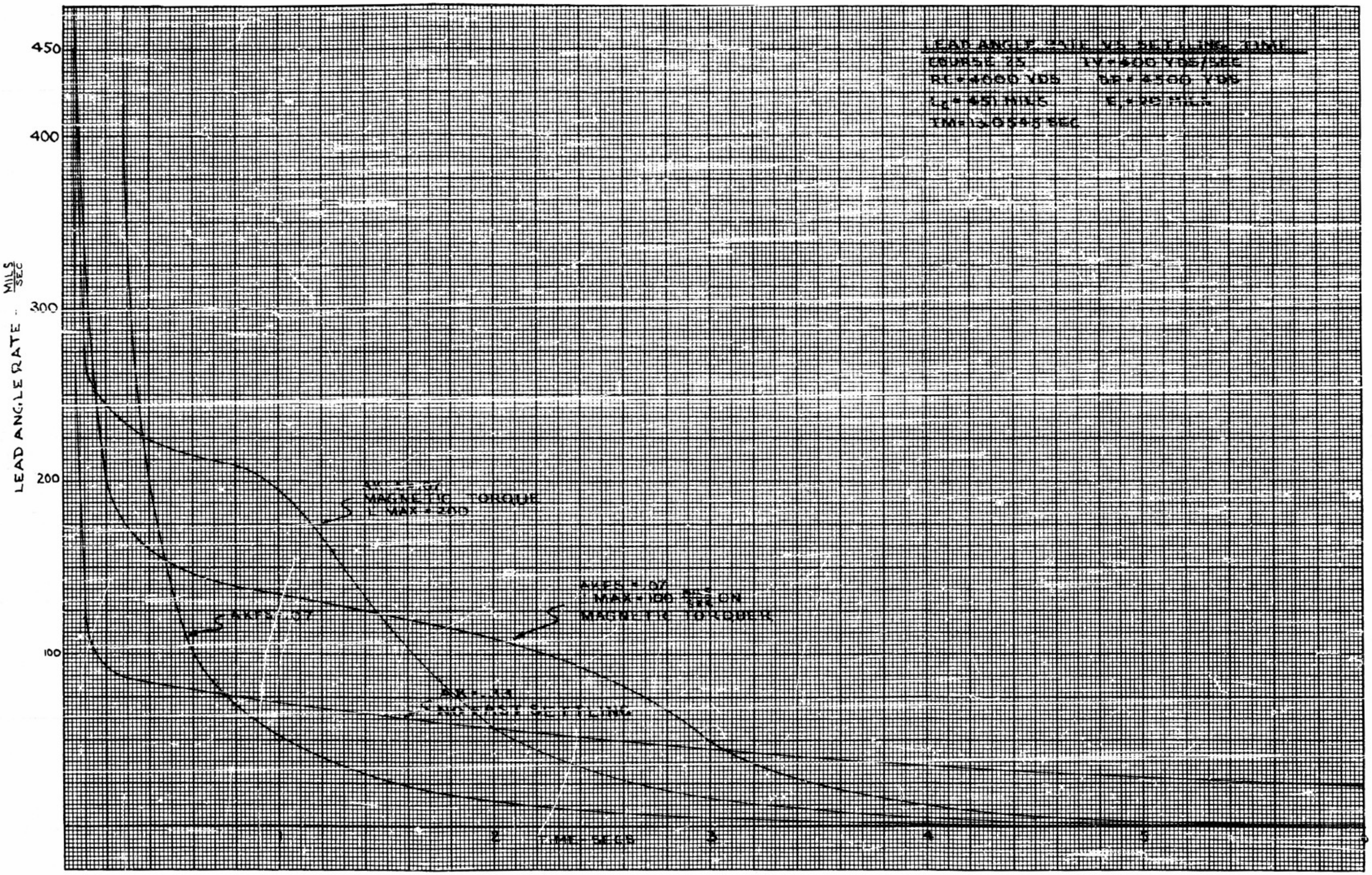

FIGURE 4-16

FAST SETTLING CURVE – LEAD ANGLE RATE vs SETTLING TIME (L_c=451 MILS)

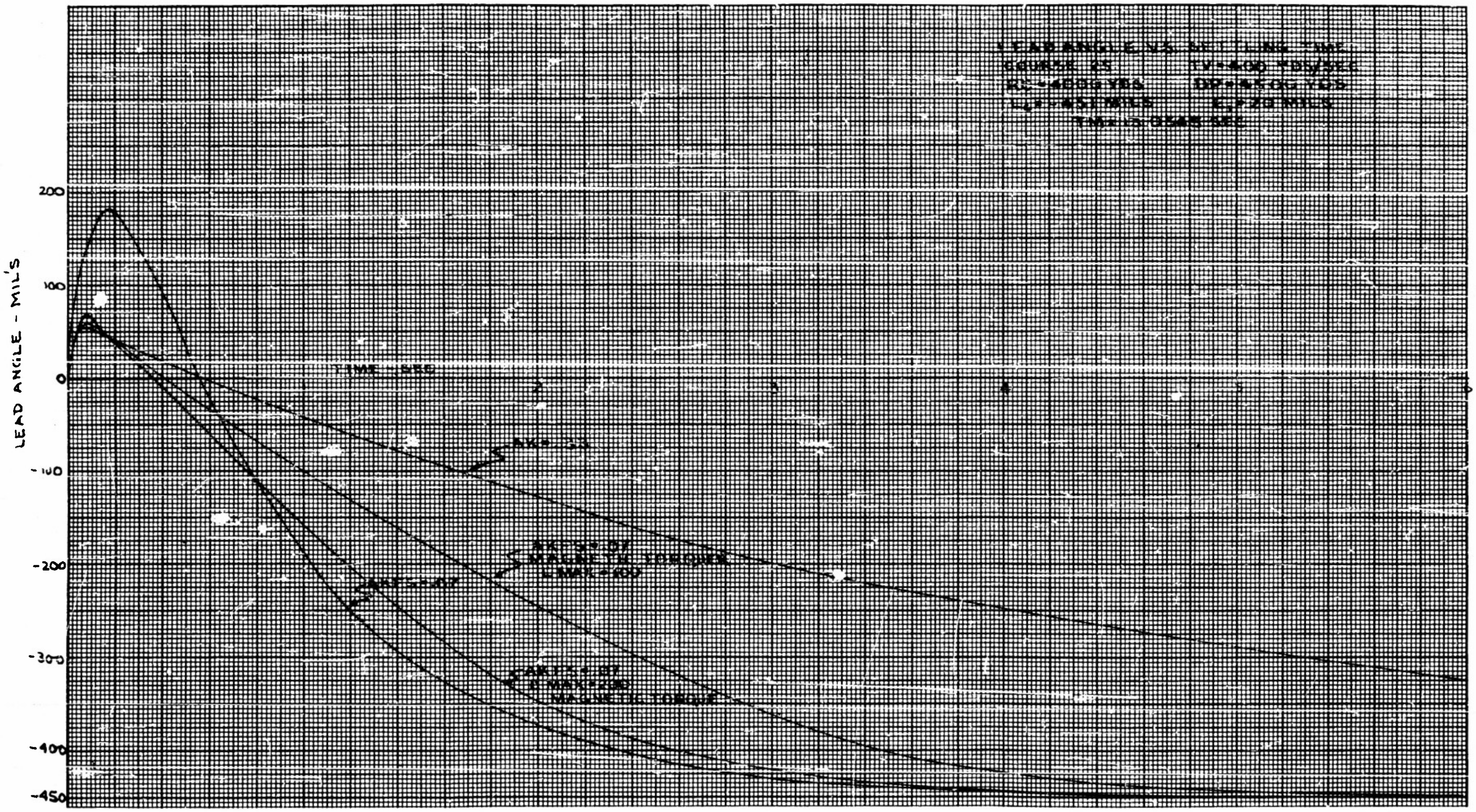

FIGURE 4-17

FAST SETTLING CURVE - LEAD ANGLE vs SETTLING TIME (L_c=-451 MILS)

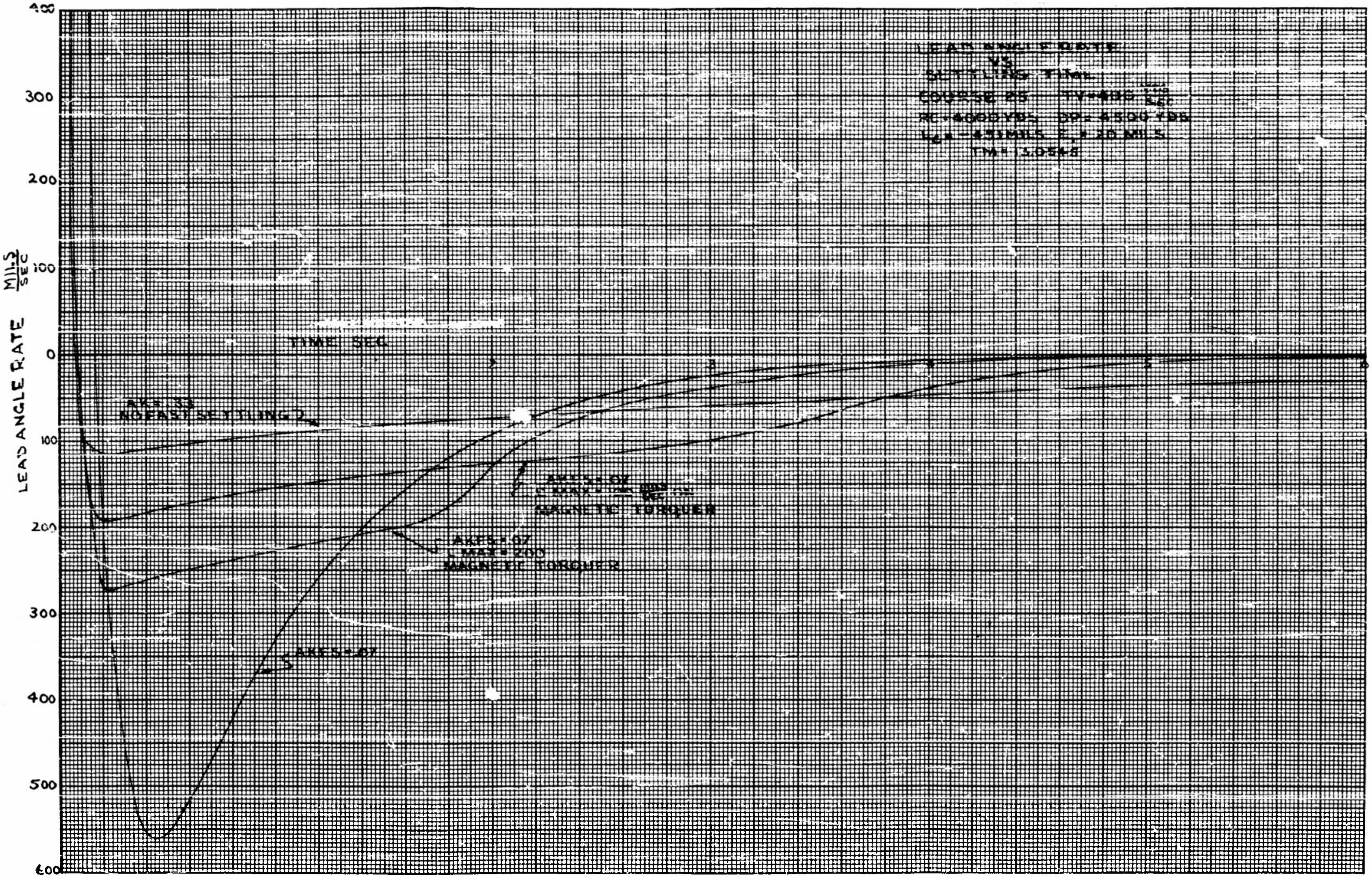

FIGURE 4-18

FAST SETTLING CURVE-LEAD ANGLE RATE vs SETTLING TIME(L_C=-451 MILS)

CONFIDENTIAL
SECURITY INFORMATION

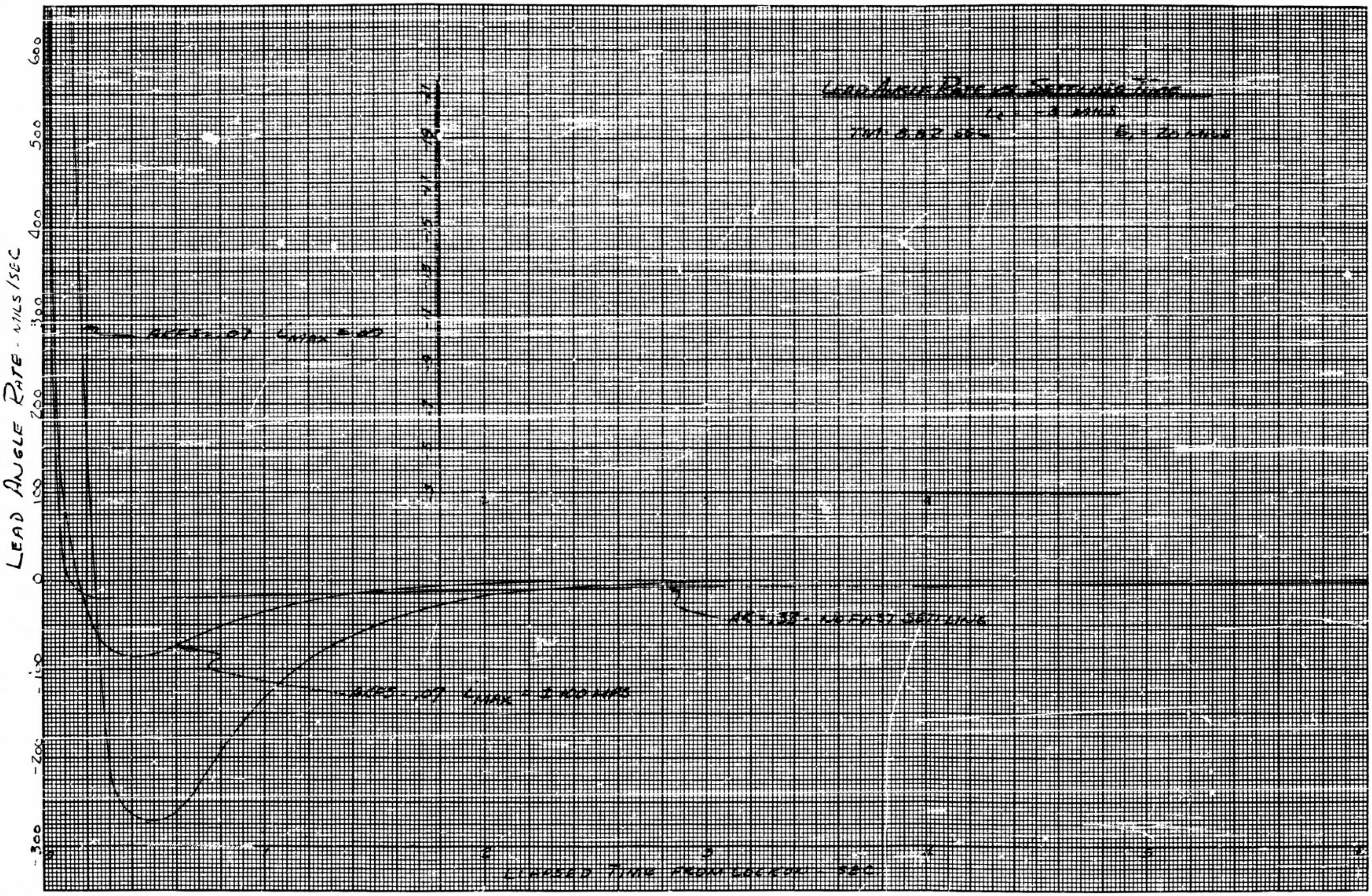

FIGURE 4 - 19
FAST SETTLING CURVE-LEAD ANGLE RATE vs SETTLING TIME (L_c=-3 MILS)

CONFIDENTIAL

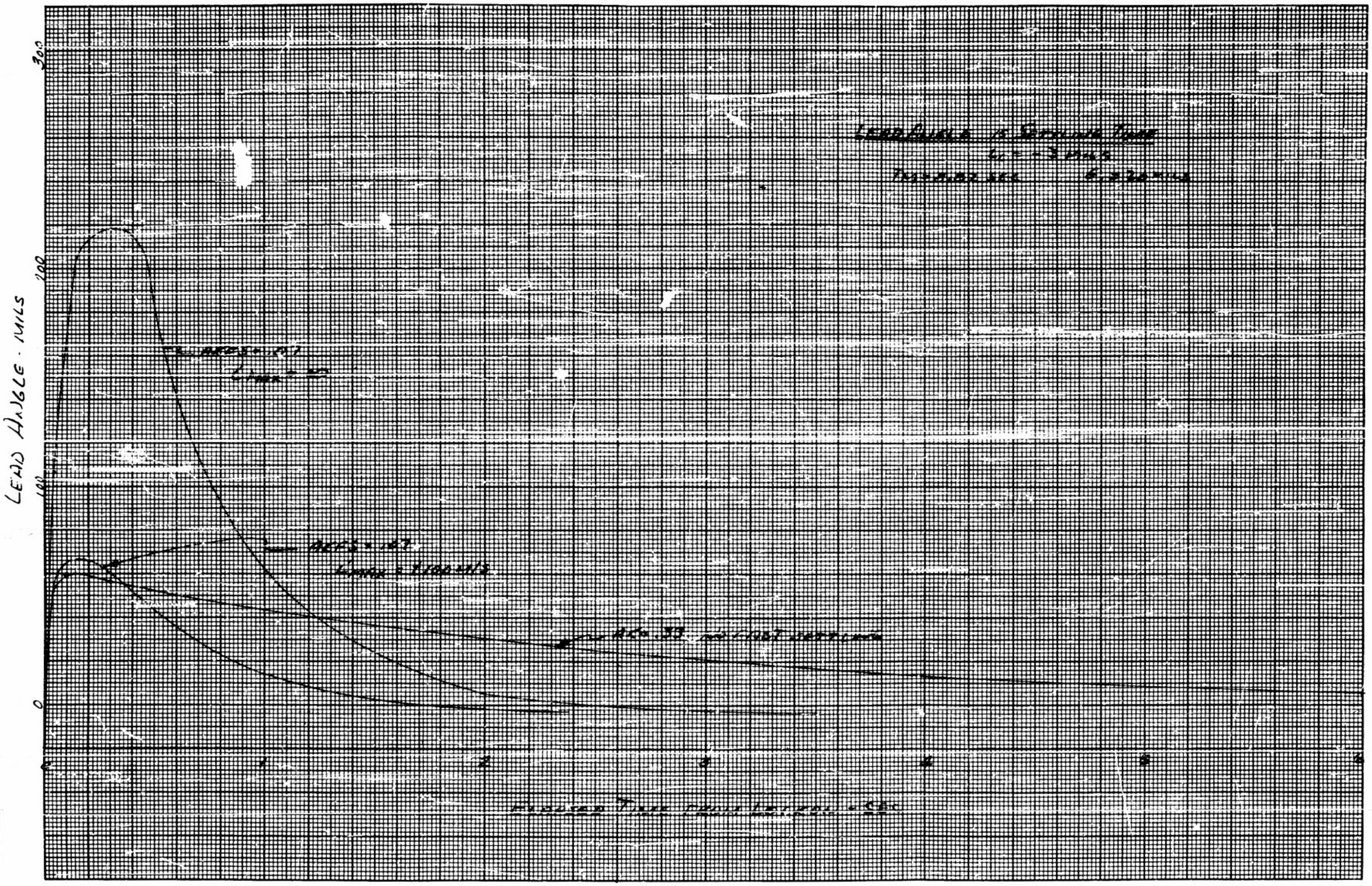

FIGURE 4-20
FAST SETTLING CURVE -- LEAD ANGLE vs SETTLING TIME (L_c=-3 MILS)

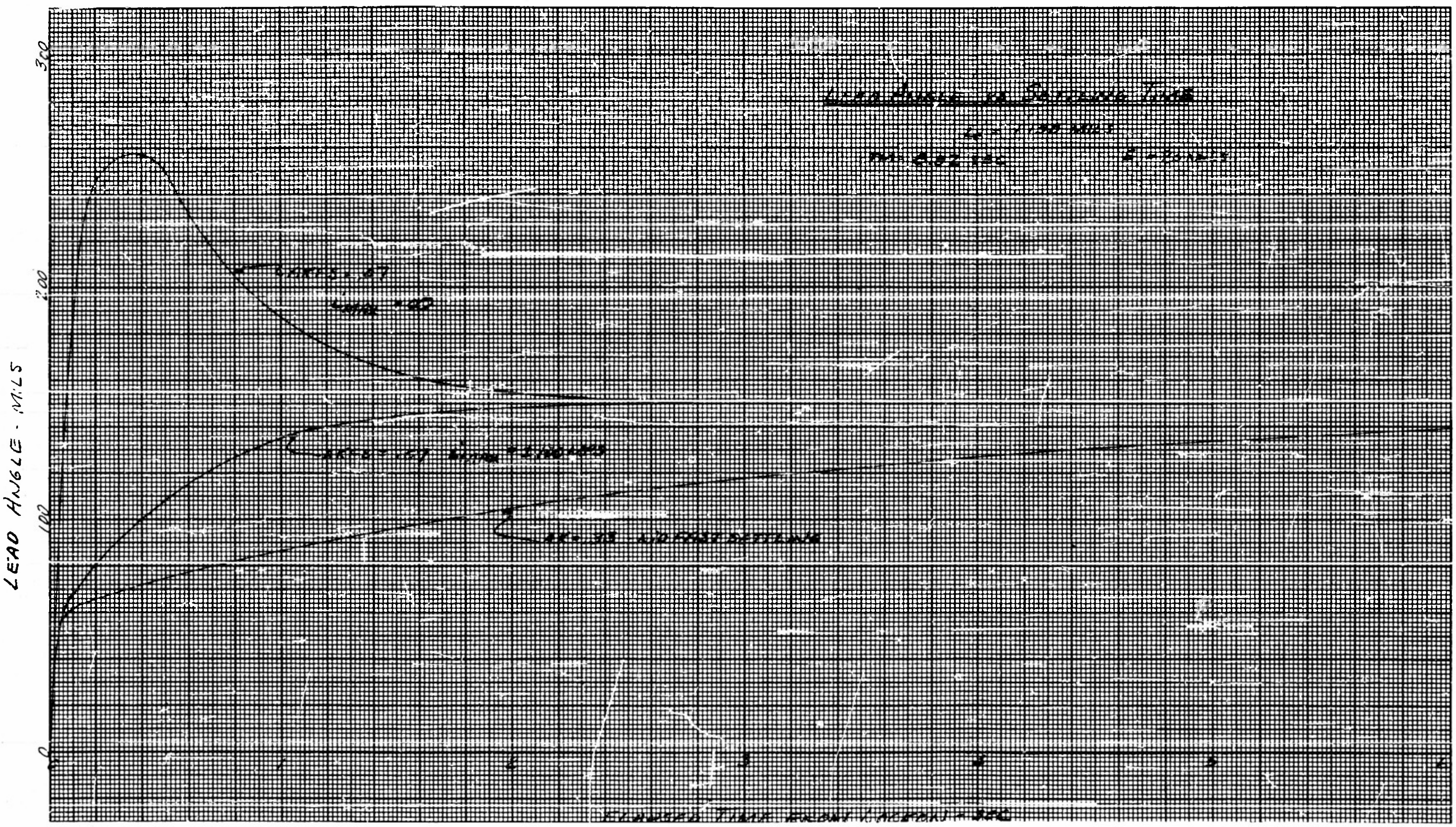

FIGURE 4-21
FAST SETTLING CURVE - LEAD ANGLE vs SETTLING TIME (L_C= 150 MILS)

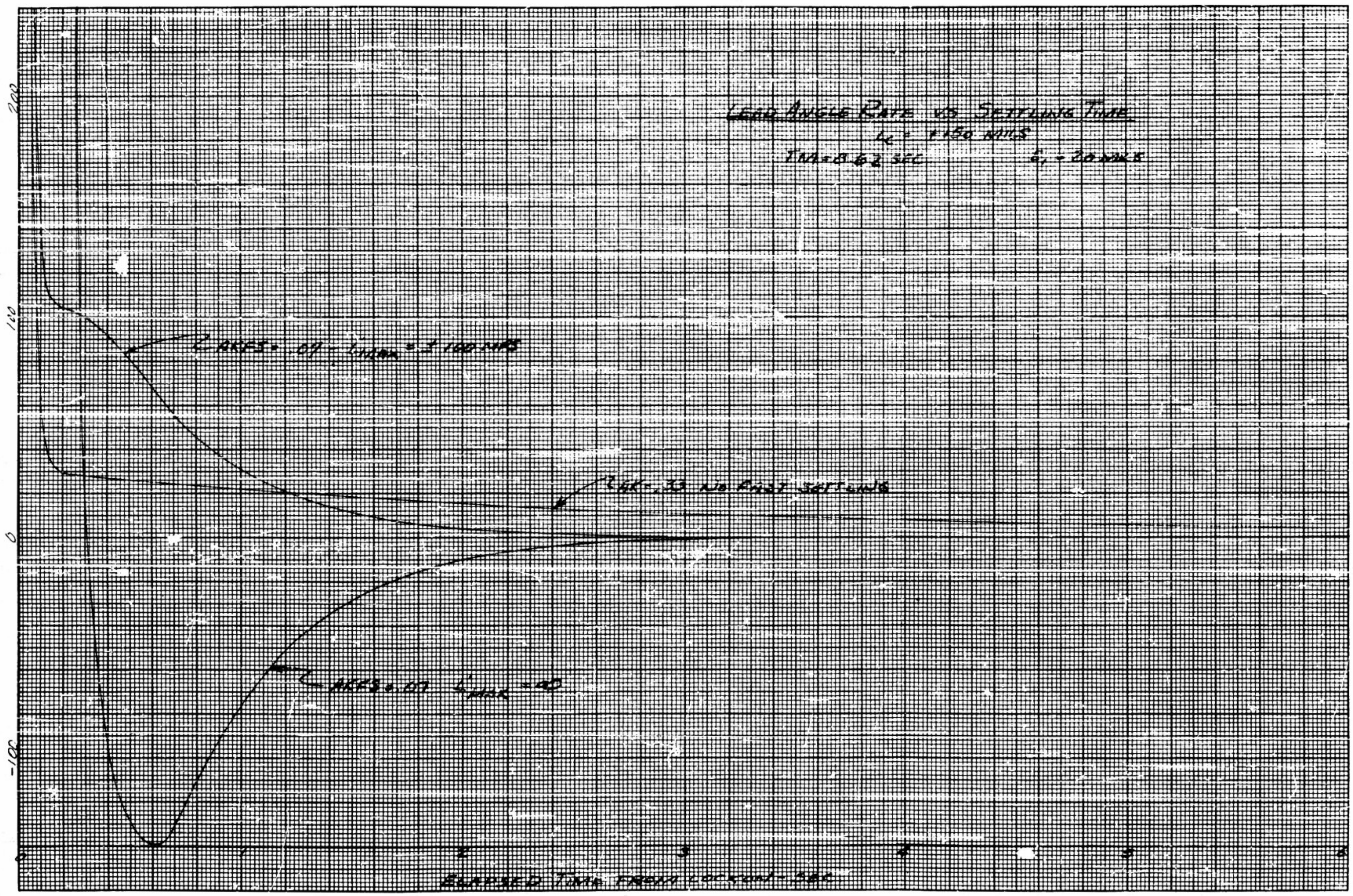

FIGURE 4-22

FAST SETTLING CURVE-LEAD ANGLE RATE vs SETTLING TIME (L_C=150 MILS)

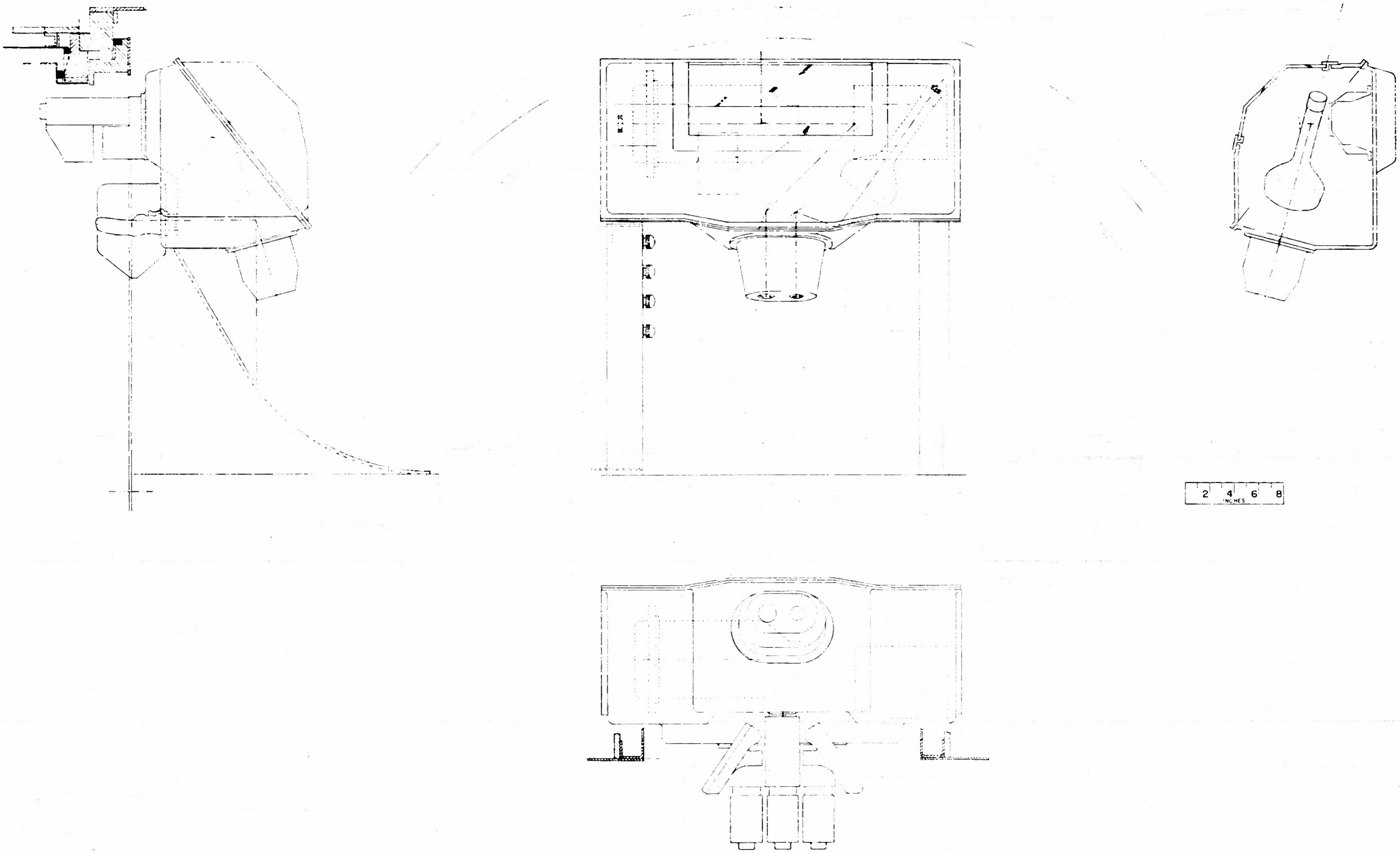

FIGURE 4–23
COMPUTER TRACKING SECTION LAYOUT

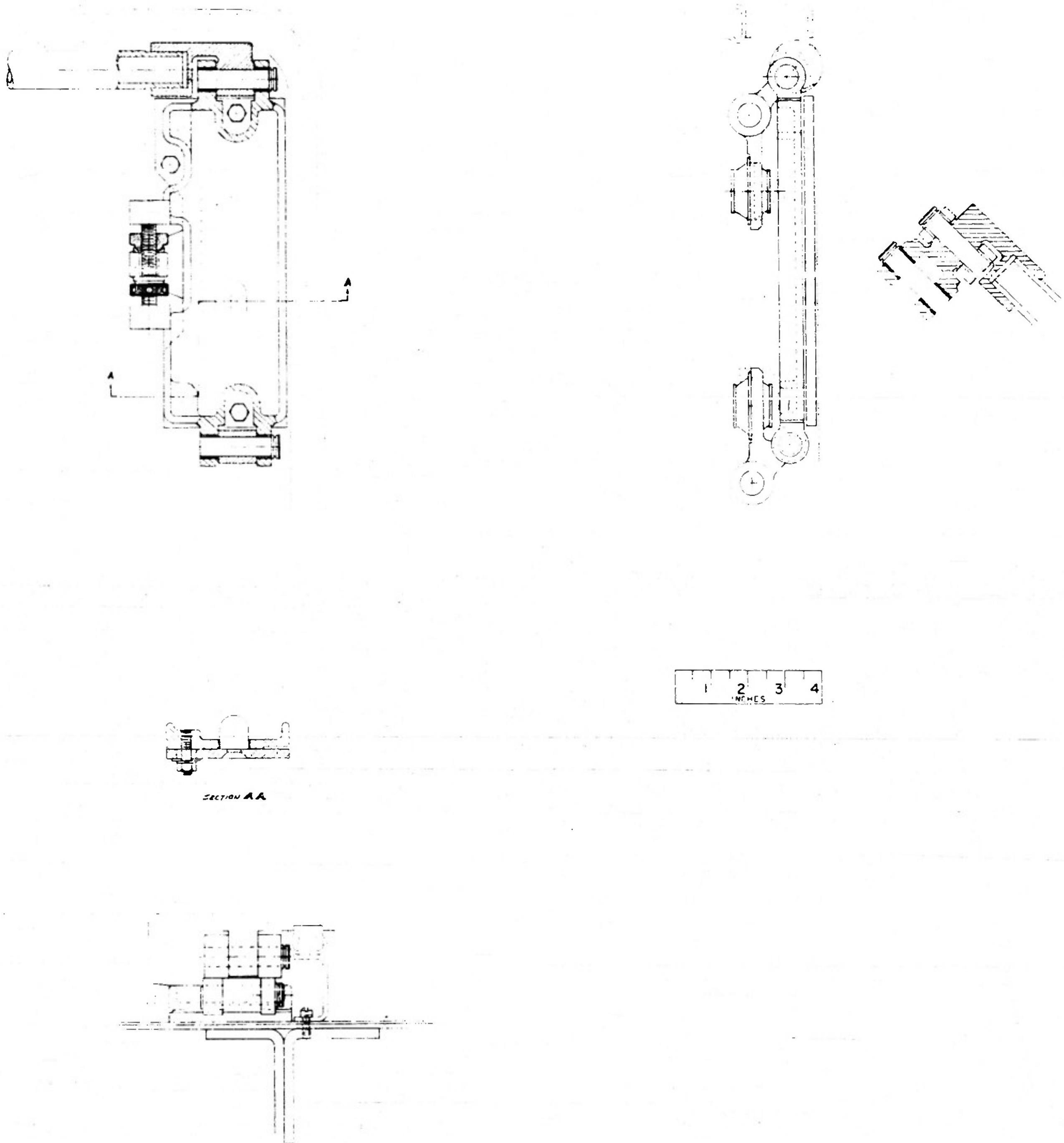

FIGURE 4-24
SHOCKMOUNT LAYOUT

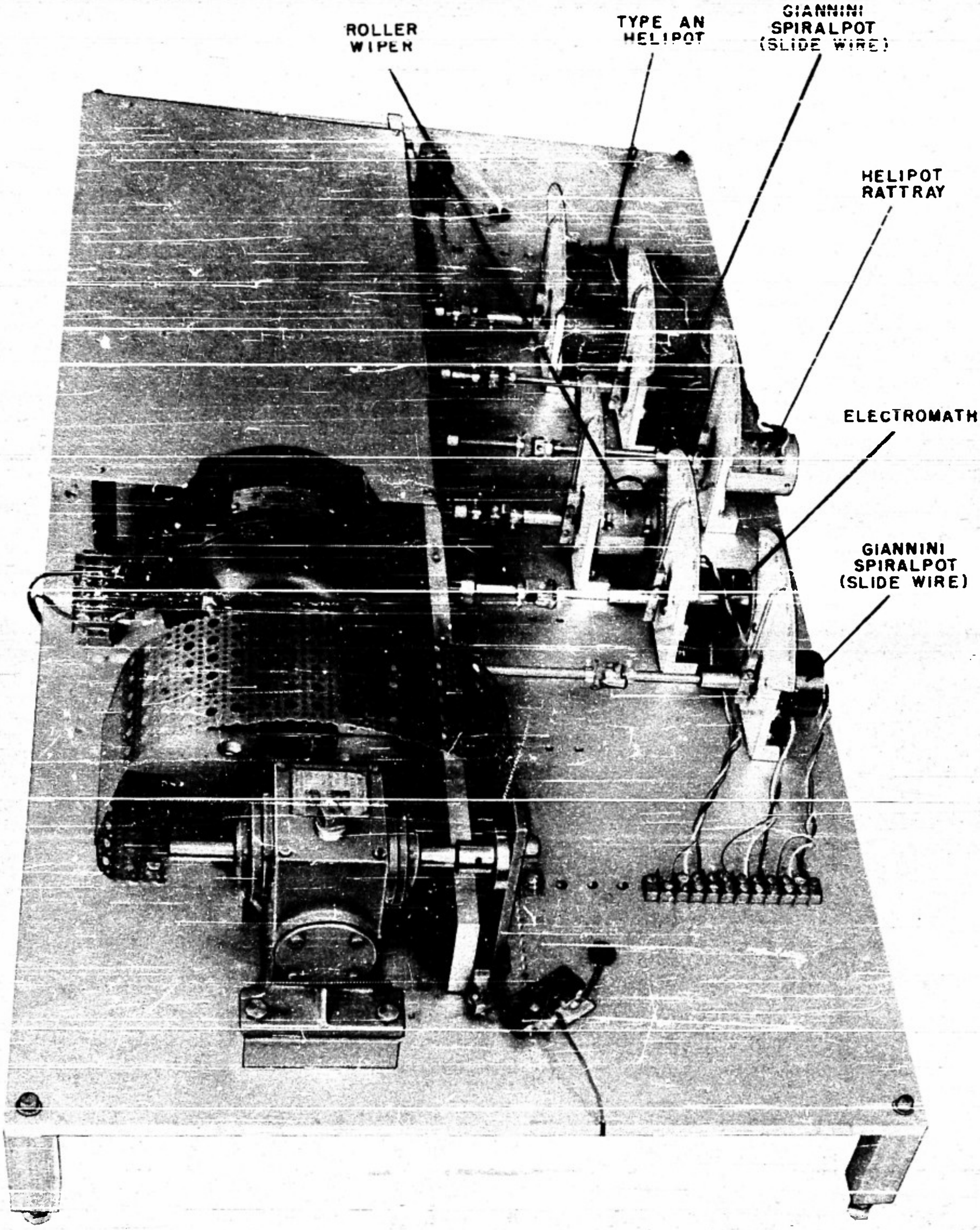

FIGURE 4-25
10 TURN POTENTIOMETER - LINEARITY vs LIFE TEST

CONFIDENTIAL
SECURITY INFORMATION

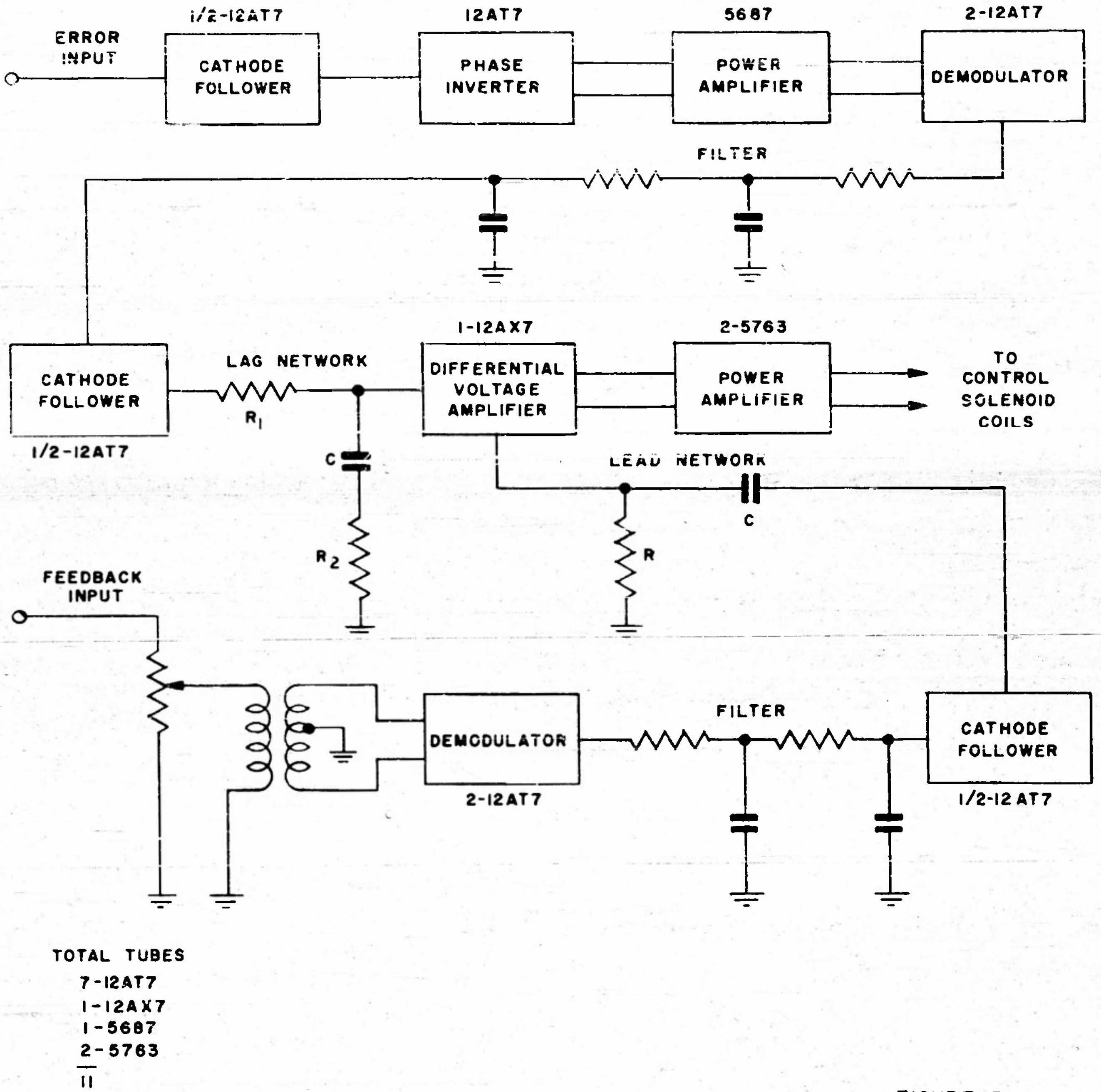

FIGURE 5-1
ELECTRONIC AMPLIFIER
BLOCK DIAGRAM

CONFIDENTIAL

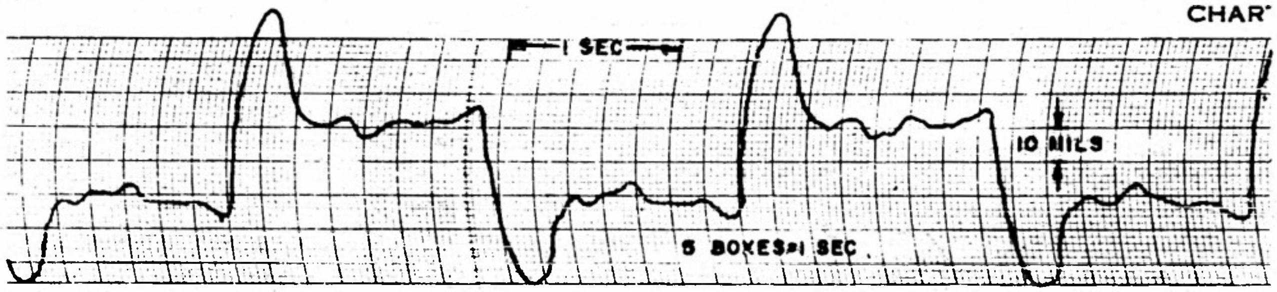

A. ACCELERATION $100^\circ/SEC^2$, ERROR 12 MILS

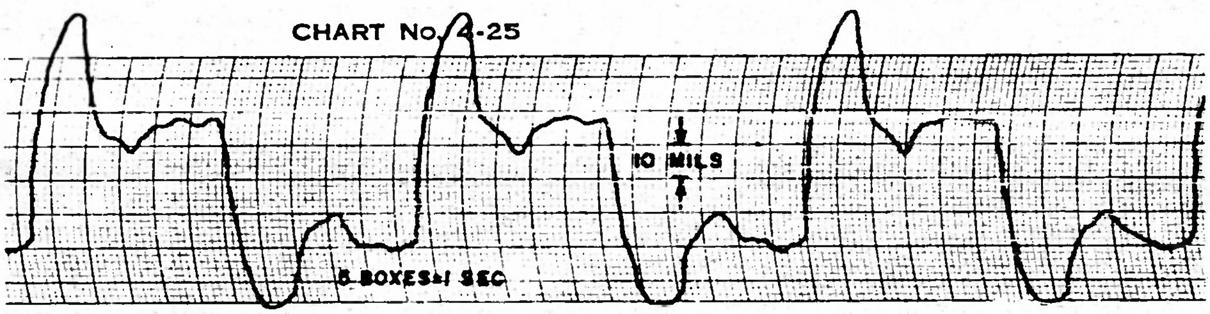

B. ACCELERATION $126^\circ/SEC^2$, ERROR 17 MILS

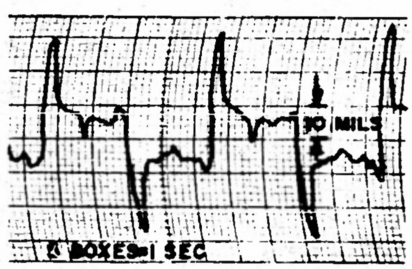

C. ACCELERATION $52^\circ/SEC^2$, ERROR 6 MILS

FIGURE 5-2
POWER CONTROL SERVO ERROR
AT CONSTANT ACCELERATION

CONFIDENTIAL
SECURITY INFORMATION

CHART No. 4-25

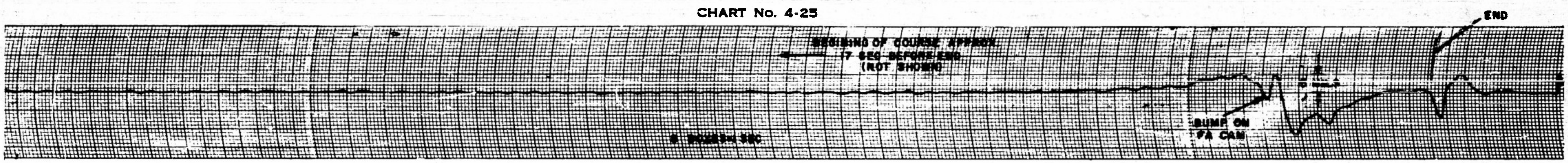

DYNAMIC TESTER
FA CAM
400 YDS/SEC VELOCITY
SLANT RANGE 670 YDS
HORIZONTAL RANGE 300 YDS
MAXIMUM ERROR 11.5 MILS

FIGURE 5-3
POWER CONTROL
SERVO ERROR-SYSTEM
FOLLOWING DYNAMIC TESTER

CONFIDENTIAL

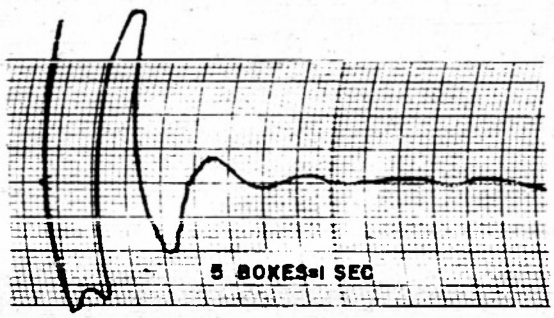

SYNCHRONIZING FROM 100 MILS OUT
TIME 1.88 SEC

FIGURE 5-4
POWER CONTROL
SYNCHRONIZING TIME

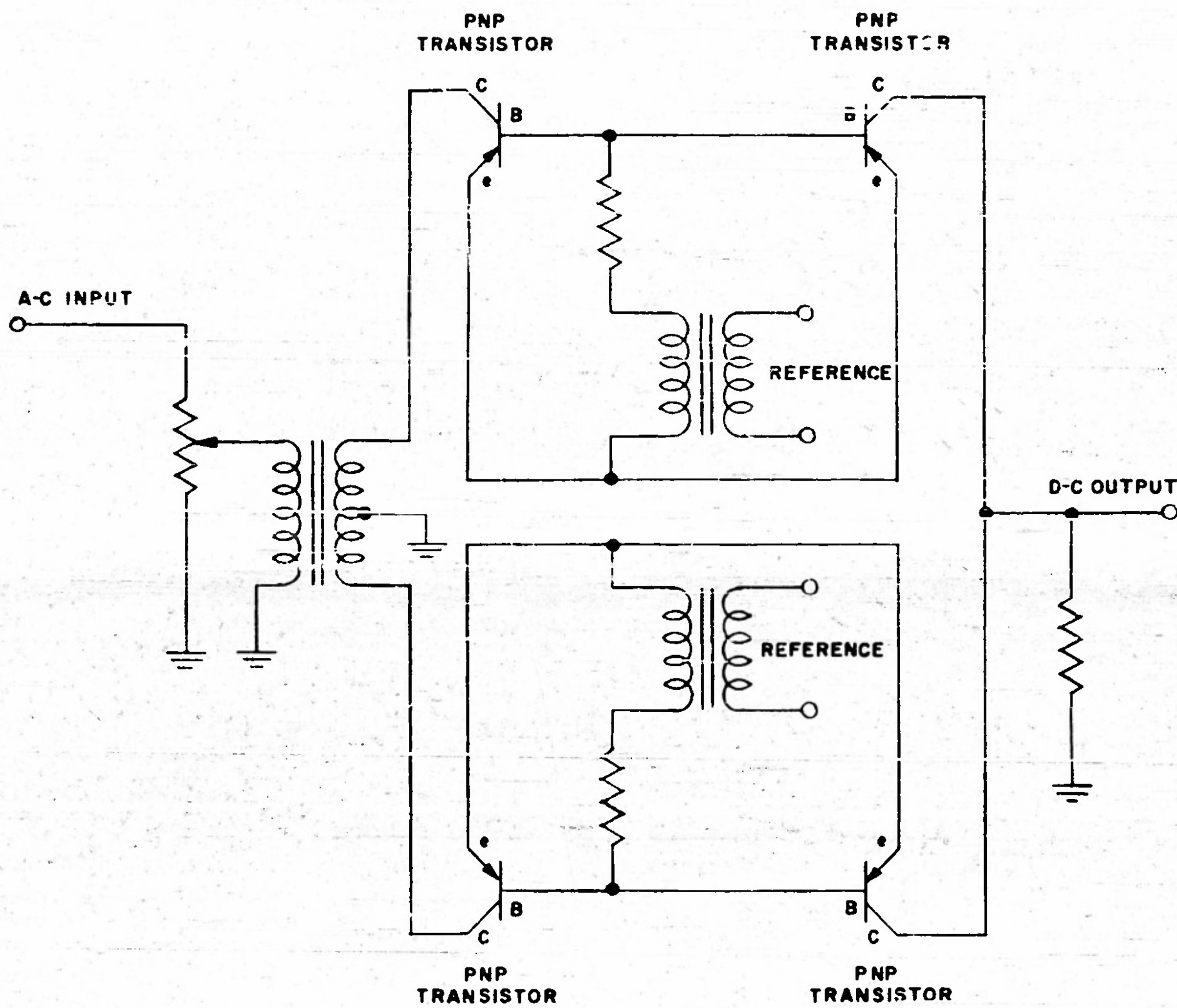

FIGURE 5-5
TRANSISTOR DEMODULATOR
SCHEMATIC

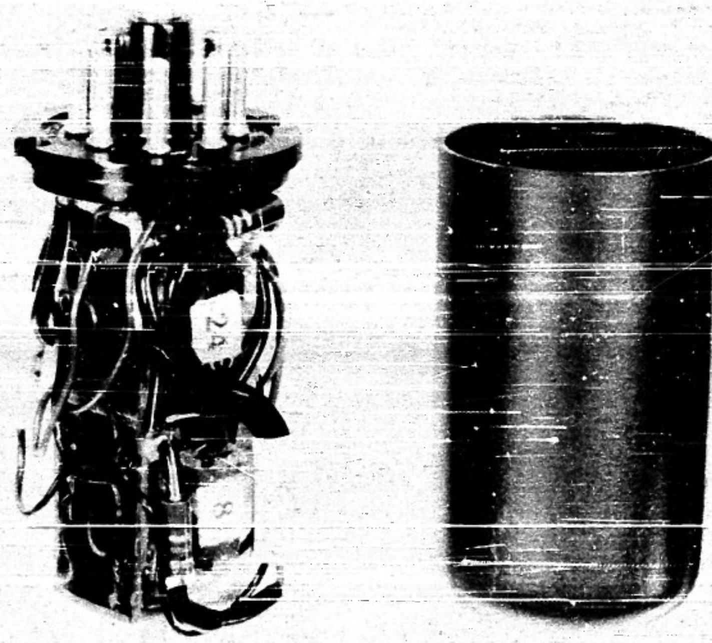

FIGURE 5-6a
DEMODULATOR PLUG IN CHASSIS
(WITHOUT TRANSISTOR SOCKETS)

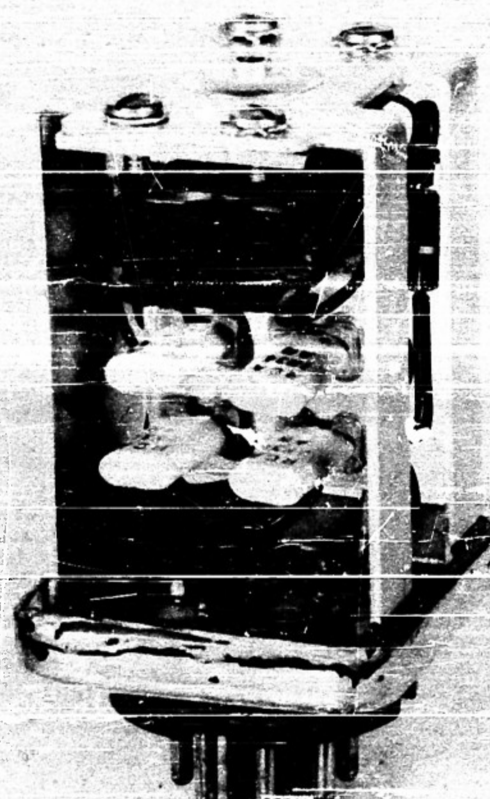

FIGURE 5-6b
DEMODULATOR PLUG IN CHASSIS
(WITH TRANSISTOR SOCKETS)

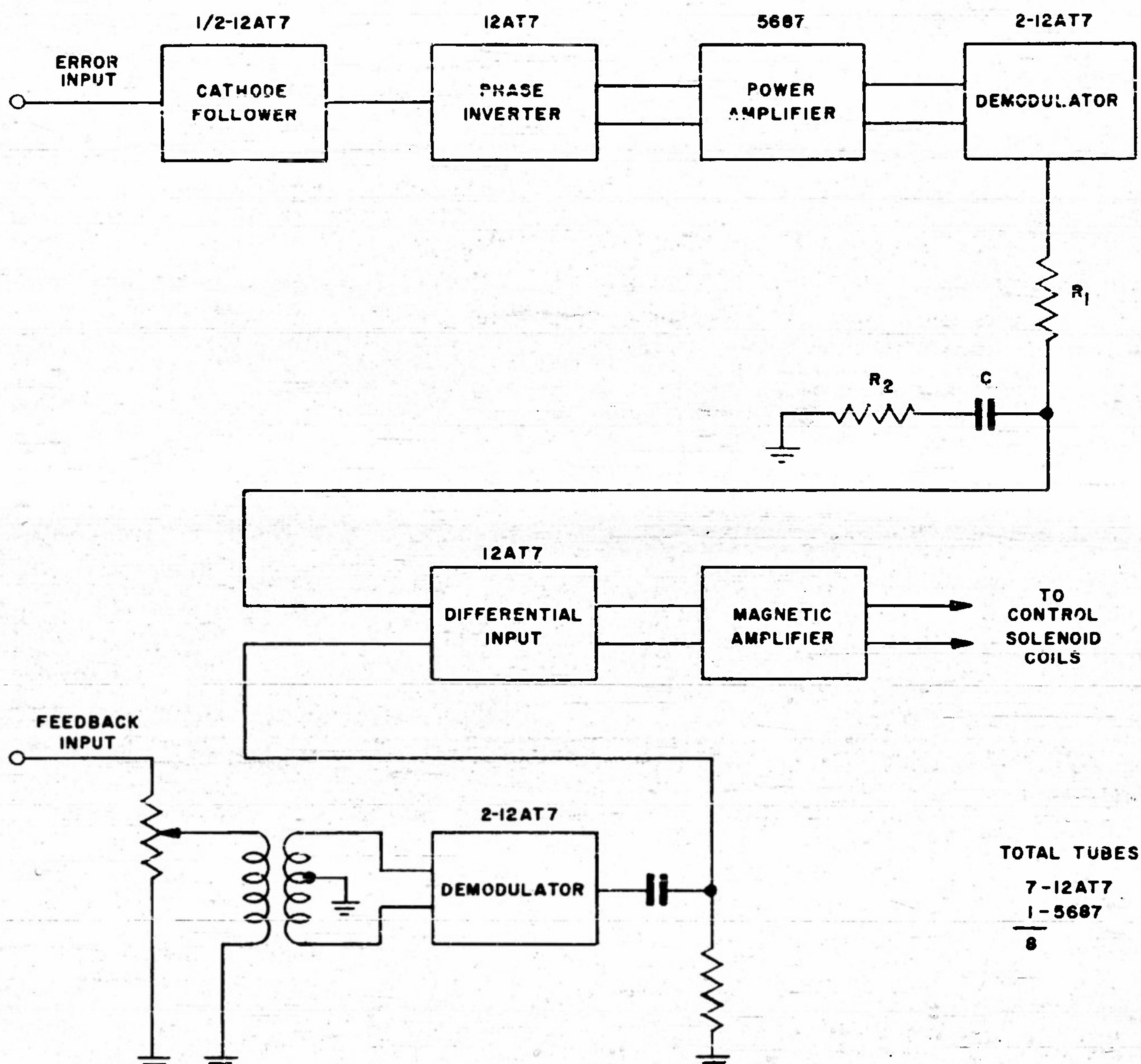

FIGURE 5-7
ELECTRONIC
MAGNETIC AMPLIFIER
BLOCK DIAGRAM

CHART No 4-25

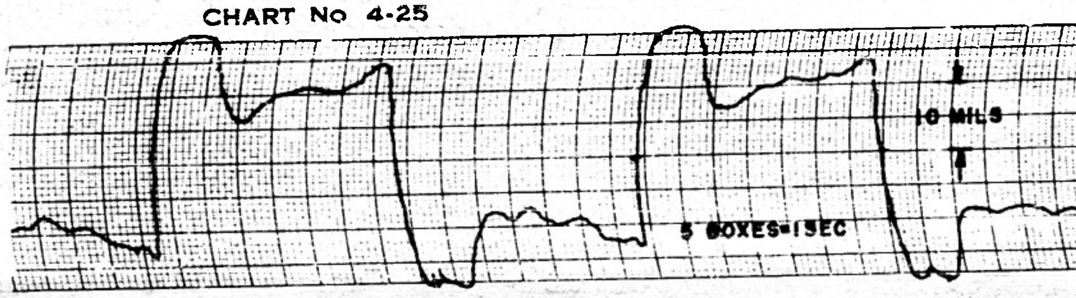

MAGNETIC AMPLIFIER CONSTANT ACCELERATION COURSE
ACCELERATION 110°/SEC^2, ERROR 12 MILS

FIGURE 5-8

POWER CONTROL ERRORS
USING MAGNETIC AMPLIFIER

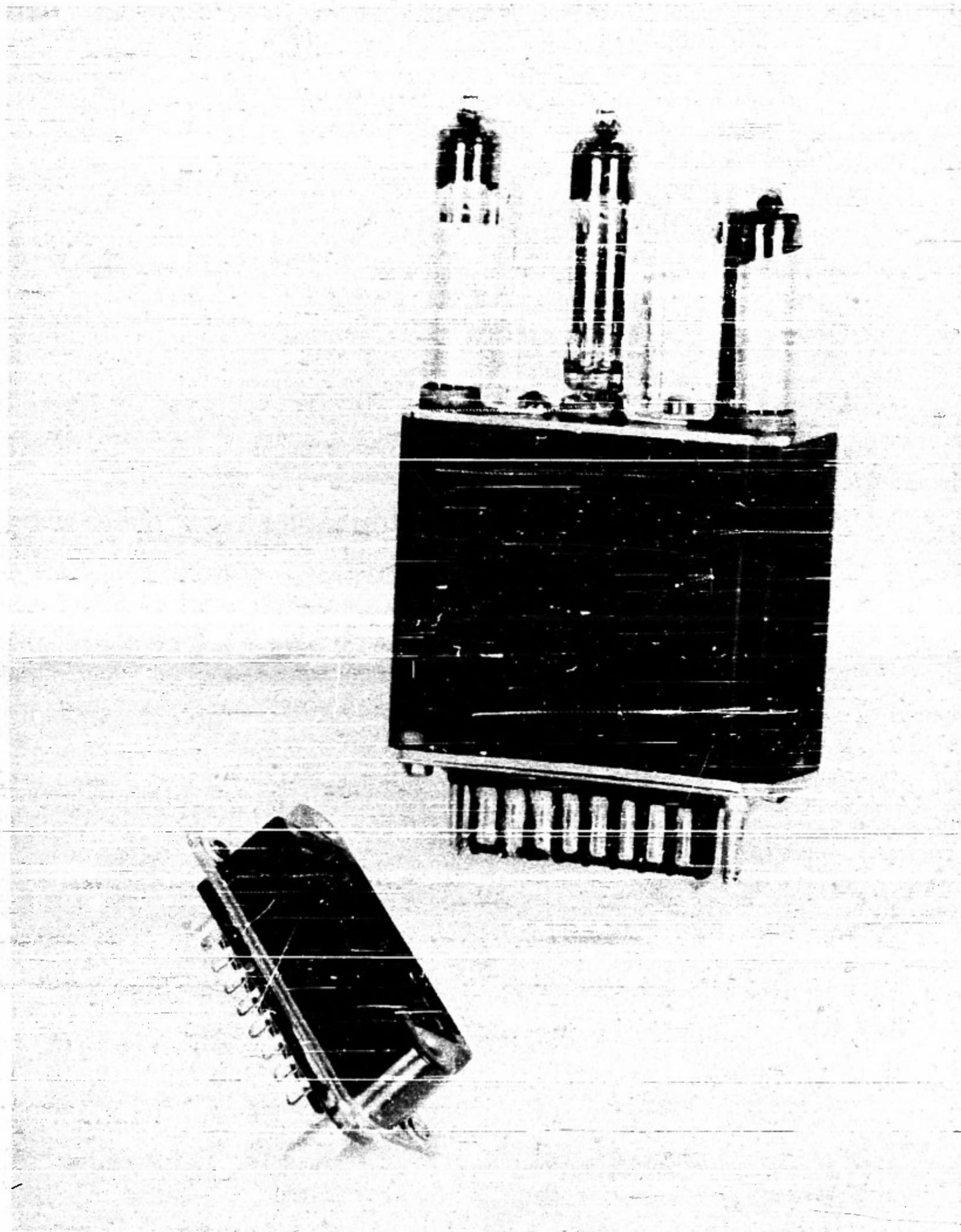

FIGURE 5–9a
SUBMINIATURE D-C POWER AMPLIFIER – IMBEDDED

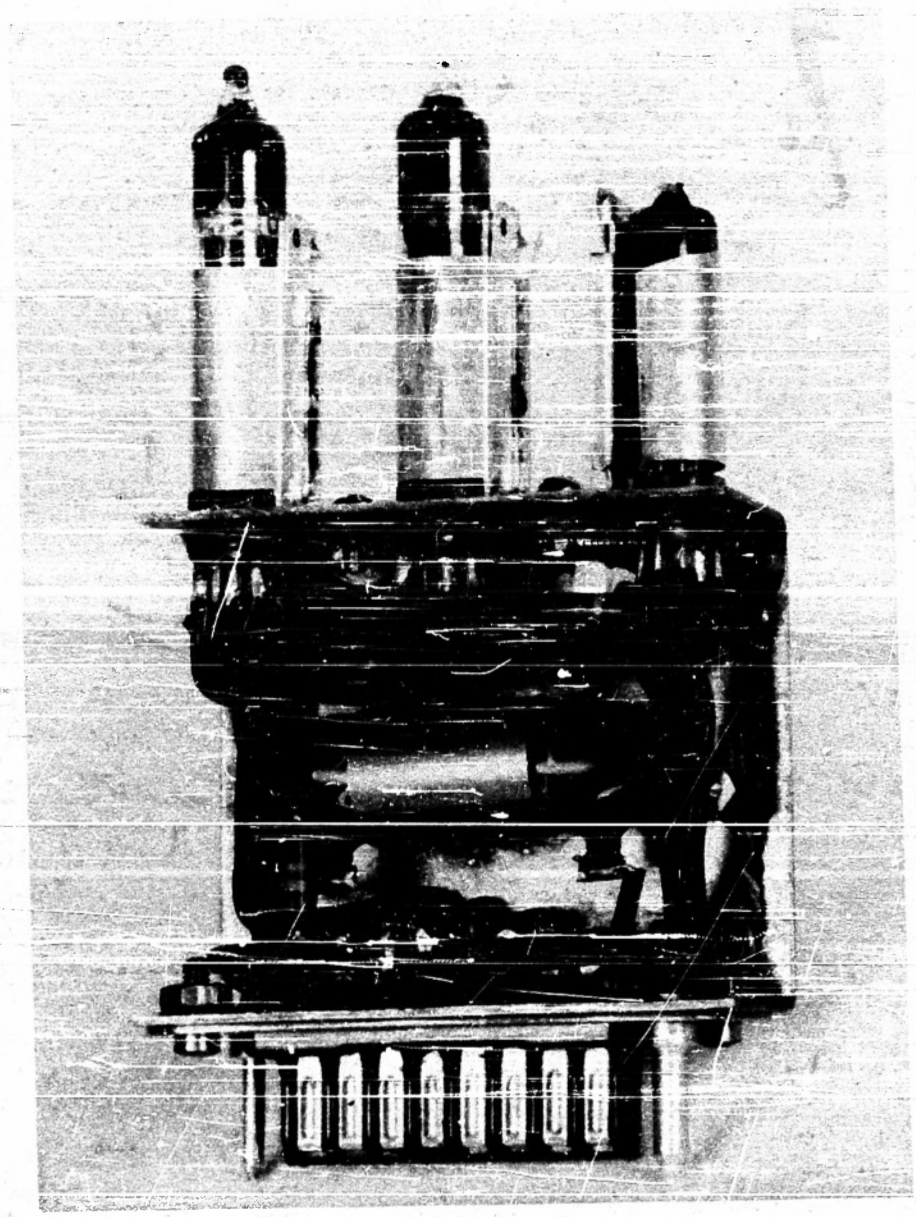

FIGURE 5-9b

SUBMINIATURE D-C POWER AMPLIFIER - NOT IMBEDDED

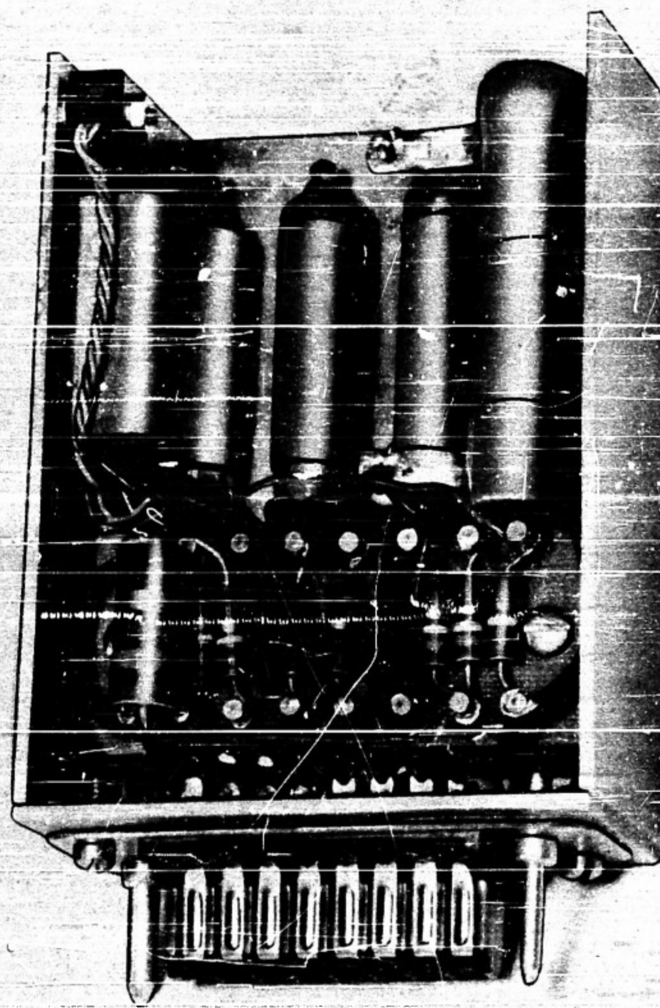

FIGURE 5-10
SUBMINIATURE DEFLECTION AMPLIFIER

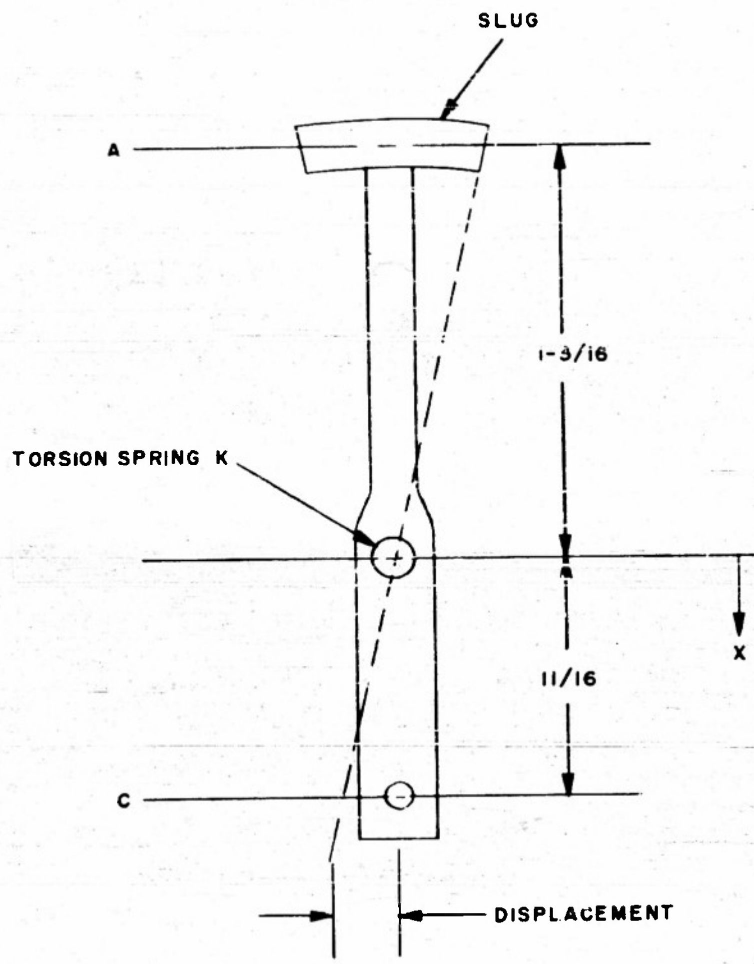

FIGURE 5-11
SOLENOID ARMATURE

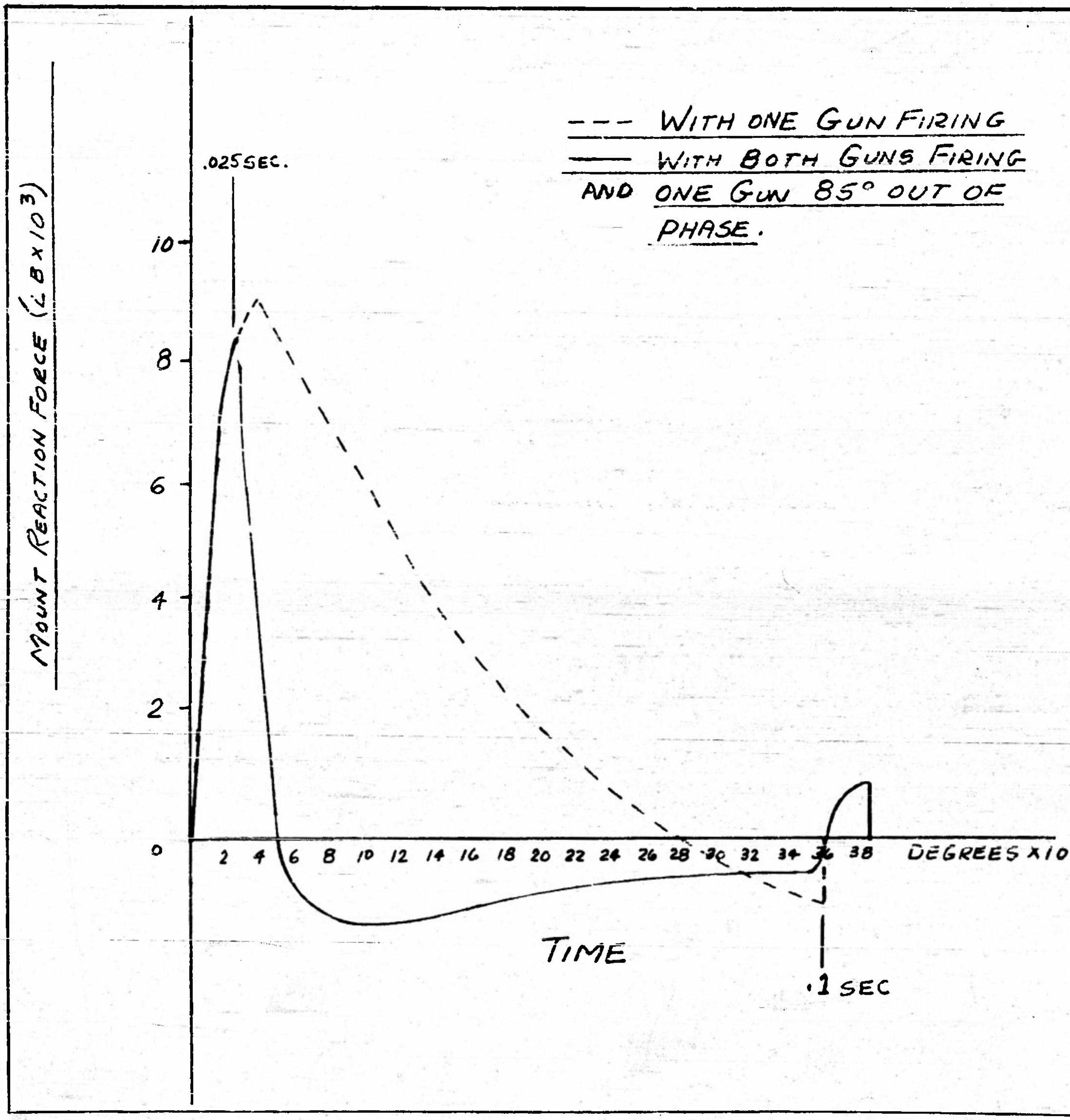

FIGURE 5-12
GUN MOUNT
REACTION FORCE
VS. TIME

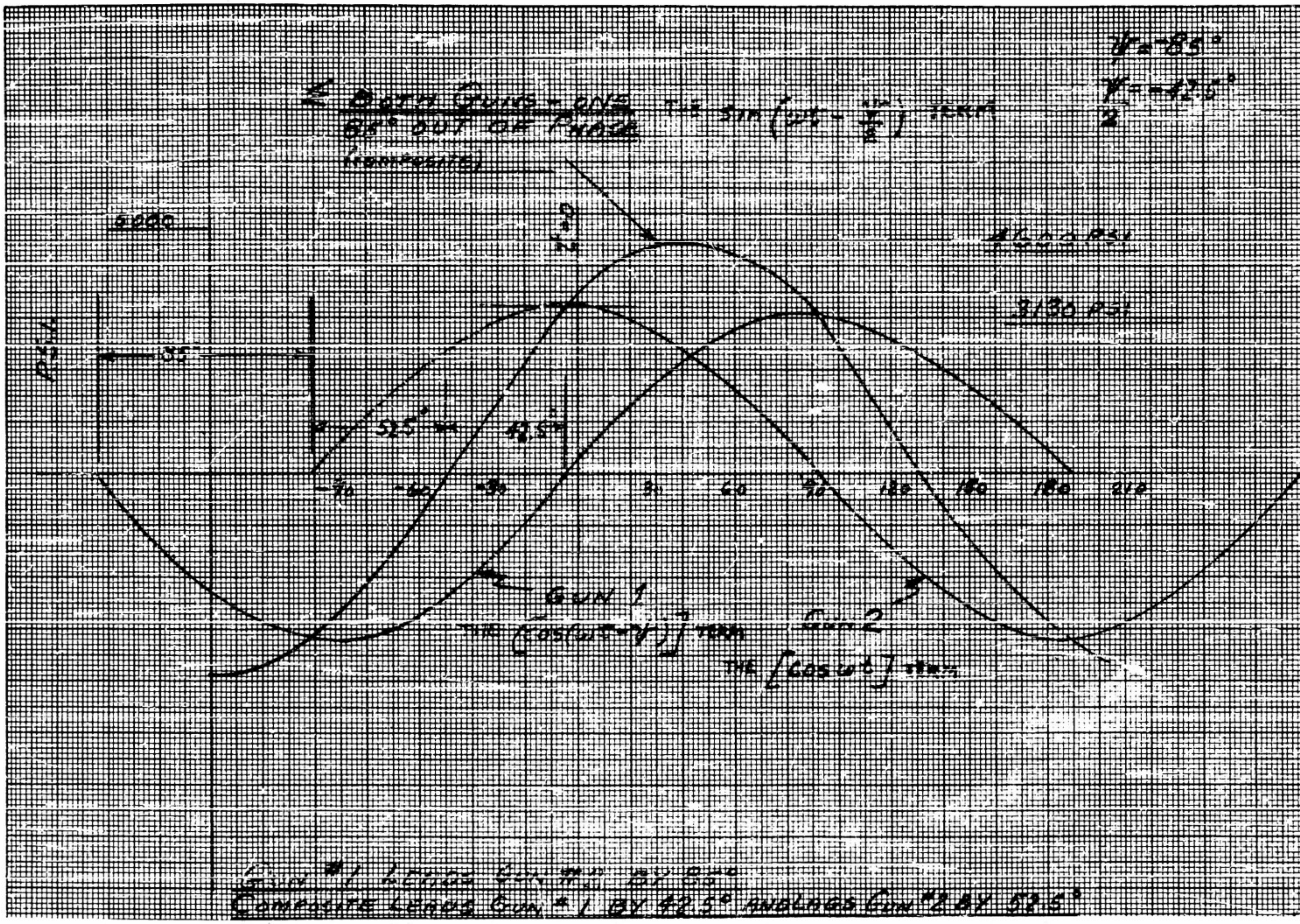

FIGURE 5-13
ASYNCHRONOUS GUN FIRING GRAPHS

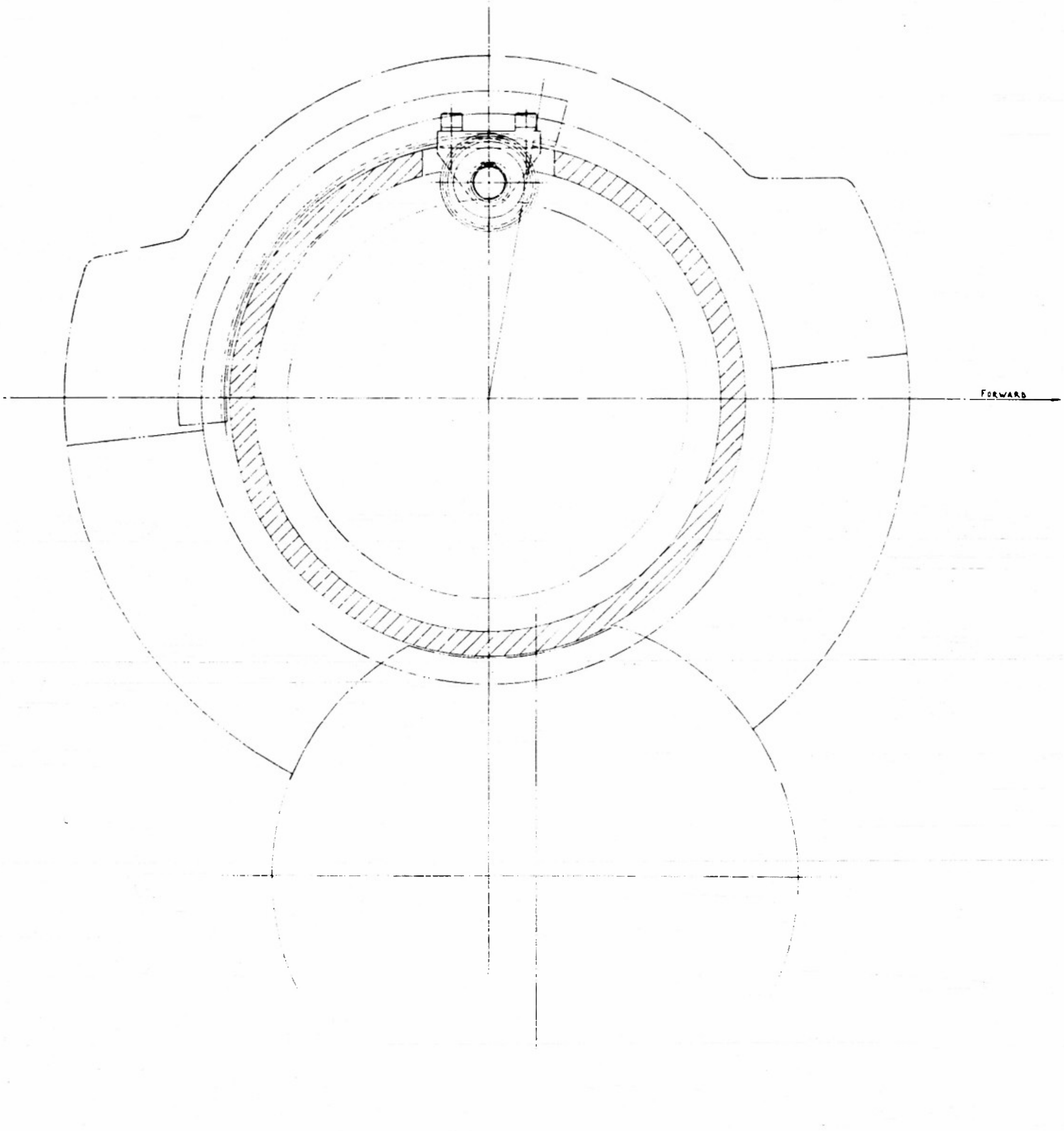

1

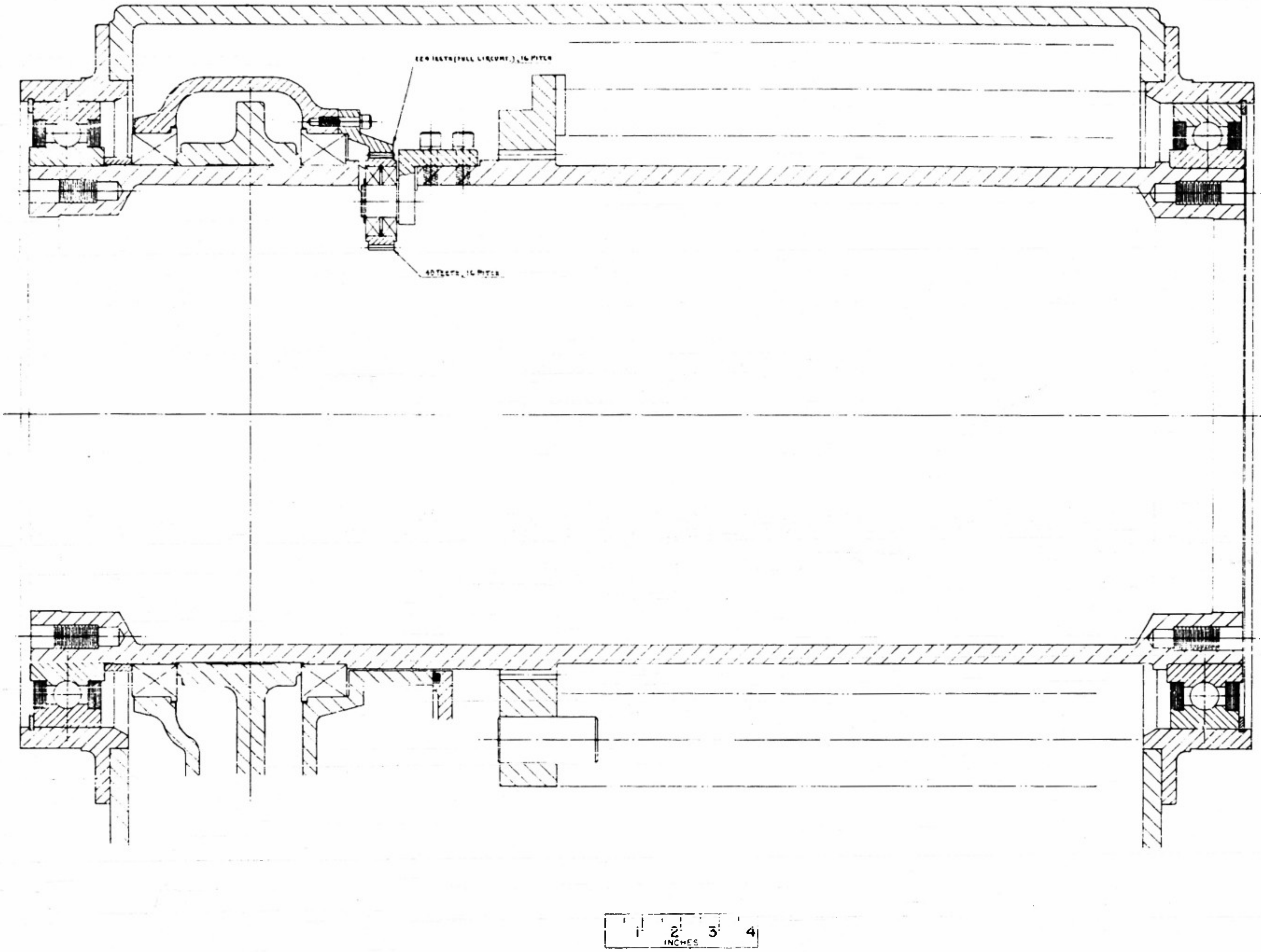

FIGURE 6-1
FE POSITION MECHANISM FOR ARMOUR GUN

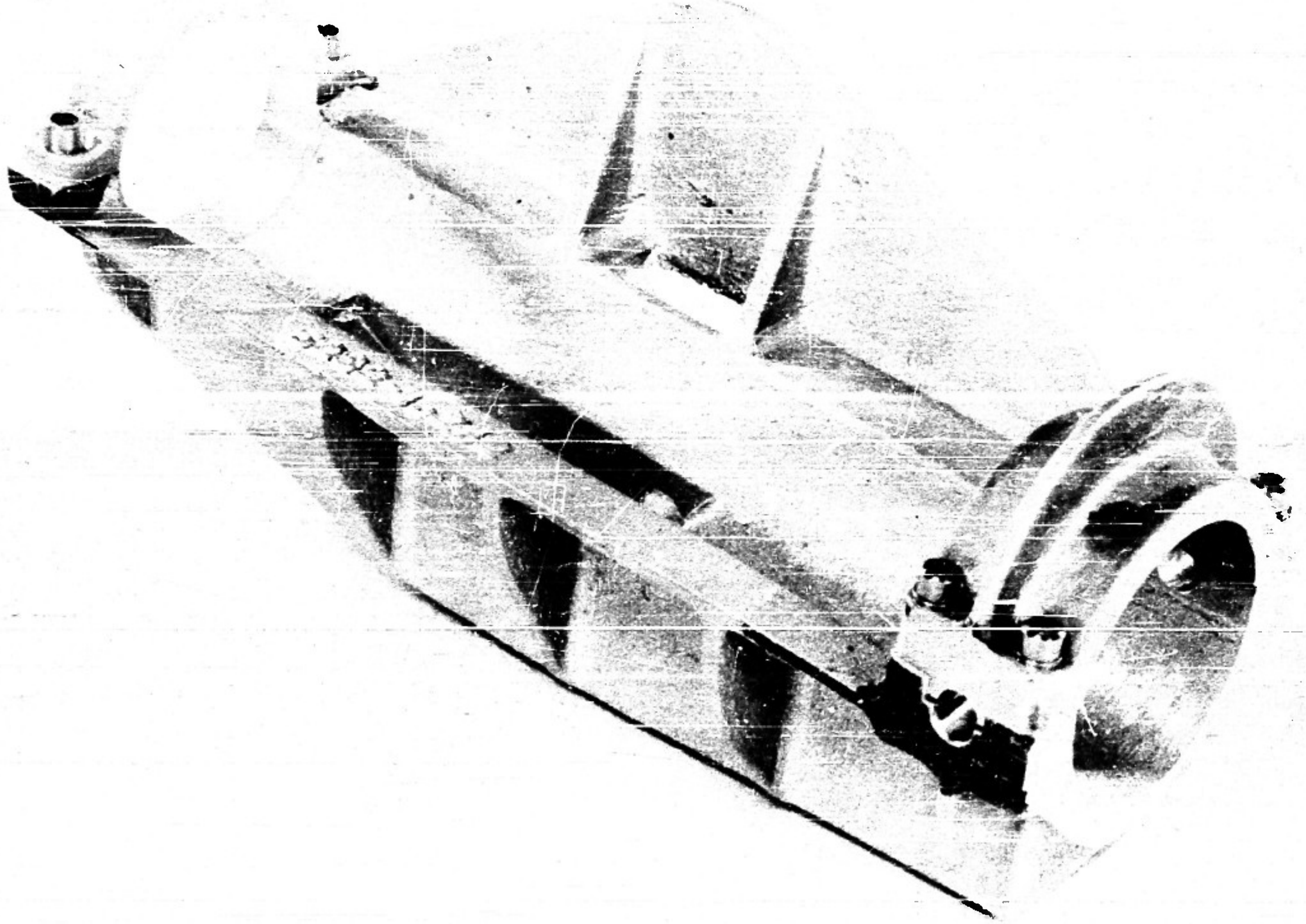

FIGURE 6-2
CRADLE FOR MOUNTING DIXON GUN

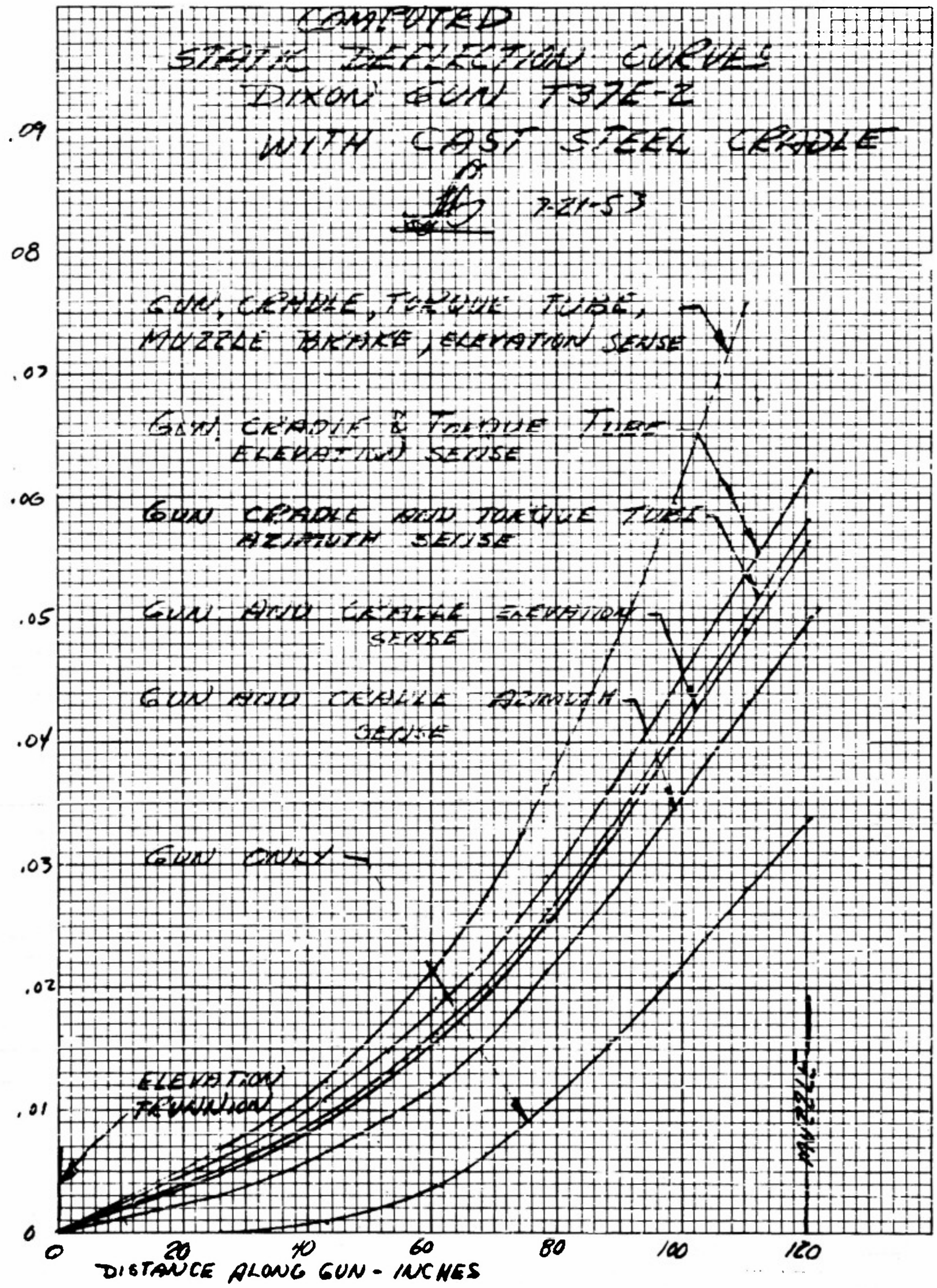

FIGURE 6-3
STATIC DEFLECTION CURVES - DIXON GUN

CONFIDENTIAL
SECURITY INFORMATION

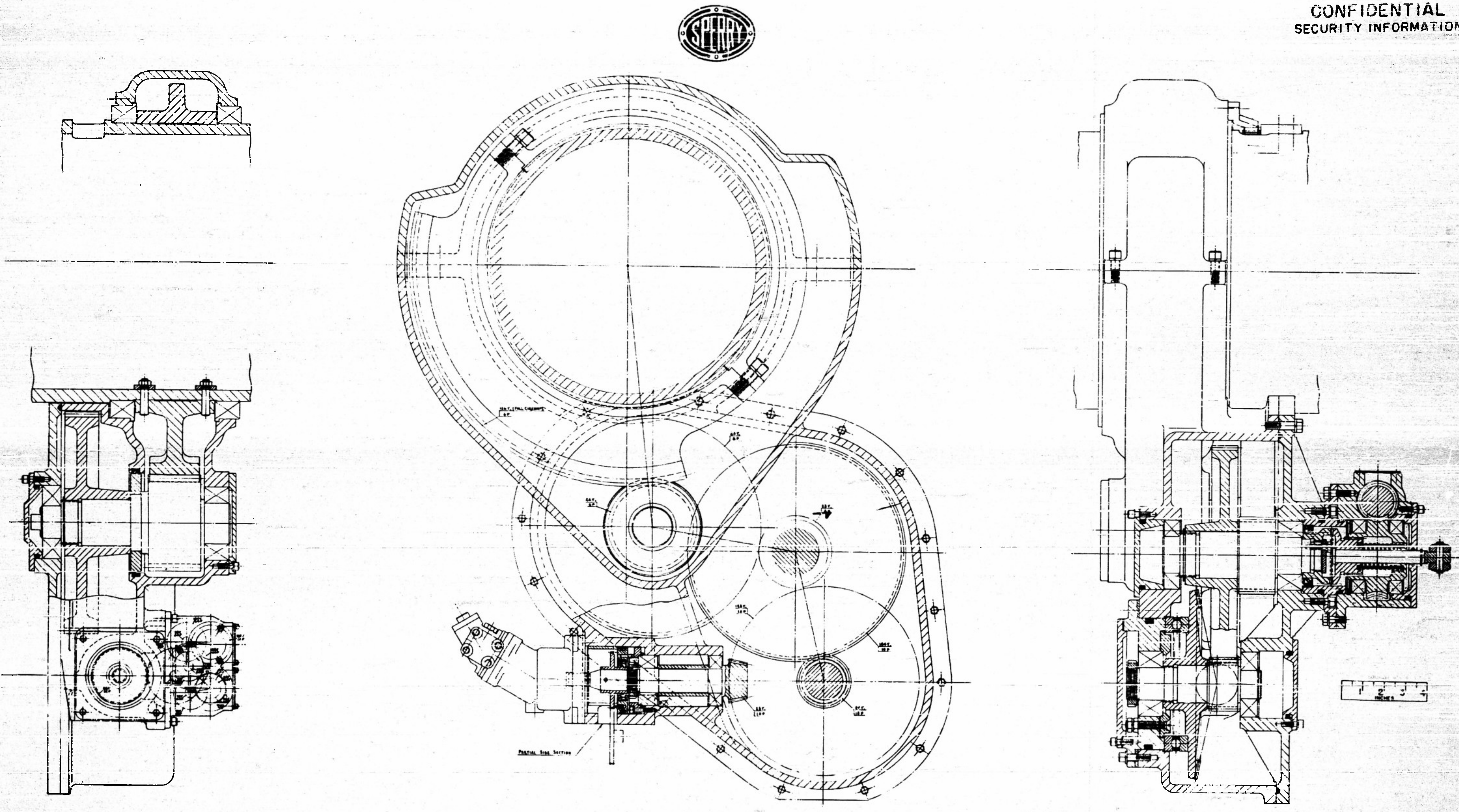

FIGURE 6-4
FE POWER SPUR GEAR - GUN ELEVATION DRIVE

CONFIDENTIAL

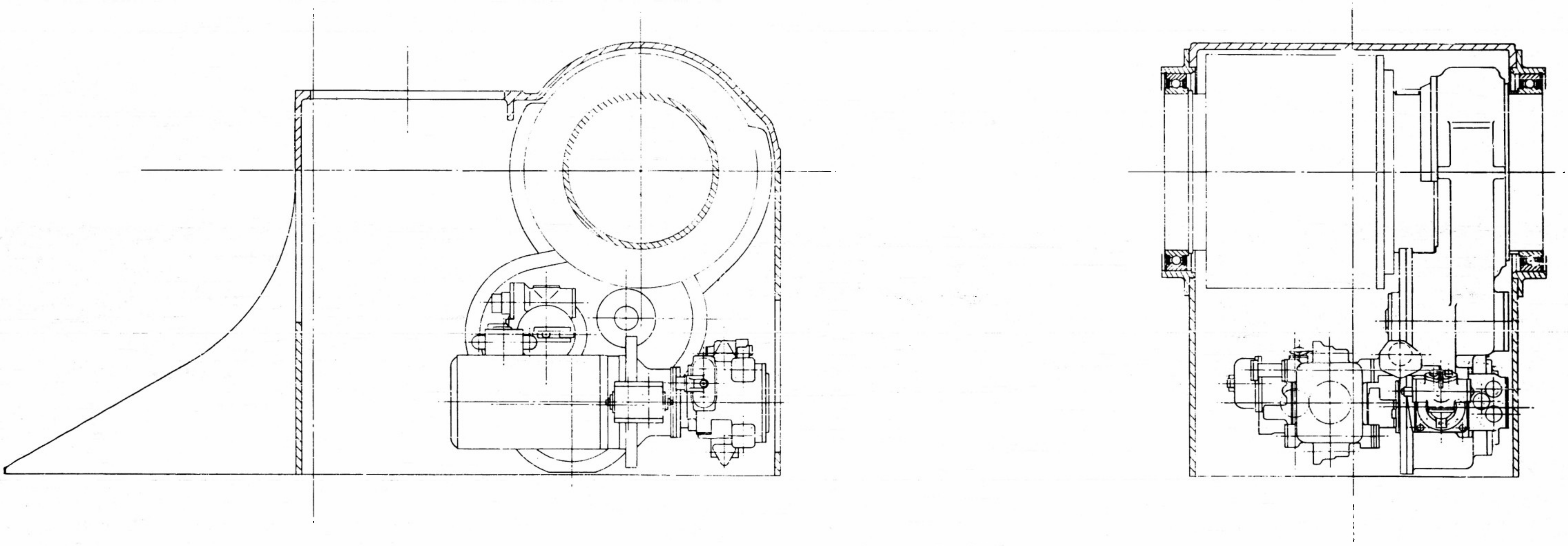

1

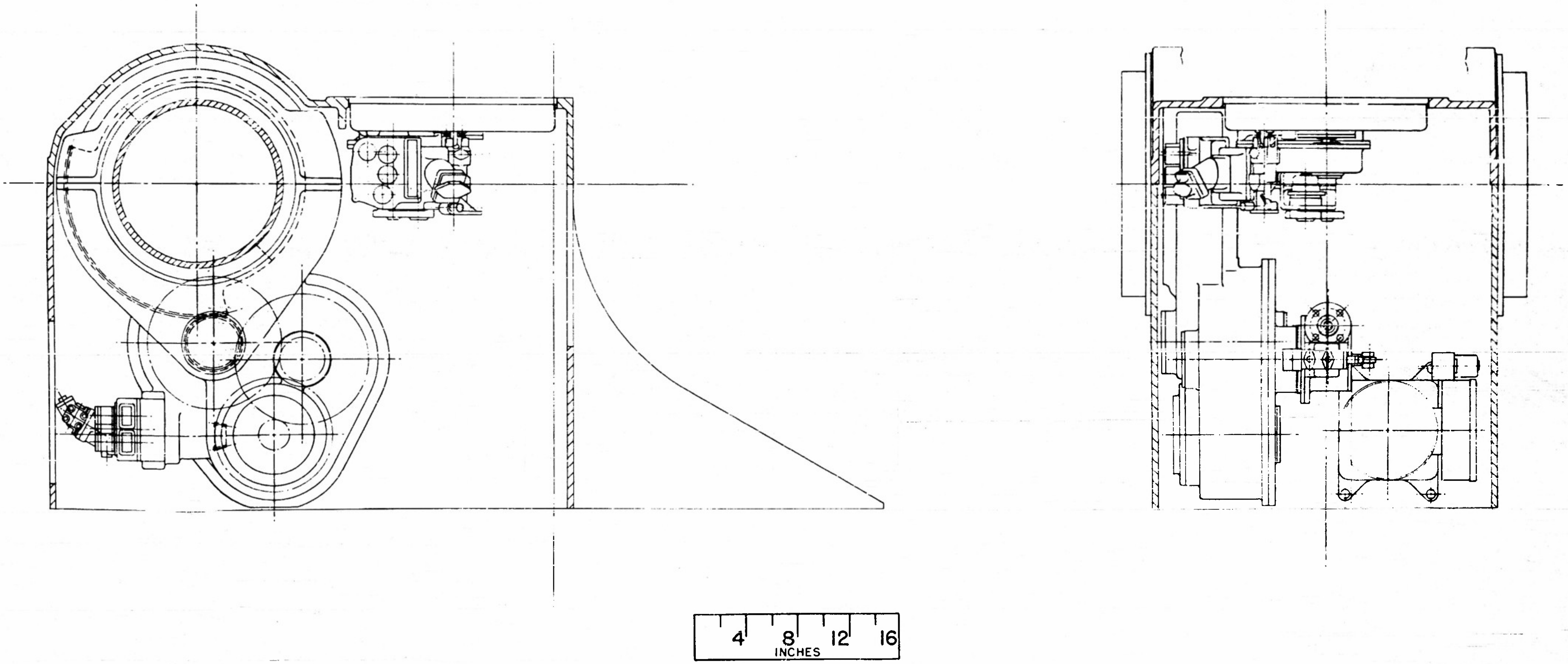

FIGURE 6—5
GENERAL GEARING ARRANGEMENT – UPPER STRUCTURE

SPERRY

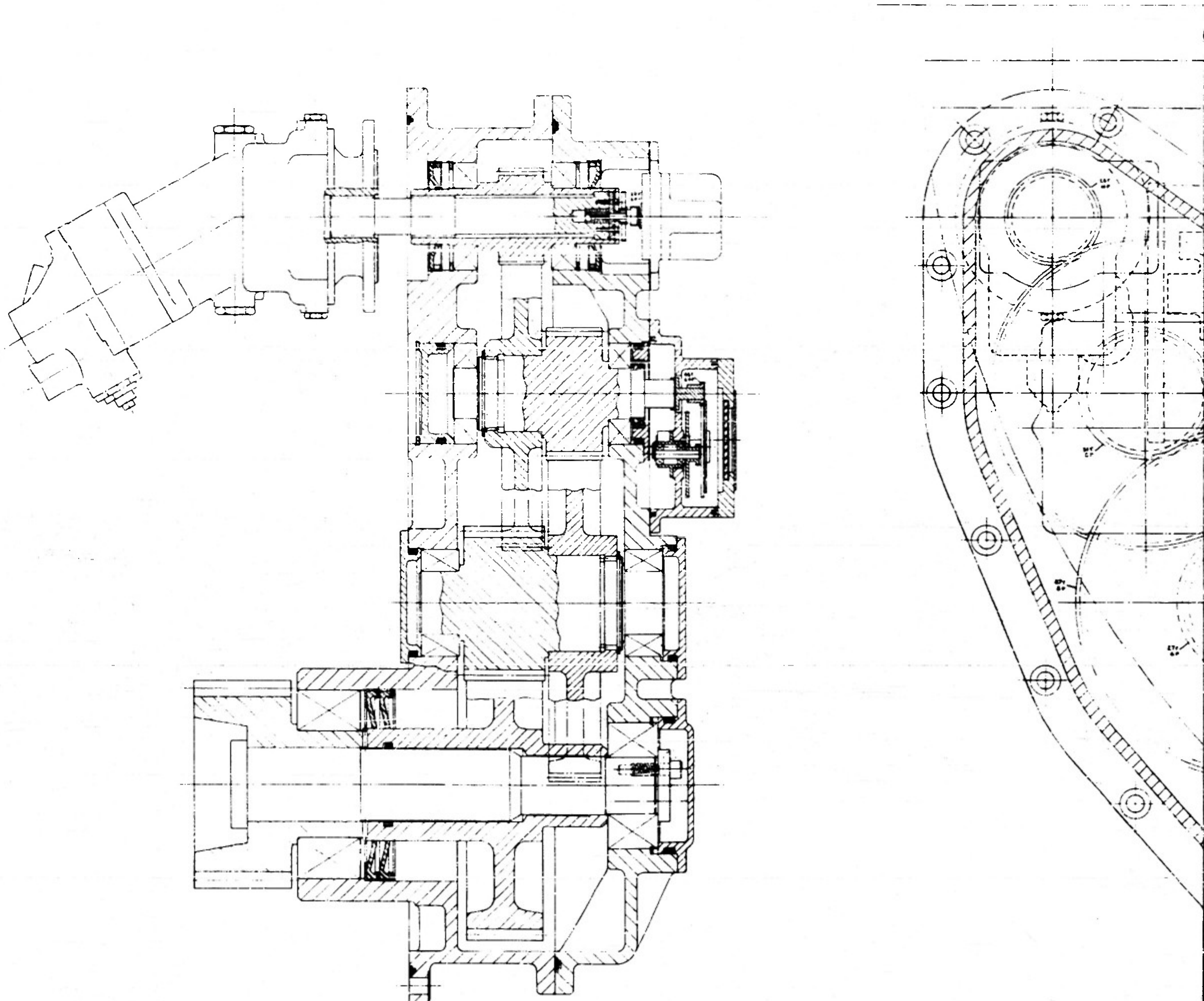

1

CONFIDENTIAL
SECURITY INFORMATION

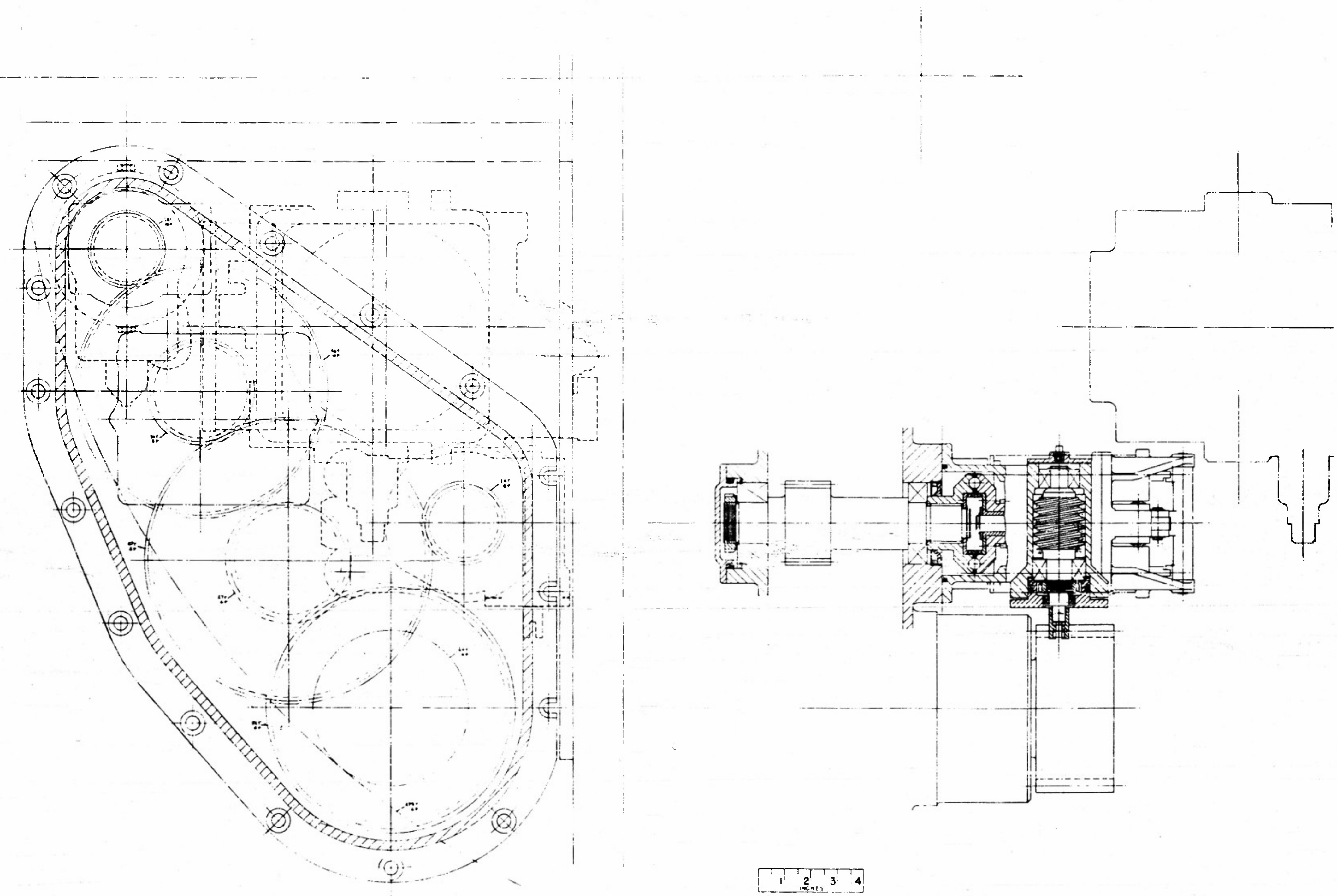

FIGURE 6-6
AZIMUTH "B" END AND GEARING ASSEMBLY

CONFIDENTIAL

2

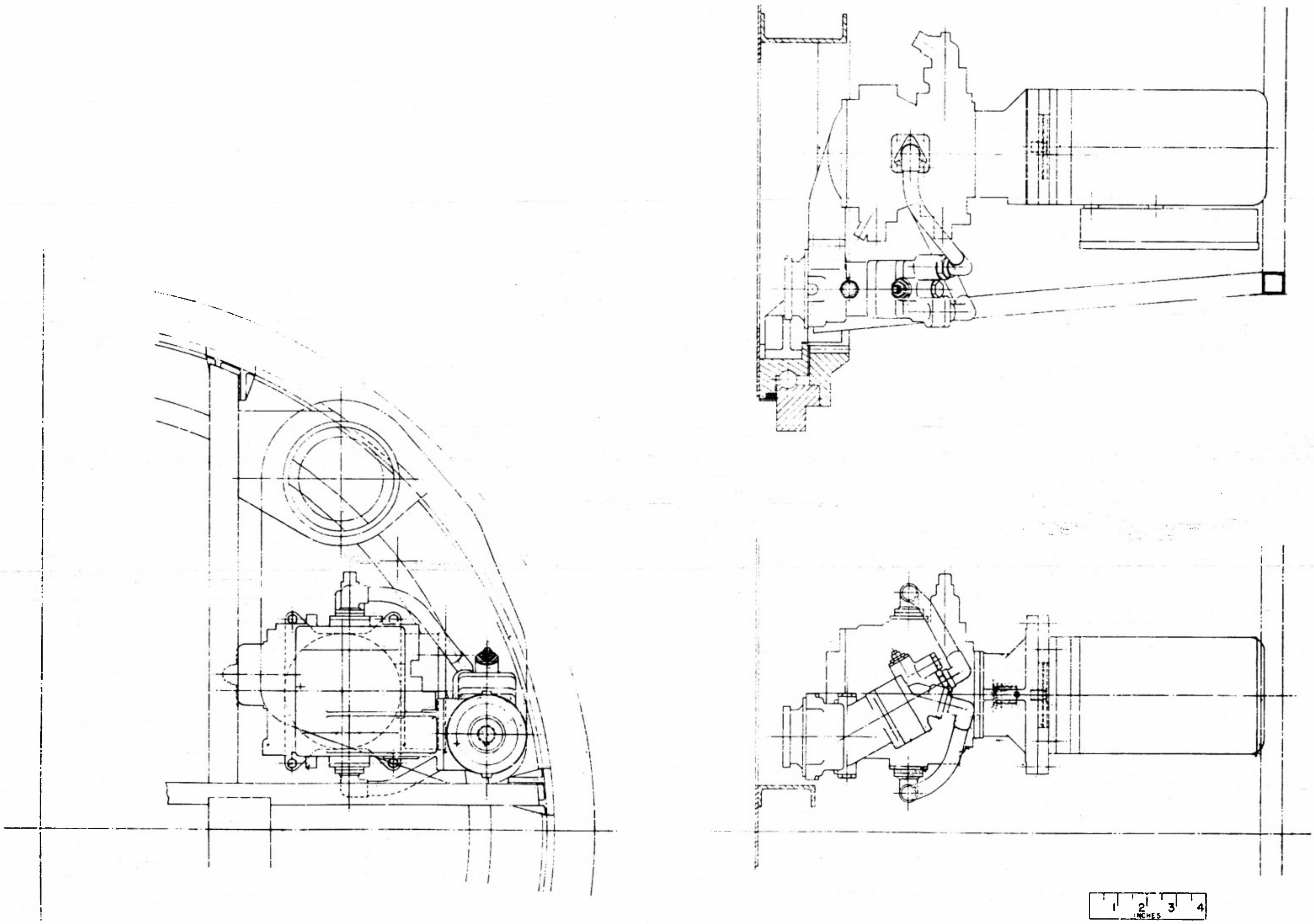

FIGURE 6-7
AZIMUTH "A" END AND "B" END

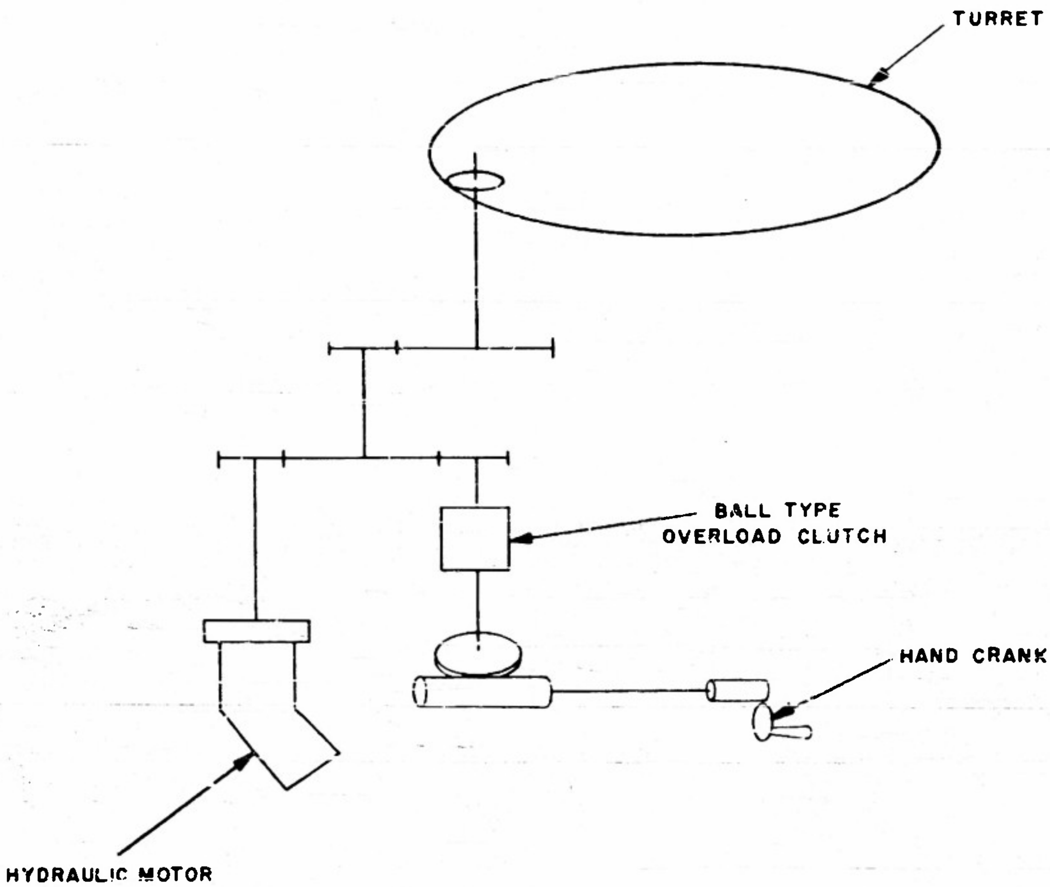

FIGURE 6-8
FA GEARING SCHEMATIC

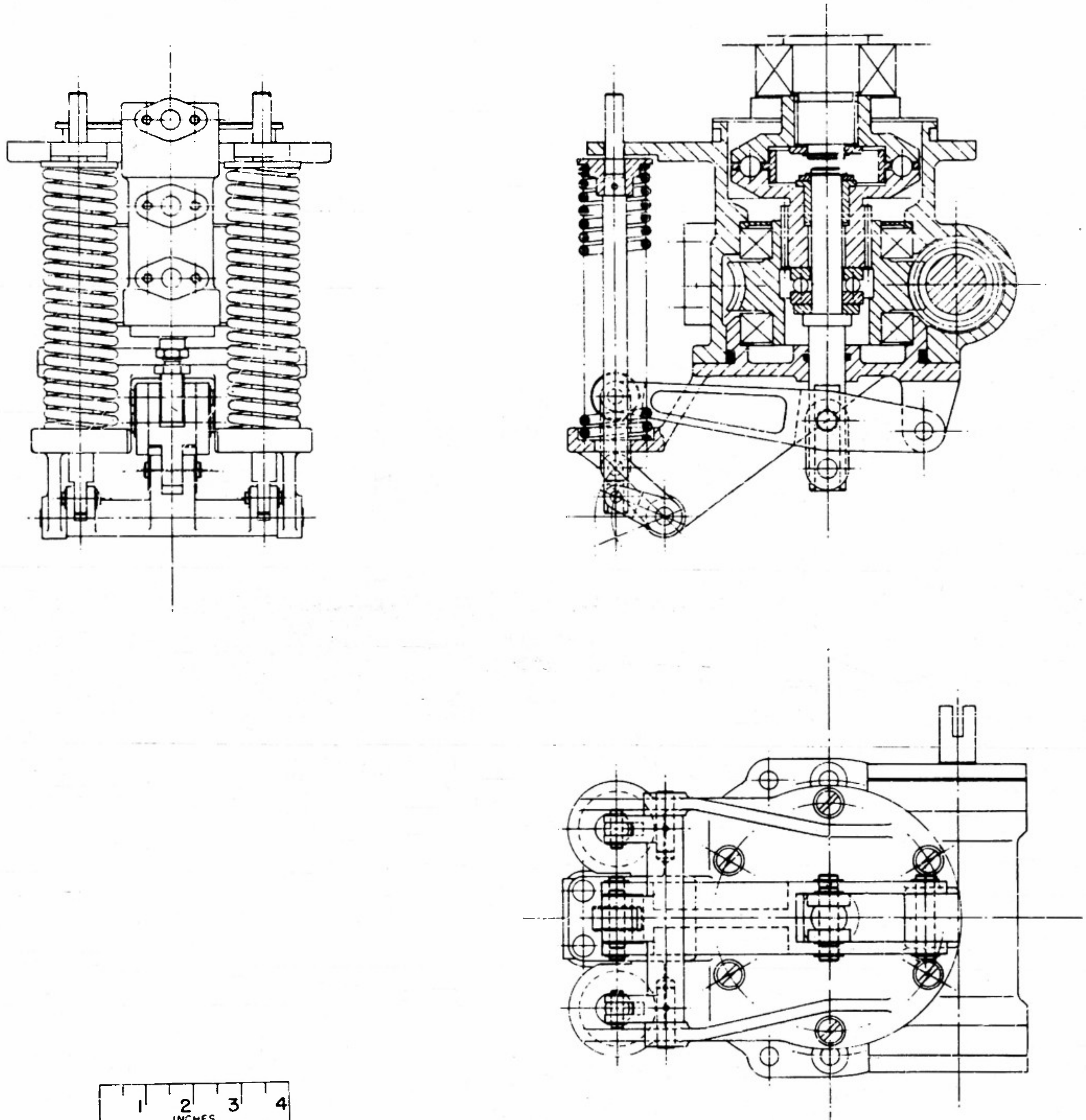

FIGURE 6--9

AZIMUTH MANUAL DRIVE AND SLIP CLUTCH

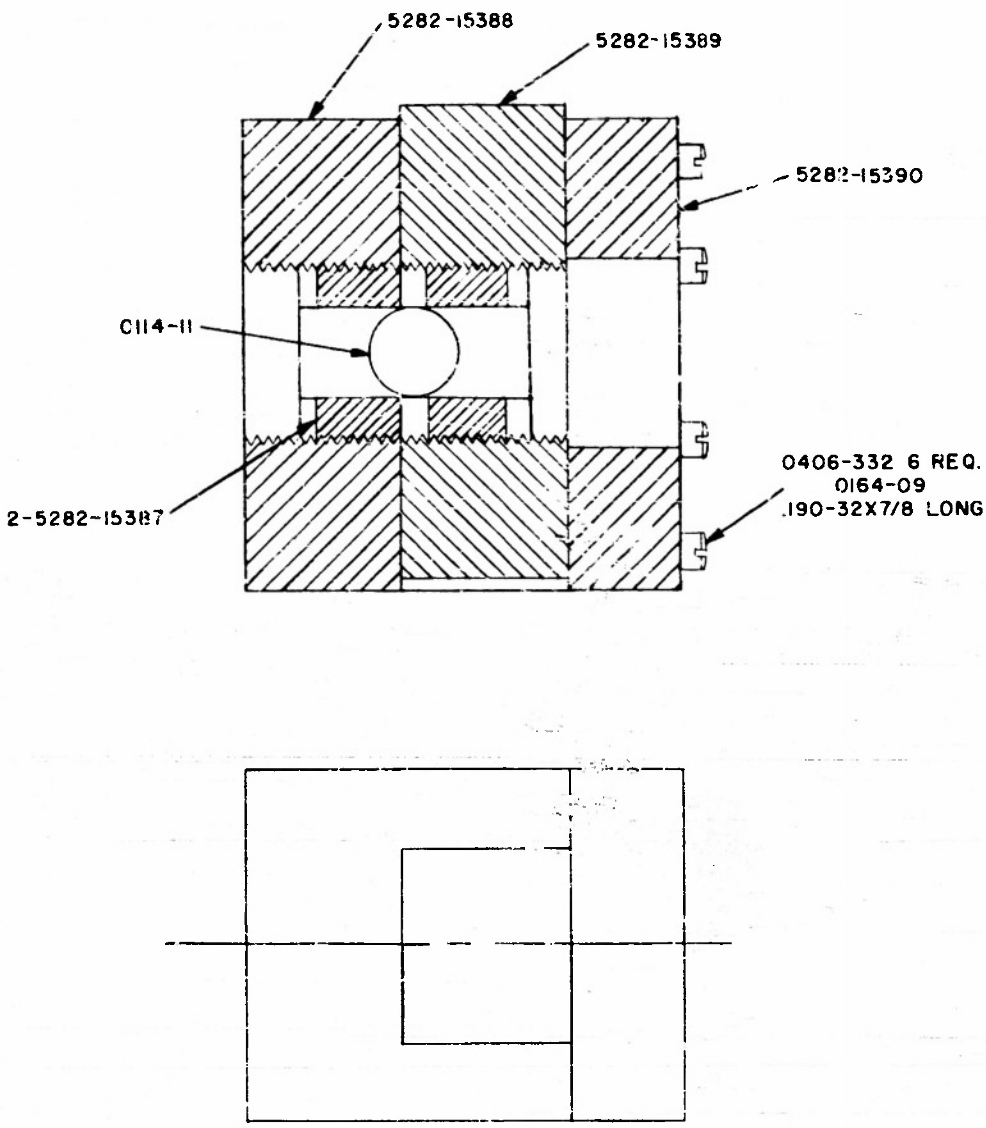

NOTE:
ALL PART NUMBERS USED ARE MANUFACTURERS (SPG) DRAWING NUMBERS

FIGURE 6-10
BALL TEST FIXTURE

CONFIDENTIAL
SECURITY INFORMATION

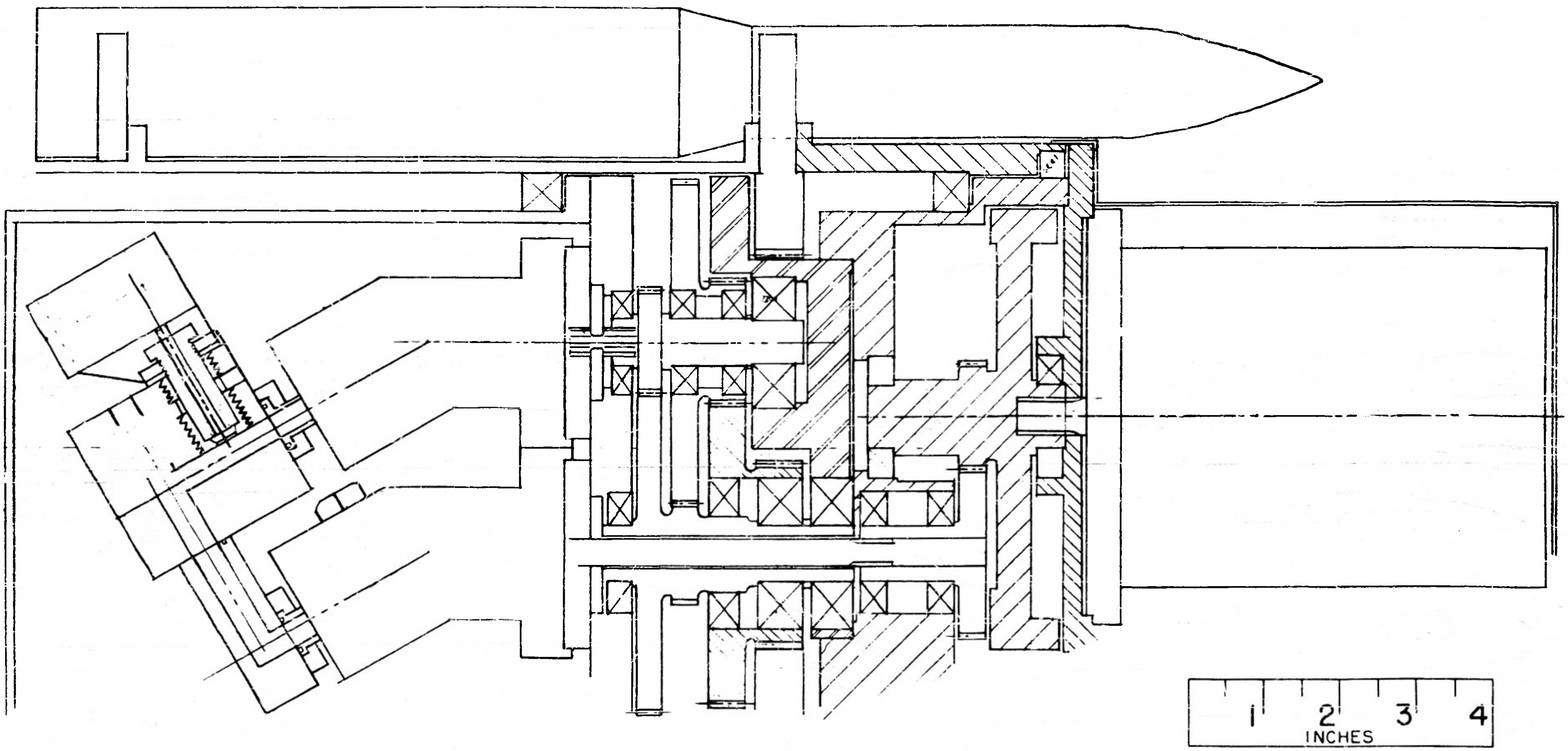

FIGURE 6-11
HYDRAULIC AMMUNITION BOOSTER

CONFIDENTIAL

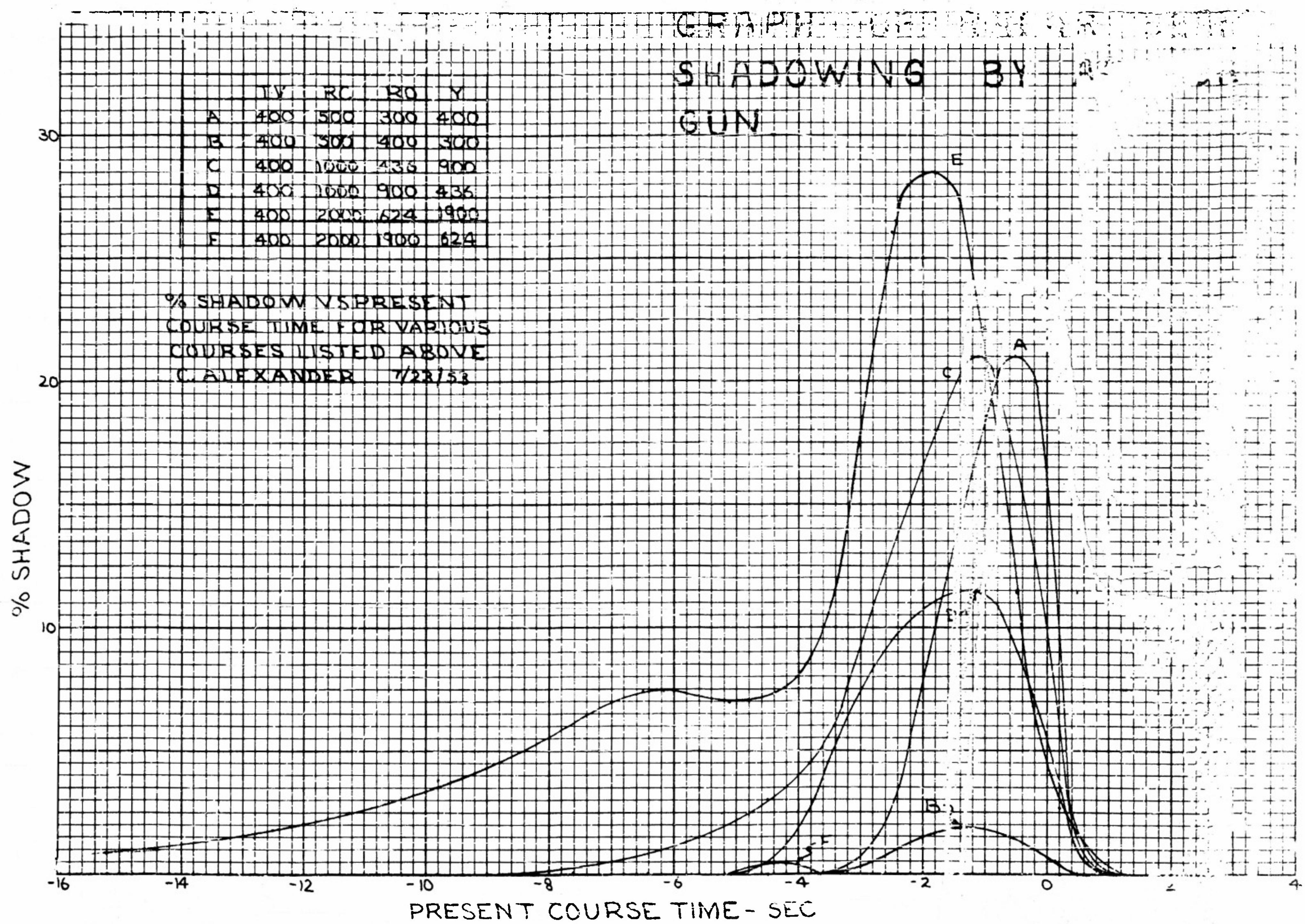

FIGURE 6-12
SHADOWING OF RADAR BEAM BY ARMOU GUN